



TECHNISCHE  
UNIVERSITÄT  
WIEN

Vienna University of Technology

# MASTER THESIS

**Evaluation of an in-house-built Peltier cooled ablation  
stage for elemental imaging of snap frozen biological  
tissue samples using LA-ICP-MS**

**Supervisor**

**Associate Prof. Dipl.-Ing. Dr.techn. Andreas Limbeck**

**By**

**Seyed Shahin Amirkhalili**

**In partial fulfillment of the requirements for the degree of Master  
of Science in Biomedical Engineering**

**at the**

**Institute of Chemical Technologies and Analytics**

**Vienna, March 2018**

---

**S.Sh. Amirkhalili, BSc**

**Dammstrasse 26-28/27**

**Vienna 1200, Austria**

من نگویم چه کن ار اهل دلی خود تو بگوی

ساقیا سایه ابر است و بهار و لب جوی

دلخ آلوده صوفی به می ناب بشوی

بوی یک رنگی از این نقش نمی آید خیز

ای جهان دیده ثبات قدم از سفله مجوی

سفله طبع است جهان بر کرمش تکیه مکن

از در عیش درآ و به ره عیب مپوی

دو نصیحت کنت بشنو و صد گنج ببر

بیخ نیکی بنشان و ره تحقیق بجوی

شکر آن را که دگر بار رسیدی به بهار

ور نه هرگز گل و نسرين ندمد ز آهن و روی

روی جانان طلبی آینه را قابل ساز

خواجه تقصیر مفرما گل توفیق ببوی

گوش بگشای که بلبل به فغان می گوید

آفرین بر نفست باد که خوش بردی بوی

گفتی از حافظ ما بوی ریا می آید

“حافظ”

“The text is a poem from a well-known Persian poet Hafez”

# Abstract

Laser ablation inductively coupled plasma mass spectrometry (LA-ICP-MS) is a prestigious analytical method for the direct elemental analysis of solid samples. Over past few years, this technique has been developed and oriented toward biological and clinical research. Good lateral resolution combined with excellent sensitivity grow the interest in the application of imaging techniques to map the distribution of elements, both metals and non-metals in biological tissues. Disparate types of tissue have been bio-imaged such as liver, brain, kidney, nail, hair and eye and tumor tissues in recent years.

For imaging experiments of biological tissues, sample preparation and pretreatment is one of the indispensable step to be cared. Up to now, there are two methods offered in literature: (i) freezing of the sample in its native state or (ii) fixation of tissue in formalin followed by embedding in paraffin. Both approaches suffer from few disadvantages which have to be considered in imaging experiments using LA-ICP-MS. Snap frozen samples without fixation definitely provide the most accurate way for analysis of metal distributions in tissue samples. Nevertheless, conventional LA- ICP- MS instrumentation is operated at ambient temperature, thus thawing of the frozen samples is required prior to measurement. This step could introduce an additional error since trace element distributions might be altered. The technique of formalin fixation and paraffin embedding (FFPE) produces stable samples which could be stored easily, but preparation needs several treatment steps with different solvents which might alter the elemental distributions within the sample.

In this work an in-house-built Peltier cooled ablation stage is proposed, which allows analysis of element distributions in frozen tissue samples in combination with a commercial LA-ICP-MS system. With this setup thawing of the sample could be completely circumvented, thereby all problems associated with sample melting are avoided. Applicability of this approach has been demonstrated by the analysis of cryo- cut tissues with 10  $\mu\text{m}$  thickness at temperature of  $-10\text{ }^{\circ}\text{C}$ .

The results of this work underline that measurement of the cryo-cut tissue sample at frozen state does have some benefits compared to conventional measurement at due to less heat dissipation into adjacent structures during the laser ablation.

Furthermore, the correlations of obtained raw signal intensity from laser ablation and ions concentrations for all target elements yielded improved sensitivity in case of frozen state measurements. In the light of the described results for LA-ICP-MS of the tissue sections, qualitative and quantitative distribution images obtained from a rat and mouse brain at both cooled and non-cooled conditions. A detailed comparison of results indicates that the use of cooled ablation cell leads to enhancement of image quality, and as a result of better sensitivity it allows analysis with better spatial resolution to yield more accurate and trustworthy analytical data.

# Kurzfassung

LA-ICP-MS (engl. *Laser Ablation - Inductively Coupled Plasma – Mass Spectrometry*) ist eine herausragende Technik für die direkte Elementanalyse von Feststoffproben. In den letzten Jahren wurde diese Technik weiterentwickelt und auch auf biologische Proben der klinischen Forschung angewendet. Die gute laterale Auflösung und eine besonders niedrige Empfindlichkeit ergeben ein gesteigertes Interesse an der Möglichkeit die Elementverteilung von Metallen und Nichtmetallen in biologischen Gewebeschnitten abzubilden. Die Abbildung der Elementverteilung wird *image* genannt. Verschiedenste Arten von Geweben, wie zum Beispiel Leber, Hirn, Niere, Nägel, Haare, Augen und auch Tumorzellen wurden in den letzten Jahren untersucht.

Für imaging-Experimente ist die Probenherstellung und -vorbereitung von essentieller Wichtigkeit. Bisher werden zwei unterschiedliche Methoden zur Probenpräparation in der Literatur genannt: (i) Schockgefrieren des unbehandelten Gewebes oder (ii) Fixierung des Materials durch Formalin und Einbettung in Paraffin. Beide Vorgehen weisen gewisse Nachteile auf, welche bei der LA-ICP-MS Messung berücksichtigt werden müssen. Bei schockgefrorenen Proben ohne Fixierung mit organischen Lösemitteln wird die Verteilung der Elemente während der Präparierung weitestgehend unterdrückt. Mit gefrorenen Proben können demnach präzisere *images* erstellt werden. Allerdings wird die Laser Ablation üblicherweise bei Raumtemperatur durchgeführt. Durch das Auftauen der Probe kann die Elementverteilung beeinflusst werden. Durch die Fixierung mit Formalin und Einbettung in Paraffin (FFPE) werden stabile Proben erhalten, allerdings können die Präparierungsschritte mit unterschiedlichen Lösungsmitteln die Elementverteilung in der Probe verändern

In dieser Arbeit wird ein nicht kommerzieller Probentisch mit einem Peltier-Element vorgestellt, der es ermöglicht, gefrorene Proben mit Hilfe eines kommerziellen LA- ICP- MS Systems zu untersuchen. Durch diesen Aufbau kann das Auftauen der Probe und alle damit einhergehenden Probleme vermieden werden. Die Anwendbarkeit wurde mit cryo-cuts bei -10 °C und 10 µm Probendicke untersucht.

Die Ergebnisse dieser Arbeit zeigen, dass die Messung der Gewebeproben in gefrorenem Zustand einige Vorteile gegenüber der Messung bei Raumtemperatur

aufweist. Als größter Vorteil erweist sich der Erhalt der Probenintegrität durch einen geringeren Wärmetransfer in umliegende Bereiche. Außerdem werden bei der Messung in gefrorenem Zustand höhere Signalintensitäten erreicht, was zu einer verbesserten Empfindlichkeit führt. Angesichts der zuvor genannten Ergebnisse wurden qualitative und quantitative Elementverteilungsbilder von Ratten- und Mäusehirnen in gefrorenem Zustand und bei Raumtemperatur erstellt. Eine detaillierte Untersuchung der Ergebnisse weist darauf hin, dass die Verwendung eines gekühlten Probenisches die *image*-Qualität verbessert. Die gesteigerte Sensitivität ermöglicht eine höhere laterale Auflösung, wodurch präzisere und zuverlässigere Daten erhalten werden können.

# Table of contents

Abstract .....	3
Kurzfassung.....	5
Acknowledgment .....	9
1. Introduction.....	11
2. Theoretical aspects.....	15
2.1 ICP-MS.....	15
2.1.1 Sample introduction.....	15
2.1.2 Plasma source.....	16
2.1.3 Vacuum interface.....	17
2.1.4 Ion optics .....	18
2.1.5 Quadrupole mass analyzer.....	19
2.1.6 Ion detection .....	20
2.1.7 Signal quantification .....	22
2.2 Laser ablation (LA).....	22
2.3 Metals in biological tissues.....	25
2.4 Imaging experiments using LA-ICP-MS .....	28
2.5 Peltier system.....	32
3. Experimental.....	34
3.1 Instrumental .....	34
3.1.1 ICP-MS .....	34
3.1.2 Laser ablation (LA) .....	35
3.1.3 Peltier-cooled stage.....	36
3.1.4 Thermometer .....	37
3.2 Chemicals and reagents .....	38

3.3	Sample preparation.....	39
3.3.1	Preparation of matrix matched standards.....	39
3.3.2	Preparation of samples for LA-ICP-MS measurements.....	39
3.3.3	Sample pretreatment for ICP-MS measurements.....	40
4.	Results and discussion.....	42
4.1	Peltier characterization.....	42
4.2	Investigation of ablation behavior at various temperatures.....	50
4.2.1	Characterization of glass using cooled stage.....	50
4.2.2	Characterization of metal using cooled stage.....	56
4.2.3	Gelatin matrix-matched standards for LA-ICP-MS as a proxy for biological samples.....	59
4.2.4	Characterization of matrix-matched tissue standards.....	62
4.3	Imaging experiments on frozen biological tissue.....	69
5.	Conclusion.....	75
6.	Outlook.....	78
	Figures.....	80
	Tables.....	83
	Literature.....	84

# Acknowledgment

Foremost, I would like to express my sincere gratitude to my supervisor Professor Andreas Limbeck, head of the Division Instrumental Analytical Chemistry at TU Wien, not only for the great opportunity he gave me to do my master thesis in his group, but also for his countless guidance, patience and encouragement. The door to Professor Limbeck office was always open and he keenly steered me in the right direction with his immense knowledge whenever I encountered troubles and difficulties in my research. He also provided me an invaluable chance to be a speaker at the 6<sup>th</sup> International Symposium on Metallomics conference in Vienna, Austria, 2017.

I would like to pay my high regard to Professor Hans Lohninger for his speedy assistance whenever I needed in statistical problems.

I am grateful to all those with whom I have worked during this project. I must enumerate few colleagues by their names who supported me greatly and were always there for me to help. My deepest appreciation to Sara Hosseinzadegan who assisted me from the beginning till the end of this project, especially for chemical preparation.

My special thanks to Stefan Smetaczek not only for his wonderful support whenever I needed, but also for reviewing my thesis. I would like to express my appreciation to Christopher Herzig who reviewed my thesis, wrote the German version of the abstract and willingly assisted me in imaging experiments.

Also, thanks to Maximilian Bonta and Winfried Nischkauer for their useful and constructive ideas and support at the beginning of this work.

In addition, I have to appreciate Lukas Brunnbauer for his extensive help in the last part of the work.

I have to thank one of my friend, Babak Dabiri, from Institute of Electrodynamics, Microwave and Circuit Engineering, for his priceless help in the last year of my study.

I owe my today's achievements to my mother, my grandmother and uncle Reza, without them I was nothing. They not only assisted me financially, but also extended their support morally and emotionally to fill the void of my father's death for more than two decades.

Last but not least, I would like to pay my special thankfulness to my adorable partner, Iva Matousova, who persistently, encouragingly and eagerly supported and inspired me to accomplish my goal. She patiently experienced all ups and downs of my study without any complaints.

Shahin Amirkhalili

# 1. Introduction

ICP-MS is a highly accepted analytical method for trace multi-element analysis and high sample throughput. ICP-MS high dynamic range and the ability of ultra-trace analysis make it so demanding in many laboratories throughout the world [1]. The applications of ICP-MS are not only confined to analysis of environmental chemistry, archeology, geology, forensic and other field of science but also it is vastly extended to the number of biological applications such as proteomics, metalloprotein, immunochemistry and pharmaceutical industry [2-4]. The major analytical tools for the analysis of biological speciation including capillary electrophoresis (CE), size-exclusion chromatography (SEC) and liquid chromatography (LC) in order to separate the target biomolecules and their following identification by mass spectrometry techniques such as electrospray ionization (ESI) or matrix-assisted laser desorption ionization (MALDI) source. Another alternative elemental MS approach is coupling of ICP-MS with laser ablation which currently appraised as one of the most versatile MS tools for analysis of solids including the analysis of heteroatom-tagged proteins in biological and medical tissues and also for analysis of elemental distributions (imaging) in thin sections of biological tissues due to its high spatial resolution, relatively high sensitivity and dynamic range of up to twelve orders of magnitude [2, 5, 6].

The combination of gel electrophoresis (GE) and LA-ICP-MS to detect heteroatom of interest was first performed by Neilsen et al [7] using LA-ICP-MS for speciation of metal bound to proteins electrophoretically which focused on Co-binding serum proteins analysis. During years of dedicated studies in this field, it has been proved that GE-LA-ICP-MS (gel electrophoresis laser ablation inductively coupled plasma mass spectrometry) suffers some critical drawbacks which are linked to sample preparation and electrophoretic separation also to the laser-matter interaction. A critical point in metalloprotein speciation is the integrity of heteroatom-protein binding should be sustained during whole preparation and separation processes. In many analyses related to heteroatom-protein using PAGE-LA-ICP-MS, the analytes are metal or semimetal containing proteins such as selenoproteins and phosphoroproteins. In this case, there is a great affinity between heteroelements and primary structure of protein (covalent bonds), thus the bond does not break during electrophoretic separation process. However, in metal-protein binding, metal losses can occur during

electrophoretic separation specially applying denaturing polyacrylamide gels (PAGE). It is worth mentioning that there are some studies regarding metal losses in protein during GE which mostly propose the use of native PAGE instead of denaturing PAGE to diminish the losses [2, 3, 8].

As of today LA-ICP-MS has been increasingly applied for imaging analysis of broad types of samples, including hair and nail [9], teeth [10], plants [11] which are called hard tissues and can be analyzed without any special preparation and pretreatment. Moreover, investigations on elemental distributions of trace metals on human or animal tissue sections, including brain samples [12], kidney and heart [13], prostate and breast cancer [14], lymph nodes and tissue from human respiratory system [15, 16] have been elevated. The main target of the distributions of metals is to assess the interaction of metals originating from drug with tissues. These kinds of tissues are named soft tissues and need some preparation before analysis using LA-ICP-MS.

As mentioned, one of the most crucial parts to be noticed before analysis of soft tissue samples is sample preparation. Up to now, there are two common methods for obtaining rather reliable results for bio-imaging experiments: 1- formalin fixation and paraffin embedding (FFPE), 2- freezing of the sample in its fresh state. However, both approaches reported to have some unignorable drawbacks which affect the morphology and integrity of the tissue prior to the experiment. In first case, the sample preparation needs several steps which can cause some metal losses or change the elemental distributions. It is reported that some metals from tissues involved leaching in formalin solution. Therefore, the real concentration of them gets decreased. Moreover, analysis of alkaline metals and some transition metals proved to be inappropriate by means of FFPE [5, 17]. In the second case, a droplet of tissue gets frozen quickly in liquid nitrogen and sorted at -70 °C to avoid proteolytic reactions, which is a prominent fact impeding general applicability of this method of preparation. For LA-ICP-MS analysis thin cuts of 10 or 20  $\mu\text{m}$  are prepared using cryotome. Snap frozen samples without fixation definitely provides the most accurate way for analysis of metal distribution (especially in terms of ions diffusion) in tissue samples with the least sample preparation and it drastically reduces the sample contamination [5, 18]. Nonetheless, current LA-ICP-MS instrumentation is operated at room temperature, thus thawing of the samples is unavoidable prior to measurement. This step can introduce an additional error since trace element distribution might be altered. The

reason can be attributed to the displacement of ions by water diffusion during thawing and then evaporation. Furthermore, it is important to reduce possible thermal effects, which may affect the sample both directly in the irradiated surface and in adjacent areas [19]. Additionally, it is also reported that rapid heating of samples during ablation is found to be a striking limitation for micro-sampling of biological samples. Therefore, decreasing sample temperature during ablation to preserve the integrity of biological sample and inhibit unwanted effect is essential [20].

To overcome the obstacles, over the past few years, there have been some publications pertaining to evaluation of thermoelectric cooler device (Peltier cooled stage) specially designed for the analysis of cryogenic tissue sections. Notwithstanding the different engineering methods to design thermoelectric devices, they all have two features in common: 1- the ability to control the temperature of the target holder and heatsink, 2- to sustain the temperature unchanged for longer time especially in case of frozen ablation. This step needs to be cared by designer meticulously since obtaining high resolution image to be morphologically representative for biological tissue is achieved by ablation with smaller spot size (between 5 to 50  $\mu\text{m}$ ) and it acquires longer time to ablate the whole tissue sample.

To the author's knowledge, there are some well credited cooled ablation stages offered by different research groups. Below few of them will be mentioned:

Konz, et.al [5], proposed a cryogenic cell which was made from polyamide with a sample holder of a high purity copper plate. The plate was cooled by a circular internal refrigeration that consisted of eight Peltier elements, located exactly under the plate. A thermocouple was responsible for controlling the internal refrigeration system. A refrigerant fluid (polypropylene glycol) was pumped through the cooling coil, which was located beneath the eight Peltier elements for heat dissipation. The constant temperature at  $-25\text{ }^{\circ}\text{C}$  was guaranteed during the measurement for more than 17 hours.

Hamilton, et.al [21], demonstrated a custom made of copper block with two piping extensions to pump ice water as a coolant through the block with conductive grease to assure heat transfer from the Peltier to the heatsink. The samples were placed on a glass affixed to the Peltier element. Only one Peltier element positioned directly on the top of the heatsink.

M.Jarošová, et.al [22], offered an open ablation cell which could provide the initial temperature around -77 °C. It consisted of a plastic cup contained a mixture of dry ice and isopropanol. Samples were placed on a parafilm and the open ablation cell was firmly stuck to the parafilm to preserve the laser system from cooling bath vapors. The existence of dry ice in the mixture was watched over throughout the ablation to assure the stability of the temperature.

Due to complexity in design and to some extent high cost of mentioned cooled system, during this work, an in-house-Peltier cooled ablation cell with a simple engineered system for routine applications has been evaluated to figure out the laser ablation effect at different temperatures on NIST, metal and mostly focused on biological tissue. For this, the Peltier has been characterized in terms of the best working range and temperature stability over time. Prior to LA-ICP-MS analysis of biological tissue, matrix- matched standards from gelatin with a known amount of analytes have been utilized for signal quantification due to its similarity to biological tissue. Afterward, cryotome sections (10 µm) of two distinct types of biological tissues each spiked at four concentration levels have been prepared and ablated at both room temperature and frozen conditions. By proving that there have been some benefits using Peltier cooled stage, qualitative and quantitative elemental distribution imaging experiments have been applied.

## 2. Theoretical aspects

### 2.1 ICP-MS

The acceptance of inductively coupled plasma mass spectrometry (ICP-MS) has grown rapidly since the launch of the first commercial instrument in 1986 till now. Today, it is frequently used in many different research fields such as geology, archaeology, environmental and life sciences, forensic science and in wide range of industry (food, nuclear, semiconductor, chemical, medicine) [23].

In last few years, several manufactures have introduced automated, compact ICP-MS instruments that show a perfect performance in respect of sensitivity, detection limits and reliability. The detection limit is in the range of milligram per liter (mg/L) to microgram per liter ( $\mu\text{g/L}$ ) in trace analysis and microgram per liter ( $\mu\text{g/L}$ ) to nanogram per liter (ng/L) in ultra-trace analysis. In terms of sensitivity, it increases from 8 to 12 MHz/ppm over a wide mass range. Moreover, most ICP-MS instruments have a dynamic range of approximately eight orders of magnitude. Besides sensitivity and detection limit, ICP-MS is good at splitting off the isotopes of the same element. Samples for ICP-MS can be either solid or liquid, a technique for direct solid analysis is coupling ICP-MS with laser ablation (LA) which will be discussed later [1, 24].

#### 2.1.1 Sample introduction

The sample in ICP-MS, routinely in liquid form, is delivered into sample introduction system. This system consists of spray chamber and nebulizer. The nebulizer takes the liquid sample and converts it to very tiny droplets. The droplets (an aerosol) are created by pneumatic action of a flow of argon gas ( $\sim 1\text{L/min}$ ). The droplets should be split off by their size prior entering the plasma. The splitting process takes place in spray chamber where the larger droplets ( $>10\ \mu\text{m}$  diameter) will fall out by gravity and running out of the drain tube at the end of spray chamber. The smaller droplets ( $<10\ \mu\text{m}$  diameter) then pass between the outer wall and the central tube where they finally emerge from spray chamber and are transported into the sample injector of the plasma torch. Figure 2.1 demonstrates a more detailed view of the ICP-MS sample introduction area.

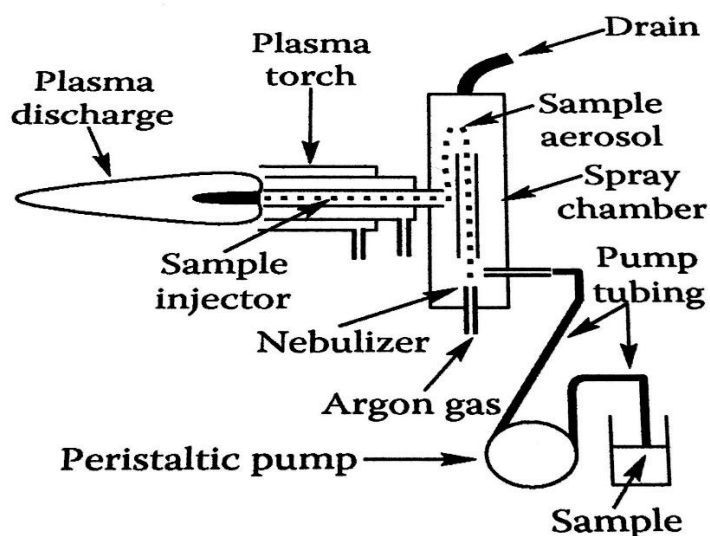


Figure 2.1: Detailed view of the ICP-MS [25]

Currently, there are more different sample introduction techniques such as laser ablation (LA, will be described later), ultrasonic nebulizers, electro thermal vaporization (ETV) and direct injection nebulizers. They are getting more and more important since ICP-MS users need higher and better performance and flexibility [1, 25].

### 2.1.2 Plasma source

Inductively coupled plasma (ICP) is an important excitation and ionization source used in optical emission spectroscopy (OES) as well as mass spectrometry (MS). Creation of inductively coupled plasma happens in the plasma torch which is usually made out of quartz, sapphire, alumina and it consists of three concentric tubes. Figure 2.2 demonstrates a more detailed view of the plasma torch and the RF coil. The sample aerosol with a carrier gas is introduced to the center of the plasma jet via the inner tube. Gas flow is around 1 L/min for the nebulizer gas to bring the sample in a form of aerosol. The middle and outer tubes are responsible for passing the gas (plasma gas) in order to form the plasma (gas flow ~12~17 L/min). Argon is usually used for gas supply. A radio frequency coil (RF, usually copper) is located nearly at the end of torch where the gases exit, oscillating the AC current makes the intense electromagnetic field around the coil. With the argon gas flowing through the torch, a high-voltage spark is applied to strip off the electron from their argon atoms. These electrons are accelerated in the magnetic field then collide with more argon atoms and therefore more electrons are stripped off. The process continues until the rate of released

electrons in collisions is balanced by the rate of recombining of electrons with argon ions. The amount of energy needed to produce argon ions is around 15.8 eV (first ionization potential) which is reported to be sufficient to ionize most of the elements. The temperature of the plasma is very high, depending on HF energy it varies from 6000 K to 10000 K. This makes evaporation, break down of molecules and finally ionizing the atoms. The ions later travel directly towards the interface of the mass spectrometer [24, 25].

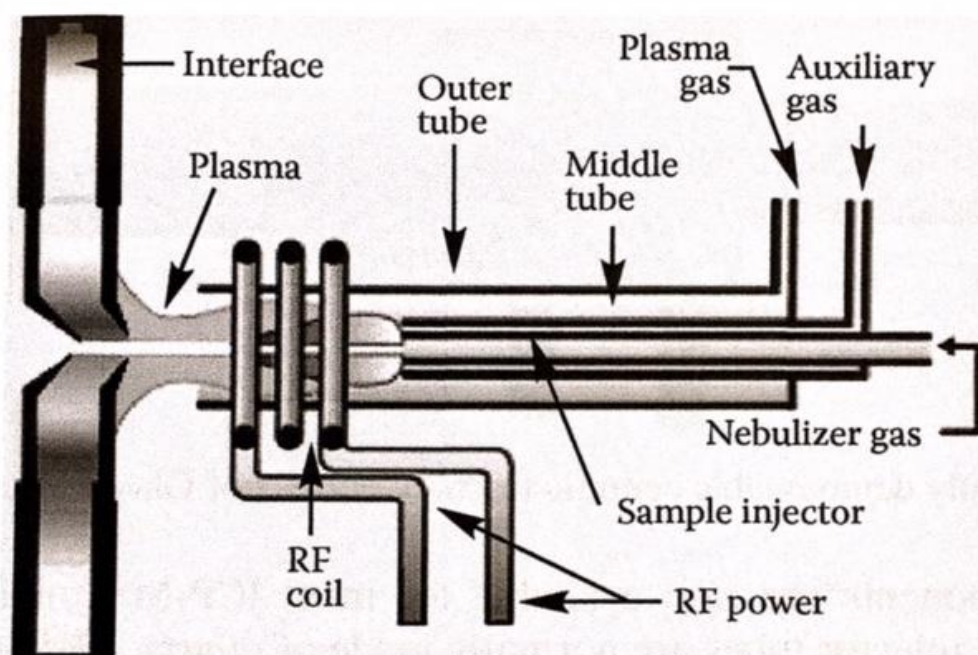


Figure 2.2: Detailed view of plasma torch and RF coil relative to ICP-MS interface [25]

### 2.1.3 Vacuum interface

The interface region is responsible for transporting ions continuously and efficiently. Since the ionization is performed at atmospheric pressure ( $\sim 760$  torr) and for mass analyzer a vacuum of  $3.8 \times 10^{-5}$  torr or less is required to avoid any collision of the ions with the background atmosphere, the pressure between the source and mass analyzer is needed to be reduced by eight orders of magnitude. This is the most challenging of ICP-MS instrumentations. Figure 2.3 shows the detailed view of the interface region. Interface is comprised of two or three metallic cones (depending on the design) with very tiny orifices, which are sustained at a vacuum of  $\sim 1$ -2 torr. After generating the ions in hot plasma, they pass through the first sampler cone, and immediately after is the second cone called skimmer which is sharper at its orifice (higher vacuum). Both

of these cones are usually made of nickel, copper or platinum, with the diameter of 1.0 mm for sampler and 0.4 to 0.8 for skimmer. There are also in some cases third cone called hyper skimmer, which reduces the vacuum and prevent the ion beam from dispersion. Finally the ions reach the mass spectrometer through the ion optics [25, 26].

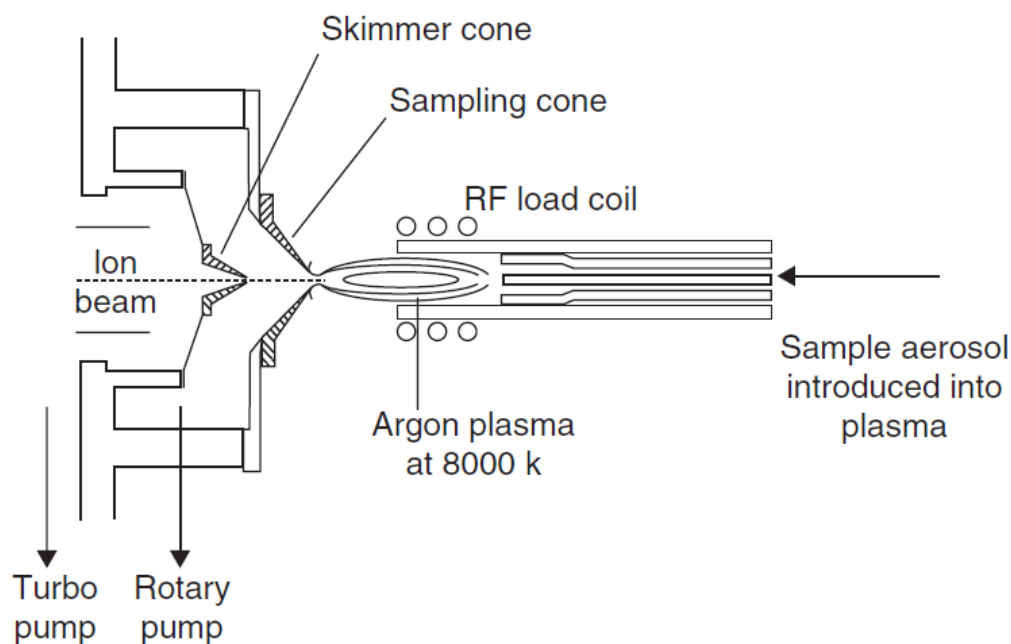


Figure 2.3: Typical vacuum interface used in ICP-MS instruments [26]

### 2.1.4 Ion optics

After transmission through the interface, the ions reach the ion optics which consist of one or more electrostatically circular lenses maintained at a vacuum of about  $10^{-3}$  with a turbomolecular pump. Focusing is obtained by the means of constant electric fields in order to deflect and accelerate the ions. The main role of ion optics is to focus the ions into the mass analyzer and to separate them from electrons, photons and neutral atoms. These species cause the signal to be instable and affect the system performance. There are different ways offered to decrease the probability of unwanted species entering the mass spectrometer such as putting the metal stop (disk) behind the skimmer (i) (which allows the ion beam move around the metal stop), set the mass analyzer off axis to the ion lens system in a way to avoid obstruction of the primary

aperture by secondary optical elements (ii) (which guides the positively charged ions steered with the lens components into the mass analyzer), using “hallow” ion mirror to deflect the ion beam by 90° (iii) (which lets the particles, photons to pass through while ions are deflected) and the current method which is quite common today is to swerve the ion beam coming from plasma by 90° (iv) (which changes and focuses the direction of the ion beam to mass spectrometer, while allowing the photons, neutral species and particulate matter to go straight through and be ejected ) [25, 27, 28].

### 2.1.5 Quadrupole mass analyzer

The mass analyzer arrays the ions merging from ion optics according to their mass to charge ratio ( $m/z$ ) and measures the plenitude of ions at each mass. The pressure of the analyzer part should be at a vacuum of roughly  $10^{-6}$  to work successfully. Nowadays the quadruple is the most common type of mass spectrometer used in ICP- MS. It is worth mentioning that low cost of build, high scan rate and easy to use close to ground potential are the benefits of quadrupole. However, few drawbacks are reported. There are other mass analyzers such as such TOF (Time-Of-Flight) or high resolution magnet sector field which offer different advantages, but are not discussed here.

The quadrupole is comprised of four parallel metal rods which are electrically connected (Figure 2.4). Direct current (DC) and alternating current (AC) voltages are applied on opposite pairs of the four rods. The applied voltages cause the merged ions from ion optics to oscillate. The ions from one  $m/z$  can pass through quadrupole and hit the detector safely, others with different  $m/z$  values are bounced off the transmission line and strike the rods. By changing the voltages different  $m/z$  ratios can be analyzed within a short time scale.

Resolving power ( $R=m/\Delta m$ ) and abundance sensitivity are two main criteria of a mass analyzer. For calculating the resolving power, the width of a peak at 10 % of its height and the mass of the peak is used. Most of quadrupole mass filters have the resolution practically between 0.5 to 1 amu. Although the higher resolution causes sharper peaks and more satisfying separations of two adjacent peaks, the downside is lower sensitivity. Abundance sensitivity is related to the tail of the peak shape of the mass which should be minimum in the neighboring tail. There are several factors which affect the abundance sensitivity. Motion and kinetic energy of the ions are two most

prominent factors which are subjected to the high potential of the plasma and the use of lenses to accelerate the ion beam might have a negative result on the instrument abundance sensitivity. It is shown that the peak of low mass boundary is not as stable as the high mass, thus the sensitivity is poorer at low mass. It can be stated that better abundance sensitivity is more preferred than high resolution [1, 28, 29].

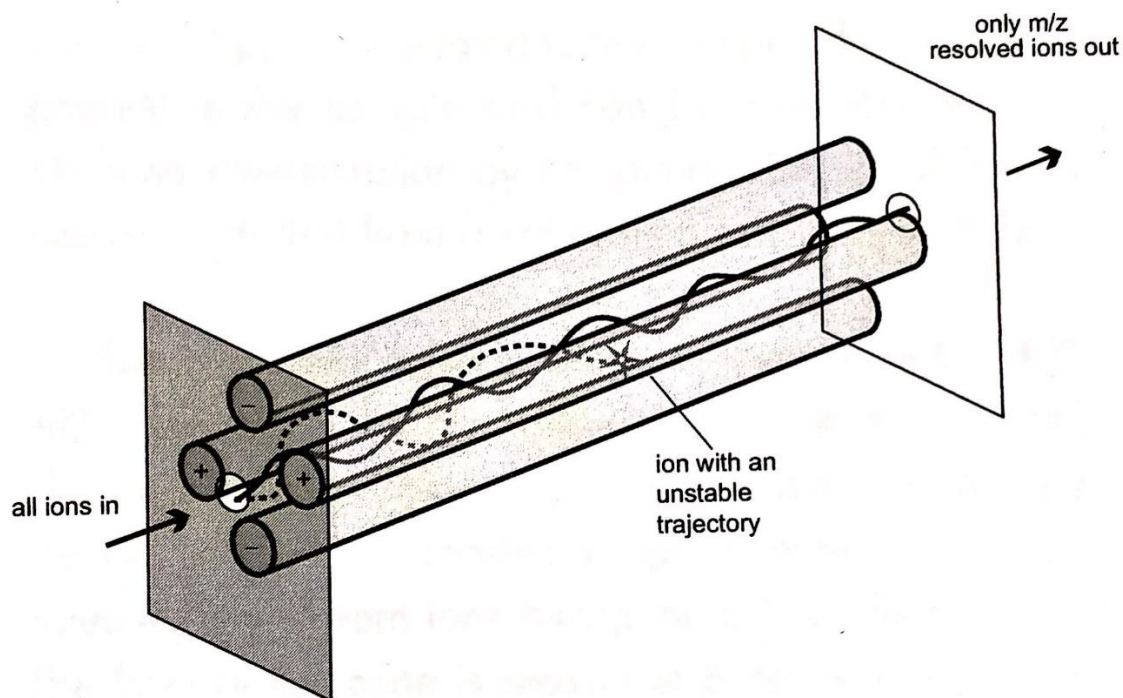


Figure 2.4: Schematic diagram of a quadrupole mass analyzer [28]

### 2.1.6 Ion detection

When the ions leave the mass analyzer, they hit the detector. There are different kinds of detectors offered since introduction of ICP-MS. The most well-known is electron multiplier for low ion count and Faraday cup collectors for high count rate. As shown in Figure 2.5, an electron multiplier consists of a curved glass coated with semiconductor material to generate the electrons from ions hitting the surface. The ions are pulled in by high voltage applied at the incoming ion gate. The collision of the ions with inner surface leads to the formation of one or secondary electrons. Due to potential gradient secondary electrons move toward the end of curved tube which results in formation of

more secondary electrons. This process continuous to create a cascade of million and million electrons [27].

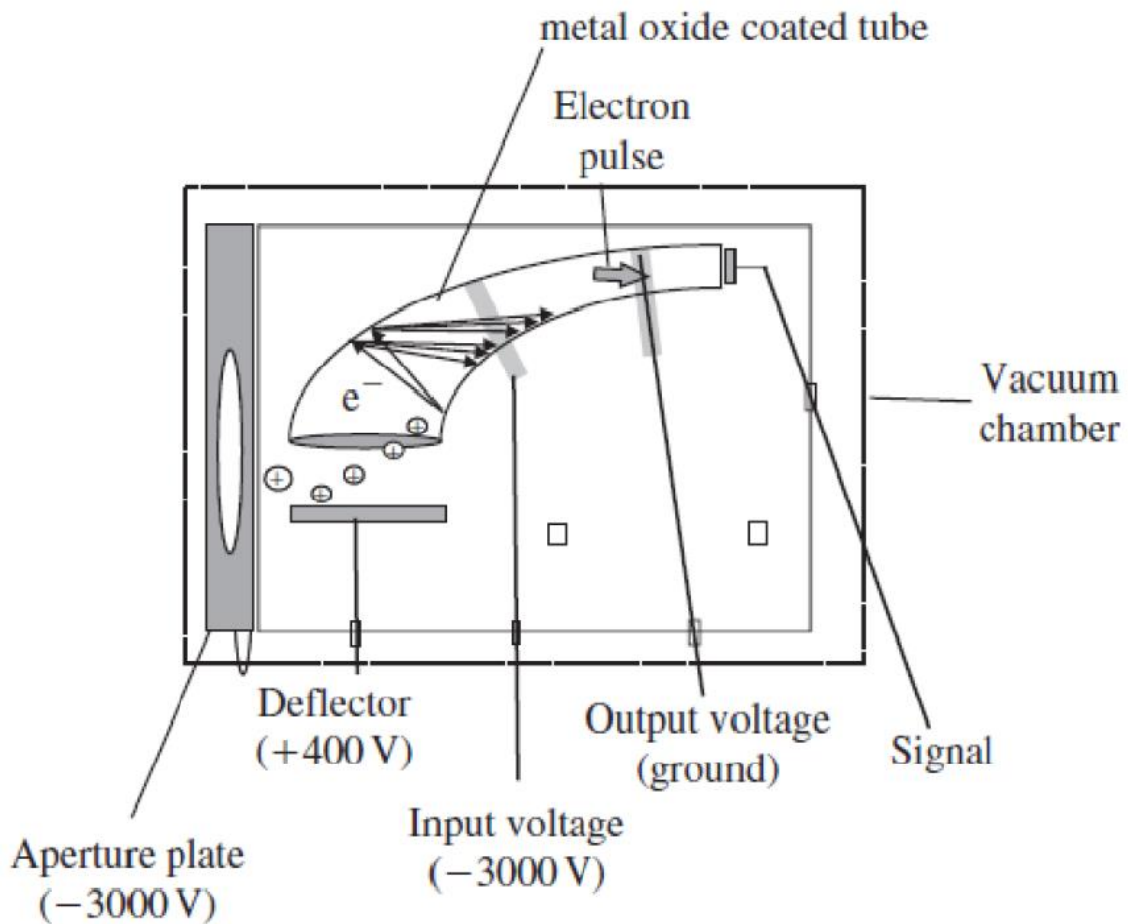


Figure 2.5: Schematic of a channel electron multiplier [27]

Faraday cup is used when ultra-trace detection limits are not requested. This method works very usefully for monitoring unknown samples that may have high concentrations of different elements. But the downside is, time-consuming of scan speed to measure the ion current, moreover it is not sensitive enough for quadrupole ICP-MS technology and therefore it is not appropriate for very low ion count rates. Nowadays, most of ICP-MS systems use detectors that are based on discrete dynode electron multiplier. They are also named active film multiplier which work in a similar way to the electron multiplier. They consist of 15-18 dynodes which are covered with metal oxide that has a great secondary electrons emission features [1, 27].

### 2.1.7 Signal quantification

Inductively coupled plasma mass spectrometry (ICP-MS) and inductively coupled plasma optical emission spectrometry (ICP-OES) are the simplest techniques to obtain analyte concentration in unknown samples. Since the signals obtained from ICP are not representative for whole elemental composition of the target samples, the instrument is calibrated by measuring the intensity for elements of interest in a number of known calibration standards that speak for a range of concentrations presumably to be faced in the unknown samples. This external standardization usually compensates for matrix components in the standards and the samples. It comes to difficulty either when matrix-matched and matrix-induced interferences are not so similar or measuring the solid samples by means of laser ablation. Unfortunately, due to the huge variety of investigated samples, there are no unique standards commercially available compatible for all samples. Therefore, additional standards have to be prepared in house with a striking resemblance to the matrix of components [1, 25]

## 2.2 Laser ablation (LA)

As mentioned before, introducing ICP-MS in 1980s followed wet chemical digestion methods, but high demand for analyzing solid materials led to development of laser ablation technique. Laser ablation inductively coupled plasma mass spectrometry (LA-ICP-MS) is extensively applied for direct elemental analysis with less effort for sample preparation. It also provides a vast analytical dynamic range from milligram per liter (mg/L) to nanogram per liter (ng/L).

In order to ablate, the solid sample material is positioned into the air tight sample chamber which is purged with an inert gas (usually Helium) before ablation. The sample is mounted on an XYZ translational stage allowing for spatially defined material ablation. When adequate energy in a form of a laser beam fires the sample, material from the surface is removed and vaporized, the created aerosol is then transferred to the plasma for atomization and ionization by means of argon as a gas carrier [1, 30]. A schematic diagram of a laser ablation system is illustrated in Figure 2.6.

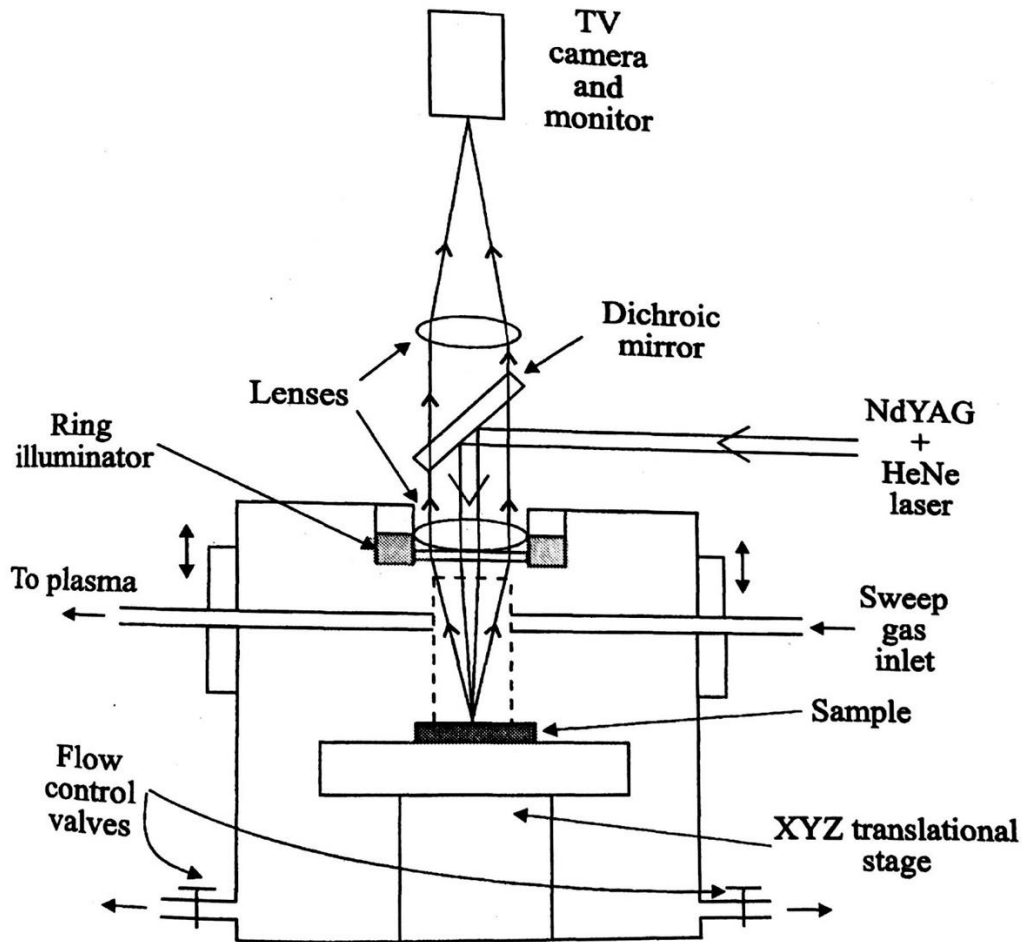


Figure 2.6: Schematic diagram of a laser ablation [1]

Different parameters influence the ablation process such as wavelength, pulse duration, mode of operation, focal length, energy of the laser and beam diameter. First development was, offering the ruby laser, operating at 694 nm which faced number of problems, including low repetition rate, large beam diameter and insufficient stability which made it inflexible for trace element analysis. Later on, neodymium doped yttrium aluminum garnet (Nd:YAG) designed, operating at 1064 nm in the infrared (IR). This also suffered lack of precision which made it unacceptable for many kinds of solid materials. The idea of shortening the wavelength by placing the optical component between two mirrors resulted in double (532 nm), quadruple (266 nm) and quintuple (213 nm) the frequency. The laser ablation system used in this work is equipped with a 213 nm Nd:YAG laser [27, 31].

Nd:YAG ( $\text{Nd:Y}_3\text{Al}_5\text{O}_{12}$ ) is Yttrium Aluminum Garnet doped with  $\text{Nd}^{3+}$  ions. These dopants are responsible for the laser effect, with the crystal field playing an essential

role for the appropriate energy levels. The solid-state lasers are characterized by high pulse powers and a relatively simple design (especially the active medium). Usually, a flash lamp is used as energy pump. In many cases, the resonator is Q-switched to shorten the relatively long flash pulse and increase performance. The main wavelength of the Nd-YAG (glass) laser is  $1.0641 \mu\text{m}$ . Due to the high performance of the Nd solid-state lasers, they are very well suited for frequency multiplication or frequency mixing. In most systems, at least a frequency doubling is present, which provides a frequency in the green wavelength range. However, frequency tripling is also typically about 350 nm. This wavelength can also be used as a starting point for further frequency multiplication down to 120 nm. The YAG laser is also often used as a pump laser of dye lasers. Medicine is another important field of its application. Today, Nd: YAG is the most demanding laser for LA-ICP-MS due to operation at 1 Hz to 20 Hz repetition rate without losing the power, easy to operate, reasonable price and allowing to make the spot much smaller regardless of sample material.

The advantages of shorter wavelength resulted in offering the UV gas lasers, such as XeCl (308 nm), ArF (193 nm) and KrF (248 nm) which are called excimer lasers. Although it offers better repetition rate up to 300 Hz and slightly better elemental fractionation effect, the excimer laser lacks good focusing to small spot size. Furthermore, the need to change the gas routinely makes it a bit more difficult to handle and it requires a more skilled operator to work with.

Pulse duration plays an important role in ablation. The shorter the laser duration, the sharper the created laser crater. The lasers discussed above are in range of nanosecond which typically have been used for LA-ICP-MS. Ablation process using femtosecond to picosecond lasers has certainly superior features and diminishes the effect of elemental fractionation with no heat effect [32].

Titanium-sapphire lasers (also known as Ti:  $\text{Al}_2\text{O}_3$  lasers) are an example for femtosecond lasers which emit red and near-infrared light in the range from 650 to 1100 nanometers, however, the price is a subject to be considered. Table 2.1 summarizes and compares the different laser properties using for ICP-MS.

Pulse duration	Wavelength	Repetition rate	Features of ablation
ns solid state (eg Nd:YAG)	213 nm 266 nm	1 Hz to 20 Hz	heat effect µm particles fractionation
ns excimer lasers	ArF (193 nm) KrF (248 nm) XeCl (308 nm)	1 Hz to 200 Hz	heat effect µm particles less fractionation
fs lasers (eg Ti:Sapphire)	650 nm to 1100 nm 250 nm to 330 nm in the UV range, 3 <sup>rd</sup> harmonic	1 Hz up to 10 kHz	no heat effects nm particles no fractionation

**Table 2.1: Summary of the different lasers properties using for ICP-MS**

## 2.3 Metals in biological tissues

The basic chemical components of living organisms from microbes to mammals are water, carbohydrate, lipids, proteins, nucleic acid and mineral salts, which all consist of six major elements (O, H, C, N, P, S), that in total make up around 96.5% of organism's weight. In human body, this increases to the number of eleven elements (O, C, H, N, Ca, Na, P, Cl, K, S, Mg), which is equal to 99% of human's mass. Figure 2.7 shows the abundance of elements in the nonliving world (the earth's crust) compared with the abundance in organisms [33, 34].

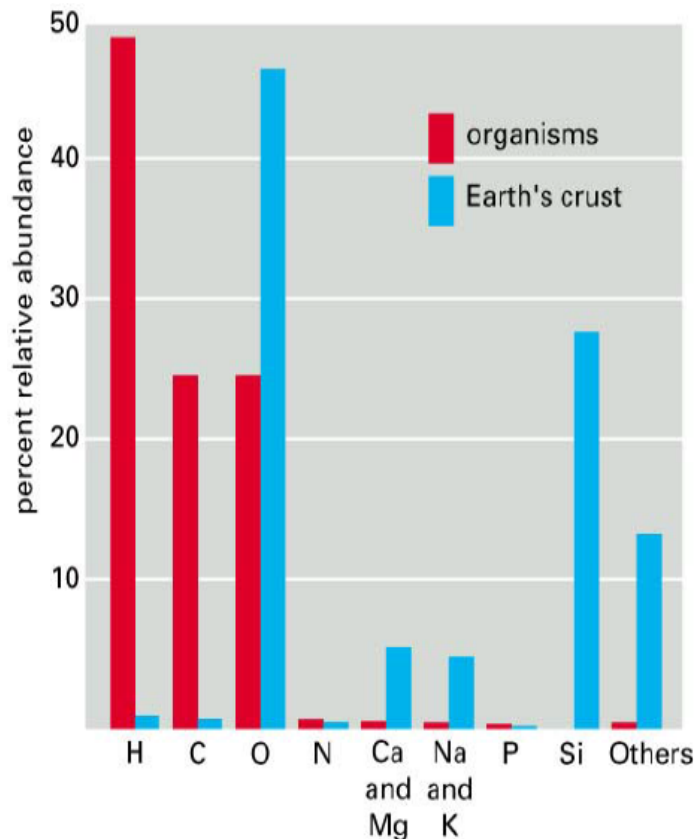


**Figure 2.7: Abundance of some elements in nonliving world compared with the abundance in organisms [33]**

The four metal elements (Na, K, Ca, Mg) are present in concentration of 100 to 1000 µg/g and the others are trace elements such as Fe, Ni, Cu, Mn and Zn which are found in lower concentration in organism tissues. The main roles and functions of these elements will be mentioned briefly.

Sodium (Na) and potassium (K) are both very significant for all kind of organisms. They belong to the alkali metal group. The functions of both are tightly connected to each other such as protein synthesis, regulation of cell volume and intracellular pH and activation of enzymes. But the most important function of Na-K pump is to create a gradient of both Na and K ions, the gradient is then used to transmit electrical signal that travels along nerves. Without this process, the nerves would not function. Moreover, the pump is used by kidney to maintain Na-K balance in the body. It also plays another role in sustaining blood pressure and control cardiac contraction. The pumping initiates with an enzyme called Na<sup>+</sup>/K<sup>+</sup>-ATPases, its function is to pump the Na out of the cell and pump the K inside the cell simultaneously [35].

Magnesium (Mg) and calcium (Ca) both belong to the alkaline earth metal group. Magnesium plays a vital role in human and all mammalian physiology. It is crucial for different organs such as bone and teeth. It acts as a co-factor of hundred enzymes including binding to ATP for kinase reactions, energy metabolism, RNA and DNA synthesis and sustenance of the electrical potential of nervous tissue and cell membranes. Magnesium deficiency is common among infant and less in adults and could lead to some malfunctions which will not be discussed here [36].

Calcium is the most abundant mineral in the body. It helps to keep the bones healthy and well structured. This transition metal also acts as a co-factor of many enzymes, for instance, clotting blood, releasing hormones and chemicals, contraction of muscles and neurotransmitter [37].

Certainly, iron (Fe) is one of the most abundant trace metal with rather the highest concentration around 100 µg/g. The body needs iron for oxygen transport proteins, in particular hemoglobin and myoglobin and for the formation of the heme group as electron acceptor or donor involved in electron transport chain. The excessive amount of iron can lead to tissue damage. On the other hand, iron deficiency is among the human common disease such as anemia and neurodegenerative diseases. The source of iron is animal meat [38].

Zinc (Zn) is the second highest found trace metal in human. Hundreds of proteins use zinc in their fundamental functions. The role of zinc in biology can range from cell growth, gene expression to protein metabolism and cell replication. Zinc deficiency can affect central nervous, epidermal, skeletal and reproductive systems. The major sources are red meat, sea food and beans [39].

Nickel (Ni), despite its low concentration in human body, plays an indispensable role in human health. It helps hormonal activity and lipid metabolism. This metal has its useful effect on digestive and respiratory systems. The over use of nickel has serious side effects such as genotoxicity, immunotoxicity and carcinogenicity. The deficiency can diminish iron resorption and leads to anemia. Furthermore, it can cause the improper function of different dehydrogenases and transaminases, and the most severe depletion leads to disorder of pancreatic enzyme (amylase), and finally affects carbohydrate metabolism [40, 41].

Manganese (Mn) is present in a tiny amount in the body. It plays an essential role in hydrolytic reactions and many biological processes. As a part of antioxidant enzyme superoxide dismutase (SOD), it assists to fight free radicals which can harm cell membranes and DNA. High and low level of manganese is mostly associated with neurological disorders like Parkinson's disease. Other problems are also reported. Manganese can be found in seeds, nuts and whole grains abundantly [42].

Copper (Cu) is another indispensable trace element in human health. It acts as co-factor of diverse enzymes. Copper is also able to behave as both an antioxidant and a pro-oxidant to neutralize the free radicals which can damage the cell wall and merge with genetic material. Copper's role in transformation of melanin for skin pigmentation, production of hemoglobin, aiding thyroid gland proper function and repairing connective tissues by creating cross-link in collagen and elastin. The excess amount of copper can lead to neurological disorders, cirrhosis of liver and hereditary diseases. Copper deficiency is linked with osteoporosis, cardiovascular disease, colon cancer, nervous system and immune system. Sea food, meat organ (liver) and whole grains are the main source of copper [43].

The discussed metals called endogenous which play significant roles in organisms. However, there are some other metals which can be absorbed by organisms from environment such as Cd, Hg and Pb. These are called exogenous and long-term exposure could result in serious illnesses even fatal.

Another group of metals employed in medical industry for diagnosis and treatment. Gadolinium (Gd) and Technetium (Tc) are applied as contrast substances for magnetic resonance imaging (MRI). Platinum (Pt) as a noble metal has been used for decades in treatment of benign cancerous tumors. There have been some repercussions reported including suppression of DNA transcription and neuro-hepatotoxicity [44].

## **2.4 Imaging experiments using LA-ICP-MS**

LA-ICP-MS (Laser ablation inductively coupled plasma mass spectrometry) is one of well-known application in terms of chemical imaging. The main advantages of this technique are high sensitivity, good potential for quantification with spatial resolution

ranging between 2 and 500  $\mu\text{m}$  and low detection limit. Beside conventional methods of imaging such as computed tomography scan (CT), magnetic resonance imaging (MRI) and positron emission tomography (PET) which represent morphology of organisms, LA-ICP-MS imaging has been widely used in analysis of biological samples to depict elemental distributions within the samples surface. In LA-ICP-MS, material is ablated, evaporated, transported to ICP, atomized in inductively coupled plasma and separated in mass spectrometer based on their mass-to-charge ratios and eventually detected by a detector [45].

Optimization of methodology for preparation of samples is crucial. Tissues must be in a form of thin slice ranging from 1 to 20  $\mu\text{m}$  in order to be ablated completely. There are various methods offered for preparation. The most common is formalin fixation and paraffin embedding (FFPE) in which soluble components are removed or may be distributed over the whole sample due to diffusion. After being embedded in paraffin the samples are cut using a microtome. The paraffin can be removed from the cut sections and be kept for longer time at ambient temperature. Other procedures for cutting do not involve such a long process for sample pretreatment. Another method which is less time-consuming involves cutting the original tissue while it is frozen [19]. Prior to analysis, tissue cuts should be stuck on glass slid or silicon wafer to be handled easily.

In principle two analysis modes for the acquisition of image data are available for LA- ICP-MS experiments. Spot-scanning and line-scanning mode are used. During a spot scan with single-point ablation, the laser stays on a defined position generating sample material from which the signal is acquired by the MS for a certain amount of time before it moves to another position. The signals can be directly linked to a specific ablation site, as for each time-resolved signal a distinct spot on the sample with clearly defined x- and y-coordinates exists. Time-resolved scanned ion intensities are produced and saved by software. During line scans, the laser is moved across the sample in a continuous manner at a given speed, with many overlapping spots being created. The spatial difference between these spots is determined by the scan speed in combination with the repetition rate of the laser. Thus, line scan is more preferred for mapping of analytes and creating images [45]. Figure 2.8 illustrates two scan types. Image quality is highly hinged upon laser parameters. Washout time of the aerosol from the sample chamber can directly affect the lateral resolution and results in indistinct image. Therefore, it is vital that laser mode, laser energy, frequency, spot

diameter, scan speed, dwell time, gas flow rate, instrument setting time (of ICP-MS) and the resulting acquisition time are set to accomplish an image with the most plausible spatial resolution. Spot size and scan speed are the most crucial parameters to be noticed. The beam diameter determines the obtainable spatial resolution of the resulting distribution images. The smaller the beam diameter the better is the resolution. However, with decreasing the beam diameter less material will be ablated, and less amount of analyte can be detected. The spot also assigns the time of measurement. As the whole sample has to be rastered, laser spot size and scan speed determine the measurement time. Commonly applied laser diameters for imaging experiments on biological samples are between 10 and 250  $\mu\text{m}$  depending on the sample to be analyzed and the desired spatial resolution. It can be decreased to below 10  $\mu\text{m}$  depending on analyte concentration and sensitivity of the detectors. Optimization of scan speed varies from quadrupole ICP-MS system to quadrupole ICP-MS system. But it is usually dependent on relationship between laser scan speed, laser spot diameter and the total scan cycle of the quadrupole mass analyzer. It is stated that up to five times higher than spot diameter can be applicable. However, typical scan speeds are equal to the value of the laser diameter to avoid a distortion of the resulting image. Scan speeds being smaller than the laser diameters have shown to yield no improvement in image quality but only extend the acquisition times. Repetition rate is one of the limiting factor for scan speed to obtain acceptable resolution. It is usually chosen between 10 and 20 Hz. A reasonable amount of laser energy results in better ablation of material. The more laser energy, the more material will be ablated. Helium is preferred as a carries gas and its flow has to be set in a way that transport efficiency of the material ablated to the ICP-MS is optimal. The final step is intensities of ions at the detector saved per time in a data file. This data is to be further processed based on time-resolved data that are matched to specific x-y coordinates of the sample to create the desired spatially resolved images of elemental concentrations.

Using LA-ICP-MS to quantify the amount of analyte in the sample is always affected by instrumental drifts and unwanted matrix dependent ablation differences. The reason can be associated with the washout time, as this might lead to a delay in the signal detected by the collectors and thus potential sample mixing within the ablation chamber or resampling of deposited material stemming from prior ablations leading to mixed signals for one ablated site hampering the potential spatial resolution achievable.

Furthermore, the vacuum conditions may change slightly during measurement time or the gas flows can vary within a small range and in consequence, the plasma temperature can be altered. To minimize these effects, applying matrix-matched standards (with a matrix as resemblance as possible to the sample) is indispensable. There are several approaches for internal standards. The easiest way is to use the analytes appearing in the sample with homogenous distribution. An example thereof is carbon. However, using carbon as internal standard has been in debate for years. Concerns about carbon will be discussed in chapter 4 in detail. Over the last few years, new developments have been achieved regarding internal standards such as the use of polymeric layers, gelatin gels as multi-element calibration standards and sputtered thin layer of gold. [19, 45-47].

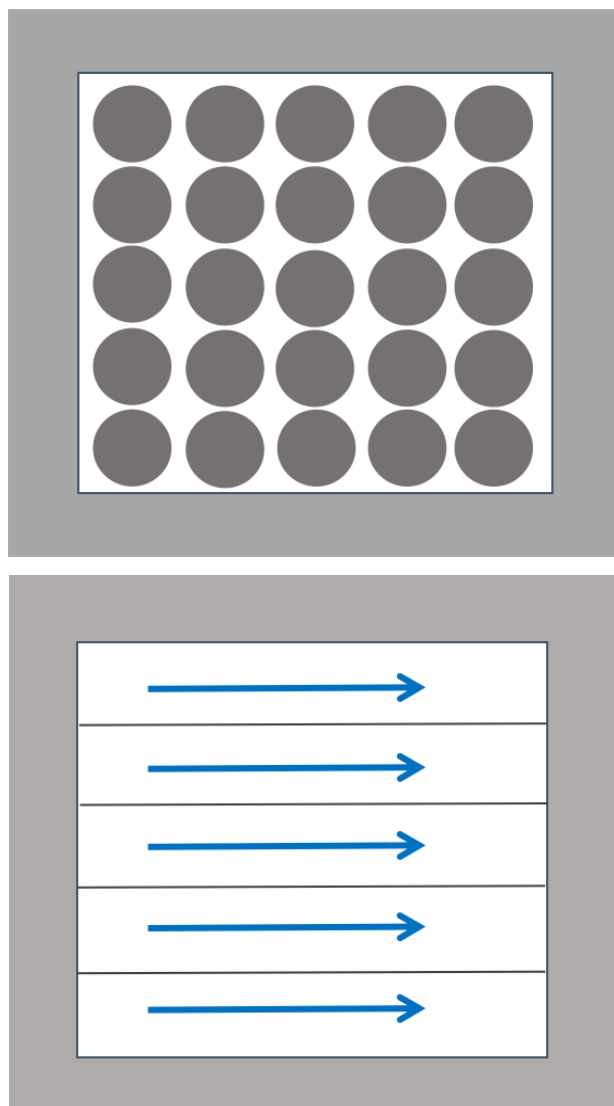


Figure 2.8: Scan types available for LA-ICP-MS

## 2.5 Peltier system

Basically, temperature control can be achieved by heat exchange with fluids or electrical heaters. The existence of heating or cooling at a pair of two semiconductors is called Peltier effect. This is named after French physicist Jean Charles Athanase Peltier. When a direct current (DC) is applied at the junctions between two semiconductors, the flow of heat from one side to another side causes a temperature difference across the two side. It is expressed by:

$$Q = \alpha TI \quad \text{Equation [1]}$$

Where  $Q$  is the total heat generated,  $\alpha$  is the Seebeck coefficient,  $T$  is the temperature and  $I$  is the current. In fact, the total amount of  $Q$  comes from the subtraction of total heat flow removed at cold side ( $Q_h$ ) and pumped to the hot side ( $Q_c$ ). Thus, the final heat power is equal to:

$$Q_h - Q_c = \alpha(T_h - T_c)I + I^2R \quad \text{Equation [2]}$$

Where  $R$  is the electrical resistance which is related to Joule's heating effect,  $T_h$  and  $T_c$  are the temperatures at hot and cold side of Peltier cell, respectively. In cooling mechanism, the heat flow to the hot side should be dissipated by the heatsink. If it does not occur well and heatsink cannot absorb more heat, the hot side temperature will go up and the cooling performance will go down. This is understandable from Equation [2] at an adjusted electrical power. The temperature difference  $\Delta T = T_h - T_c$  is constant, thus by increasing  $T_h$ ,  $T_c$  will clearly increase. The four parameters including  $\Delta T_{max}$ ,  $Q_{max}$ ,  $V_{max}$  and  $I_{max}$  mainly characterize the behavior of a Peltier cell. Where  $Q_{max}$  is the maximum amount of heat at cold side at  $I = I_{max}$  and  $\Delta T = 0$ , whereas the maximum  $\Delta T$  is achieved when  $Q = 0$ . The maximum  $\Delta T$  is obtained at  $V_{max}$  and  $I_{max}$ , the maximum current is the input current and maximum voltage is the DC voltage for maximum performance. To conclude, the Peltier heat flow is proportional to the electric current and the heat generated by Joule's effect is proportional to the square of the current [48, 49].

It is worth noticing that there are some more factors influencing the design of a Peltier cell including the size of thermocouple, the electrical current, the junction temperature and the properties of the semiconductors, which all should be cared by the engineer in order to maximize the coefficient of performance (COP) and minimize the junction temperature [50, 51].

# 3. Experimental

## 3.1 Instrumental

### 3.1.1 ICP-MS

During this work an iCAP Qc quadrupole ICP-MS (Thermo Fisher Scientific, Germany) was used. The system splits off ions from photons and neutral atoms employing a 90° deflection lens. This improves the sensitivity especially for low mass ions. Data acquisition was conducted using Qtegra software provided with the instrument. A picture of the device is shown in Figure 3.1.



**Figure 3.1: ThermoFisher Scientific iCAP Q ICP-MS instrumentation used for the performed experiments**

Solution nebulization ICP-MS measurements of digested samples were carried out using a Peltier cooled spray chamber equipped with a concentric quartz glass nebulizer for sample introduction. Samples were introduced using an ESI SC-2DXS auto sampler (Elemental Scientific, Inc., Omaha, NE). Instrument parameters were optimized on a daily basis for maximum  $^{115}\text{In}$  signal and minimum  $^{140}\text{Ce}^{16}\text{O}/^{140}\text{Ce}$  ratio using a tuning solution provided with the instrument. Measurements were carried out employing the standard measurement parameters suggested by the manufacturer. By coupling with a laser ablation system (section 3.1.2), direct solid sample introduction was performed.

Before every experiment the measurement parameters concerning the MS instrumentation were optimized using NIST 612 (National Institute of Standards and Technologies, US) for maximum  $^{115}\text{In}$  signal. Instrumental parameters used for all ICP- MS measurements are given in Table 3.1.

ICP-MS instrumentation	Thermo iCAPQ
auxiliary gas flow	0.8 [L/min]
cool gas flow	15 [L/min]
dwel time per isotope	0.01 [s]
RF power	1550 [W]
cone	Ni
measured isotopes	$^7\text{Li}$ , $^{59}\text{Co}$ , $^{115}\text{In}$ , $^{140}\text{Ce}$ , $^{232}\text{Th}$ , $^{27}\text{Al}$ , $^{88}\text{Sr}$ , $^{137}\text{Ba}$ , $^{208}\text{Pb}$ , $^{238}\text{U}$ , $^{12}\text{C}$ , $^{63}\text{Cu}$ , $^{58}\text{Ni}$ , $^{64}\text{Zn}$ , $^{55}\text{Mn}$ , $^{56}\text{Fe}$ ,

Table 3.1: Parameters applied for ICP-MS instrumentation

### 3.1.2 Laser ablation (LA)

For LA experiments, a NWR213 laser ablation system (ESI, USA) equipped with a frequency quintupled 213 nm Nd:YAG was used. A picture of the laser is shown in Figure 3.2.



Figure 3.2: New Wave 213 laser ablation device employed for the performed experiments

Coupling with ICP-MS instrumentation was achieved using PTFE tubing (inner diameter 2 mm). For cell washout, Helium was used as carrier gas which was mixed with Argon upon entering the plasma. Depending on the experiment, different ablation methods and laser parameters were used (detail will be discussed later). A summary of the optimized laser ablation parameters used for the different experiments is shown in Table 3.2.

Laser ablation	NIST measurement	Metal measurement	Biological and gelatin measurement	Imaging measurement
average influence	3.31 [J/cm <sup>2</sup> ]	3.31 [J/cm <sup>2</sup> ]	3.64 [J/cm <sup>2</sup> ]	9.75 [J/cm <sup>2</sup> ]
laser diameter	80 [μm]	80 [μm]	80 [μm]	40 [μm]
scan speed	5 [μm/s]	10 [μm/s]	-----	120 [μm/s]
dwel time in case of spot scan	10 [s]	10 [s]	5 [ s]	-----
repetition rate	20 [Hz]	20 [Hz]	10 [Hz]	10 [Hz]
carrier gas flow (He)	0.75 [L/min]	0.75 [L/min]	1 [L/min]	1 [L/min]
make-up gas flow (Ar)	0.8 [L/min]	0.8 [L/min]	0.8 [L/min]	0.8 [L/min]
warm up time	10 [s]	10 [s]	10 [s]	5 [s]

Table 3.2: Parameters applied for laser New Wave 213

### 3.1.3 Peltier-cooled stage

The use of temperature-controlled devices is commonly applied in science to understand the precise effect of temperature in various applications. A Peltier used in this work was built in house (Vienna University of Technology) consists of Substrate holder (target holder), two semiconductor cooling components, two thermistors, two carbon foils to transfer heat to sample surface and to body with a wide range from - 40 °C to 150 °C (QUICK-OHM, Wuppertal, Germany) and the body which is called heatsink made of bulky aluminum. The Peltier gets connected to a power supply which provides a DC current. The power supply allows the user to set the favorite temperature, also to monitor the temperature of the surface of substrate holder and the heatsink. Figure 3.3 illustrates a picture of the Peltier and its components. Characterization and the detailed function of the Peltier-cooled stage will be explained in chapter 4.

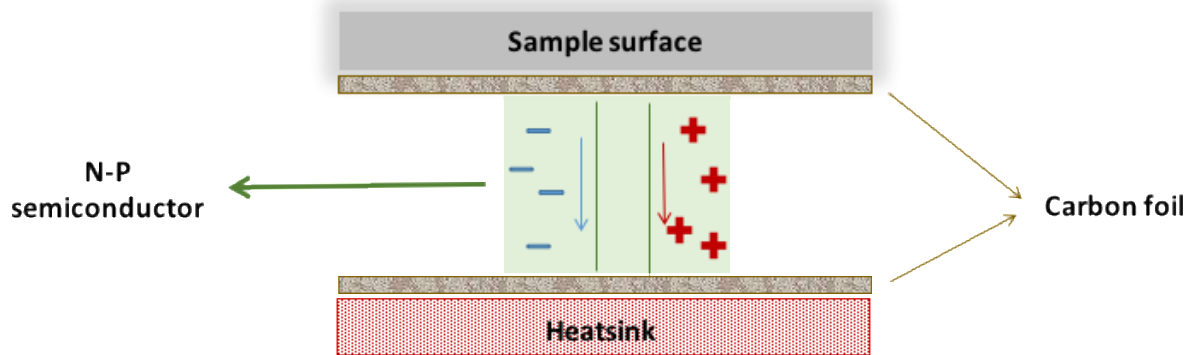


Figure 3.3: Picture of Peltier and its components

### 3.1.4 Thermometer

A thermometer (FLUKE 53/54 SERIES 2, USA) was used in this work in order to measure the temperature of the surface of NIST and silicon wafer (will be discussed in chapter 4). The Fluke 53/54 series 2, 60 HZ Dual-Input Digital Thermometer with Data Logging offers fast response and laboratory accuracy ( $0.05\% + 0.3\text{ }^{\circ}\text{C}$ ) in a rugged, handheld test tool. A wire which is a temperature sensor is located on the desired area then the temperature is shown on the thermometer. Figure 3.4 shows the thermometer (Institute of Electrodynamics, Microwave and Circuit Engineering of Vienna University Technology). To assure the correct and accurate measurement, the desired area was

covered by thermal grease (KERAFOL, Keramische Folien GmbH, Germany). It prevented air from penetrating into the measured area and maximize heat transfer.



Figure 3.4: Fluke thermometer

## 3.2 Chemicals and reagents

Throughout the experiments high purity water (resistivity 18.2 M $\Omega$  cm) prepared with an Easypure purification system (Thermo, USA) was used. For preparation of stock solution of target analytes their salts including copper (II) chloride dihydrate p.a. (Merck), zinc chloride p.a. (Fluka), Magnesium chloride hexahydrate 99% (Aldrich), sodium chloride p.a. (Merck), potassium chloride p.a. (Merck), nickel (II) chloride hexahydrate (Sigma Aldrich), calcium chloride p.a. (Merck), manganese (II) chloride tetrahydrate (Sigma Aldrich) and, iron (II) chloride tetrahydrate (Sigma Aldrich) were used. For standard calibration, gelatin powder p.a. (Neuberts Enkel, Vienna) was used. For surface modification of silicon wafers, (3-Aminopropyl) triethoxysilane 99% (Aldrich) and acetone 99.8% (Acros Organics) were used. For digestion of frozen tissue droplets Nitric acid 65% (Merck) and hydrogen peroxide 30% (Merck) were consumed. For normalization of the signals single element ICP standard In (Merck, 1000 mg /L) was applied with required dilution. The tissue digestion procedure was carried out in 15 mL conical polypropylene centrifugation tubes with a V-bottom (VWR, Germany).

### 3.3 Sample preparation

#### 3.3.1 Preparation of matrix matched standards

Tissue samples for matrix matched calibration were prepared according to the method described by the literature Hare et al [52]. Porcine liver and kidney which were purchased from a local market were mixed and homogenized using a hand-held blender (Braun, Type 4169, Mexico) then left in the ultrasonic bath for 30 minutes to have more smooth and homogenized material. A stock solution of target analytes including 1.0 g/L Mn, Ni and Cu, 2.0 g/L Zn, 4.0 g/L Ca and Fe and 10 g/L Na, K and Mg was made from their chloride salts in 1% HNO<sub>3</sub>. A set of samples consisting of 5 g homogenized tissue spiked with 0.5 mL of 1:5 and 1:2 diluted and undiluted stock solution was prepared. To one tissue sample 0.5 mL of 1% HNO<sub>3</sub> was added instead of the stock and it was marked non-spiked and used as blank. Indium with final concentration of 75 mg/L was added to all samples as internal standard. The tissues were further homogenized using vortex and ultrasonic bath. Frozen tissue droplets for laser ablation analysis were prepared by dropping 100-300 mg of the tissue samples into liquid nitrogen and stored at -70 °C to avoid any sample degradation. To determine the accurate concentration, a representative amount of the frozen tissue droplets were digested with HNO<sub>3</sub> and H<sub>2</sub>O<sub>2</sub>, measured with liquid ICP-MS.

The same strategy was applied to prepare gelatin matrix matched calibration. Five concentration levels of metals in gelatin were prepared. About 3 g of gelatin powder was weighed in polymer tubes, 15 mL of purified water, 2 mL of the stock solution of analytes and 100 µL of 1000 mg/L indium nitrate solution in 1% nitric acid as internal standard were added. The samples were homogenized by using vortex, ultrasonic bath and heated up to about 60 °C. It took about half an hour for the samples to become clear (homogenous solutions). They were poured in Petri-dishes and kept in the fridge at 4 °C overnight to become solid. Standard solutions preparation for the gelatin samples was the same as biological tissue.

#### 3.3.2 Preparation of samples for LA-ICP-MS measurements

The frozen tissue droplets of the tissue samples as well as the frozen gelatin samples were cut using a cryostat (Thermo Fisher Scientific, Germany) with 10 µm thickness at

-20 °C. The sections were collected on 10×10 mm with the thickness of 200 nm Silicon Wafers (Infineon Technology Austria AG). For surface modification of the wafers a mixture of 1 mL (3-Aminopropyl) triethoxysilane, 50 mL acetone and 10 µL water was prepared. Silicon wafers were left in the solution for 10 minutes then the slides were transferred into high purity water and were left for 10 minutes. Finally, they were dried to be used as tissue sample plates. To assure that sections stuck on silicon were still frozen, they were kept inside a cool box full of dry ice (IGA-Gas Company, Vienna, Austria) immediately after cutting and later stored at -70 °C. Figure 3.5 shows a picture of cryostat used in this work.



**Figure 3.5: ThermoFisher Cryostat**

### 3.3.3 Sample pretreatment for ICP-MS measurements

For determination of the metal concentrations in the prepared tissues accurately, the frozen tissue droplets from the matrix-matched standards were weighed (approx. 200 mg each) and dissolve completely in a mixture of 2 mL 65% HNO<sub>3</sub> and 0.5 mL 30% H<sub>2</sub>O<sub>2</sub> in loosely capped tubes at 80 °C in an oven for 3h. The obtained solutions were diluted to 10 mL with high purity water (resistivity 18.2 MΩ cm) ensuing clear solutions and measured as liquid using ICP-MS.

In case of gelatin digestion, about 100 mg of the samples was dissolved in in 1 mL of a 4:1 (v/v) conc. HNO<sub>3</sub> and 30% H<sub>2</sub>O<sub>2</sub>. The samples were heated up for half an hour to 40 °C to get dissolved completely. 8 mL of purified water was added and an aliquot of 250 µL was taken and mixed with 250 µL of conc. HCl, 8.5 mL of 1% HNO<sub>3</sub> and 10 µL of 100 ppm europium solution as internal standard. The concentration determination was performed in 4 replicates for each concentration level to decrease the errors occurred during sample preparation and furthermore to obtain a satisfactory reproducibility. This preparation method was performed as described by Hare et al [52].

## 4. Results and discussion

### 4.1 Peltier characterization

An in-house-built Peltier stage (Vienna University of Technology) consists of target holder (25×45 mm), two semiconductors N type and P type (cooling component, Peltier-element), two thermistors, two thermal conductors (carbon foil with wide temperature range, QUICK-OHM, Wuppertal, Germany) to transfer heat to the sample surface and the body which is called heatsink is made of bulky aluminum, was used. In accordance with the laws of thermodynamics, heat from the (warmer) area being cooled will pass from the cold side to the hot side. The target holder is for placing and cooling the sample. The semiconductors from one side cool the target holder and from another side transfer the dissipated heat via carbon foil to the heatsink, if this does not perform properly, the hot side temperature will ascend, and the cooling performance will descend. A perfect heat sink would be capable of absorbing an unlimited quantity of heat without exhibiting any increase in temperature. Since this is not possible in practice, the designer must select a heat sink that will have an acceptable temperature rise while handling the total heat flow from the TE device(s). Two thermistors (temperature-dependent resistors) connected to two thin wires are placed at the side of the target holder and the bulky aluminum, allowing the precise control over temperature of the substrate holder and heatsink. Direct current (DC) is provided by a power supply which allows the user to select and control the temperature. The user is able to set a desired temperature and observes the actual temperature on the surface of target holder and the temperature of the bulky aluminum, respectively. The capacity of the Peltier is between [-20 °C to +20 °C].

Since this project is aimed at ablating and analyzing various materials such as glass, metal and specially, biological tissues at different temperatures, a precise and proper characterization of the cooled ablation stage is necessary. Moreover, long term stability of temperature for imaging of biological tissues should be guaranteed during ablation. To achieve this, two set of experiments were carried out. In first experiment, the cell behavior without ablation process and outside the laser chamber was investigated. To do this, the Peltier-cooled stage was connected to its power supply at ambient temperature. Six different temperatures (+20 °C, 0 °C, -5 °C, -10 °C, -15 °C and -20 °C)

were tested separately at different time, running all measurements were not possible sequentially due to heating up the Peltier cell, hence the Peltier cell had to get cooled down again to reach the ambient temperature. Three significant factors including set temperature, actual temperature of the surface of sample holder and body temperature (heatsink) were recorded every two minutes in a span of 30 minutes. Figures 4. (1-6) show the relation between three mentioned factors for each temperature.

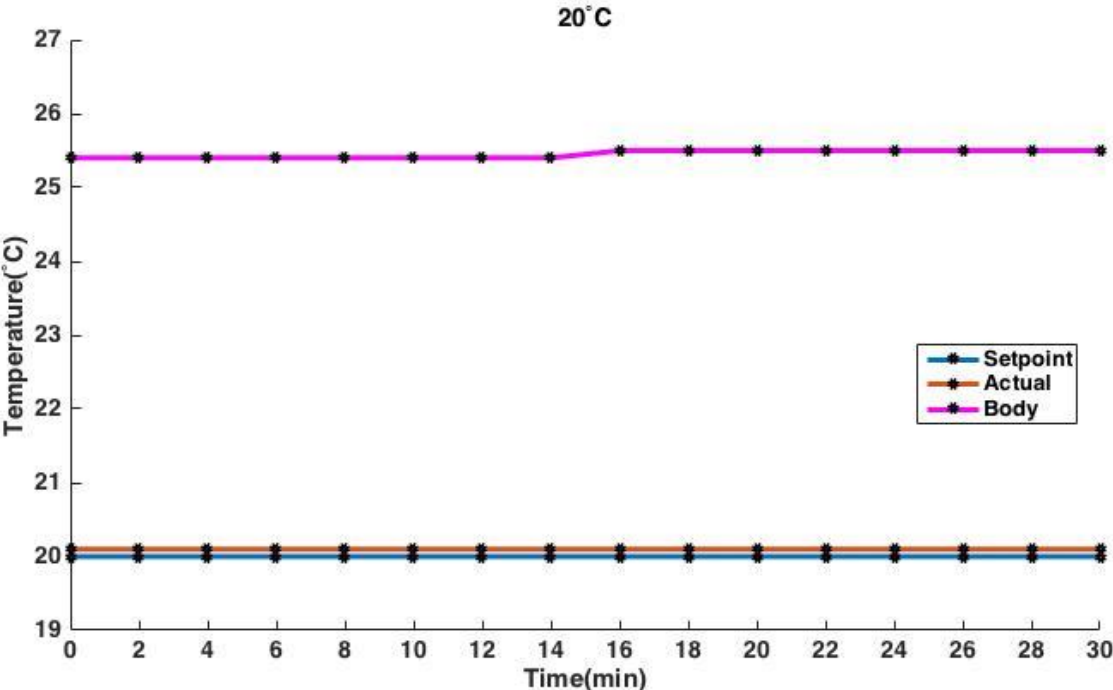


Figure 4.1: Peltier behavior at 20 °C

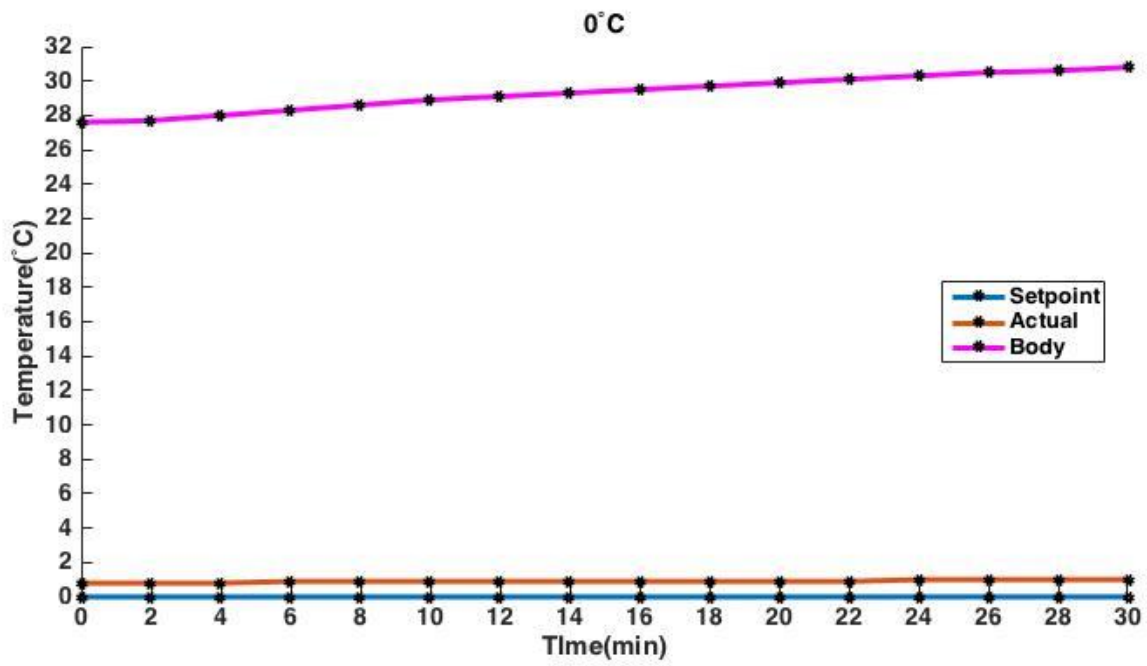


Figure 4.2: Peltier behavior at 0 °C

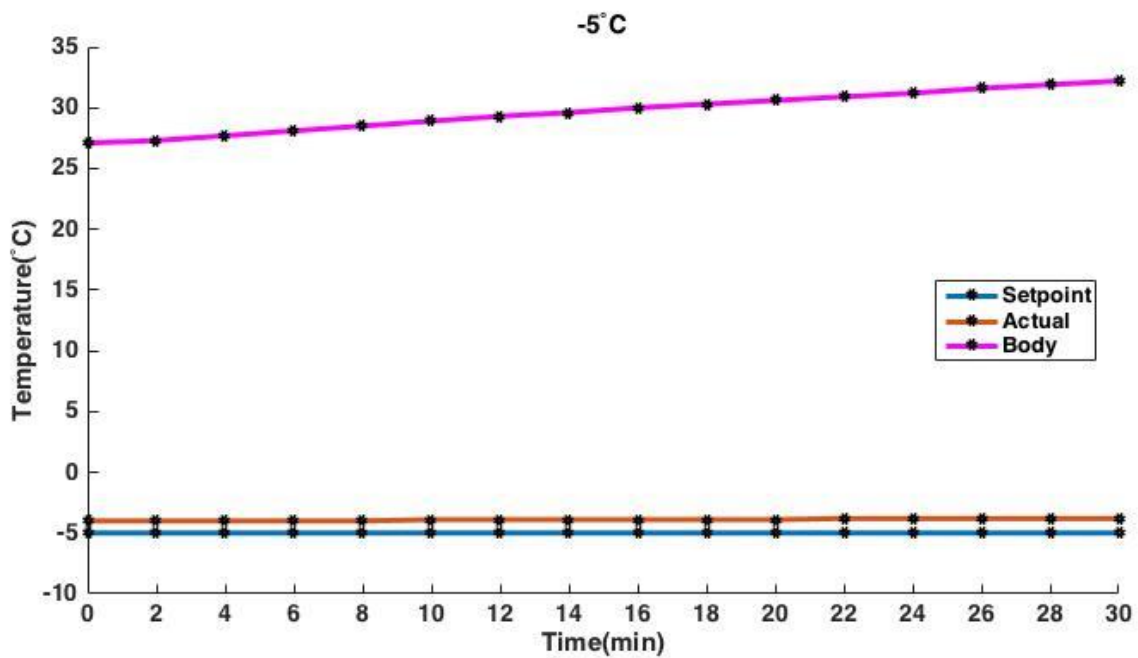


Figure 4.3: Peltier behavior at -5 °C

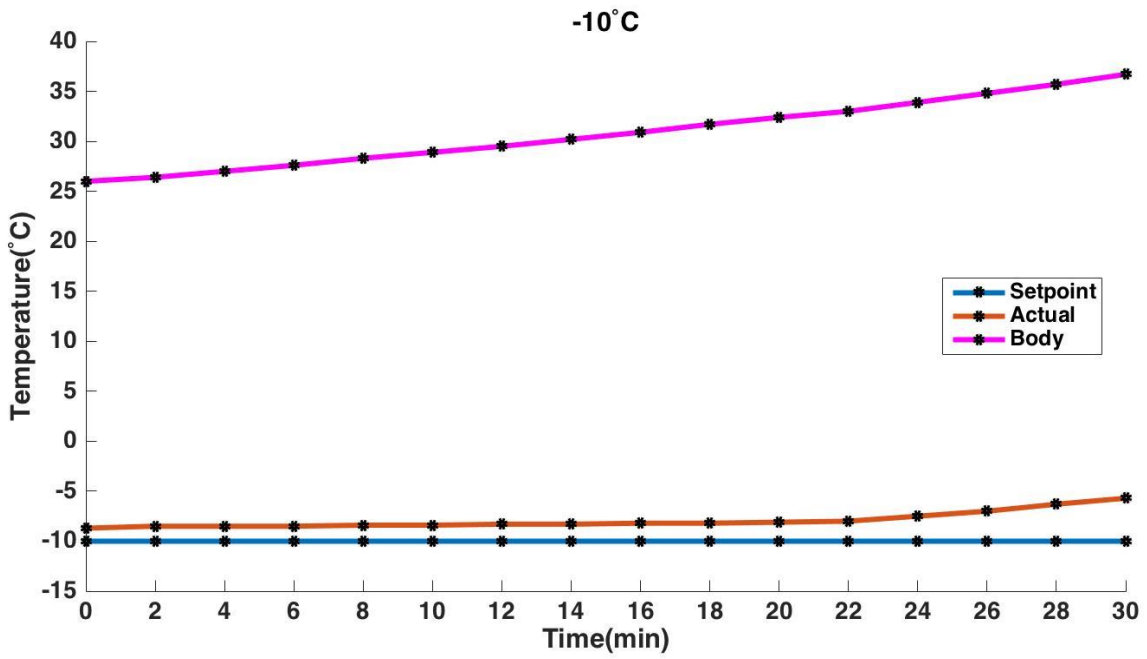


Figure 4.4: Peltier behavior at -10 °C

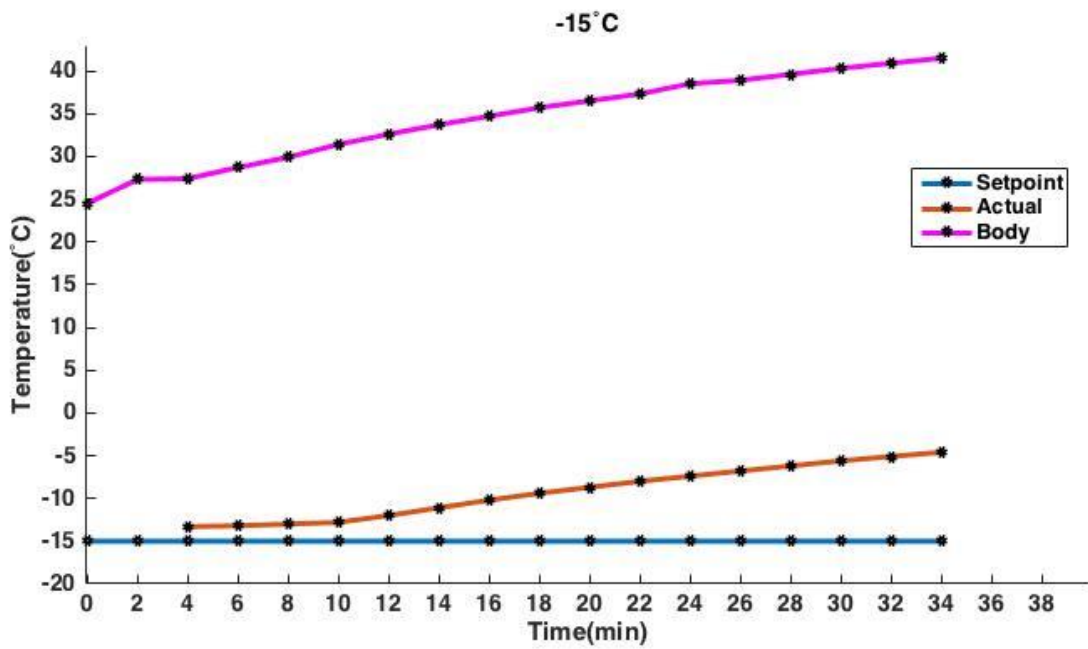


Figure 4.5: Peltier behavior at -15 °C

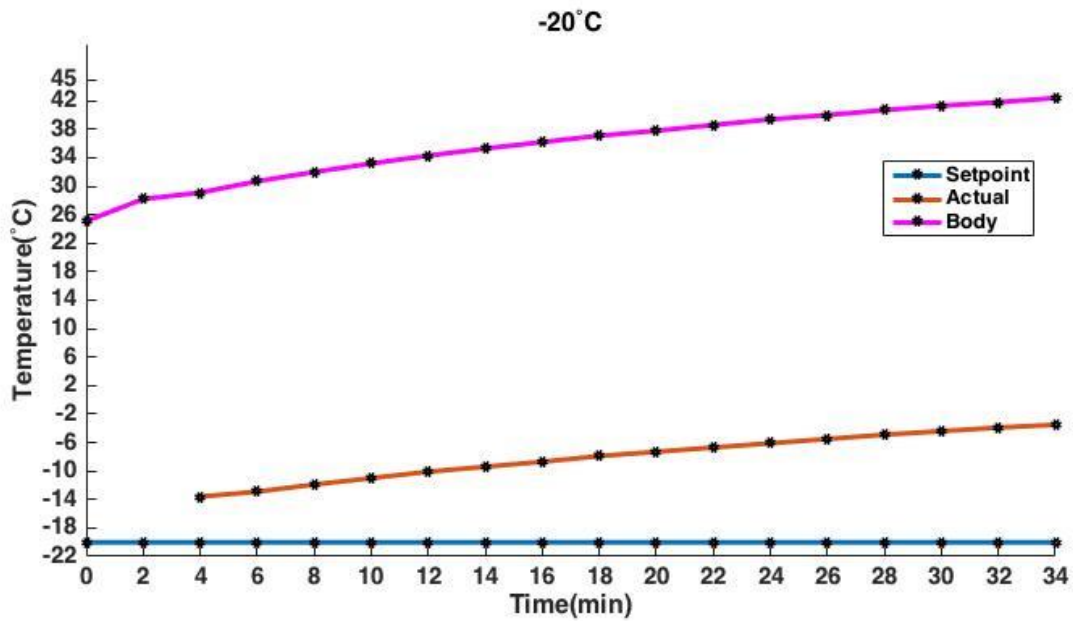


Figure 4.6: Peltier behavior at -20 °C

A precise look at all the graphs indicates that the behavior of Peltier for temperatures above zero is not problematic. The reason can be explained by less heat dissipation to the heatsink. Thus, the heatsink temperature does not increase so much. To explain more, at 20 °C, if  $T_1$  is considered as the actual temperature (target holder) of the start point of the experiment (time=0) and  $T_2$  considered as the temperature (target holder) at the end of experiment (time=30 min),  $\Delta T$  is equal to 0 °C which shows the acceptable stability of the device, also the heatsink temperature change in this span is only 0.1 °C. At temperature 0 °C, the  $\Delta T$  is 0.2 °C which indicates that for 30 minutes performance of cooled stage the target holder loss is absolutely ignorable and the heatsink becomes warmer only for 3.2 °C.

Temperatures below zero are more challenging. At -5 °C, the target holder becomes warmer for 0.3 °C in duration of 30 minutes, however, the heatsink temperature becomes warmer for around 5 °C. At -10 °C,  $\Delta T$  is equal to 3 °C, and the heatsink becomes warmer for around 11 °C. Figure 4.5 shows that at -15 °C, the actual and body lines become steeper after 10 minutes of the initiation of measurement, the loss at the target holder is around 9 °C and heatsink reaches 41.5 °C. The condition exacerbates at -20 °C, where the loss at the target holder is more than 10 °C and heatsink experiences an increase around 17 °C. In Figure 4.5 and 4.6, the actual lines

start with approximately four minutes delay. To state better, there is an interval between turning on the power supply and stabilization of temperatures on the target holder surface. Figure 4.7 shows this interval for more temperatures.

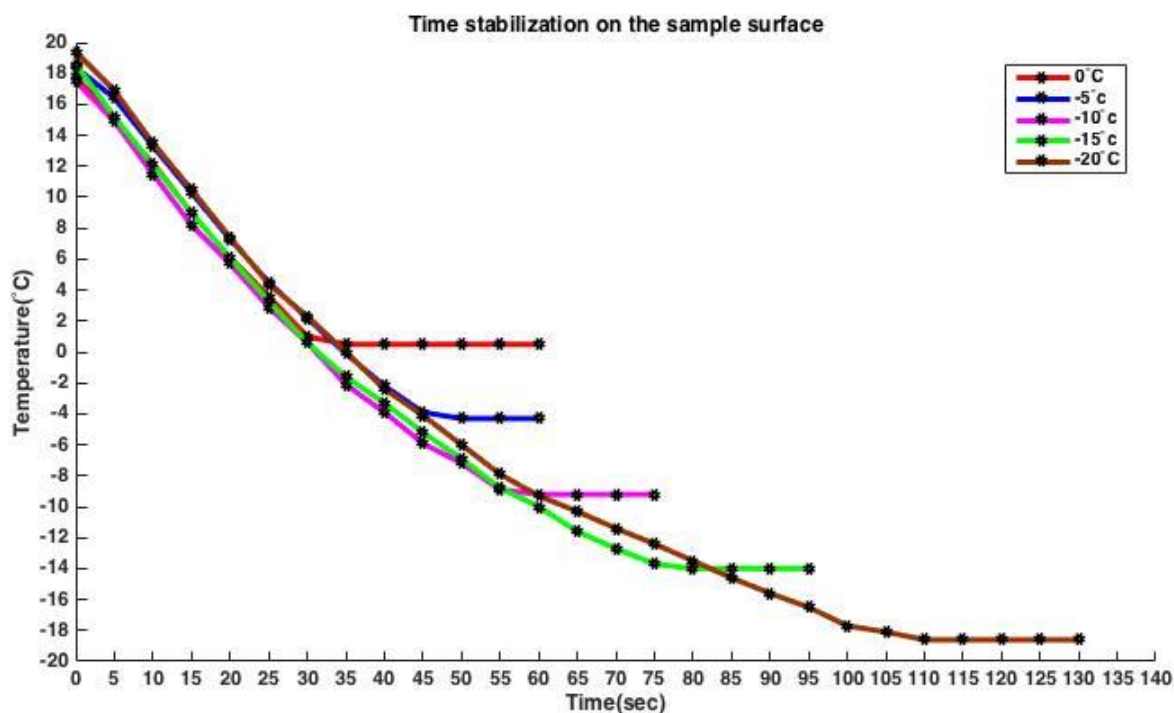


Figure 4.7: Time stabilization on the sample surface

In the second set of experiments, the cell behavior with laser ablation was investigated. To do this, a long-term single line ablation with Helium flow of 0.75 mL/min, scan speed of 5  $\mu\text{m/s}$  and beam size of 40  $\mu\text{m}$  for duration of 600 seconds was employed. An accurate comparison of the results of the cooled stage behavior at ambient temperature under laser ablation indicates that the heatsink becomes warmer sooner when the stage is inside the chamber while laser is firing. Therefore, longer possible measurements can be obtained by the correct selecting of only few temperatures below zero. Figures 4. (8-10) show the Peltier behavior at three temperatures:

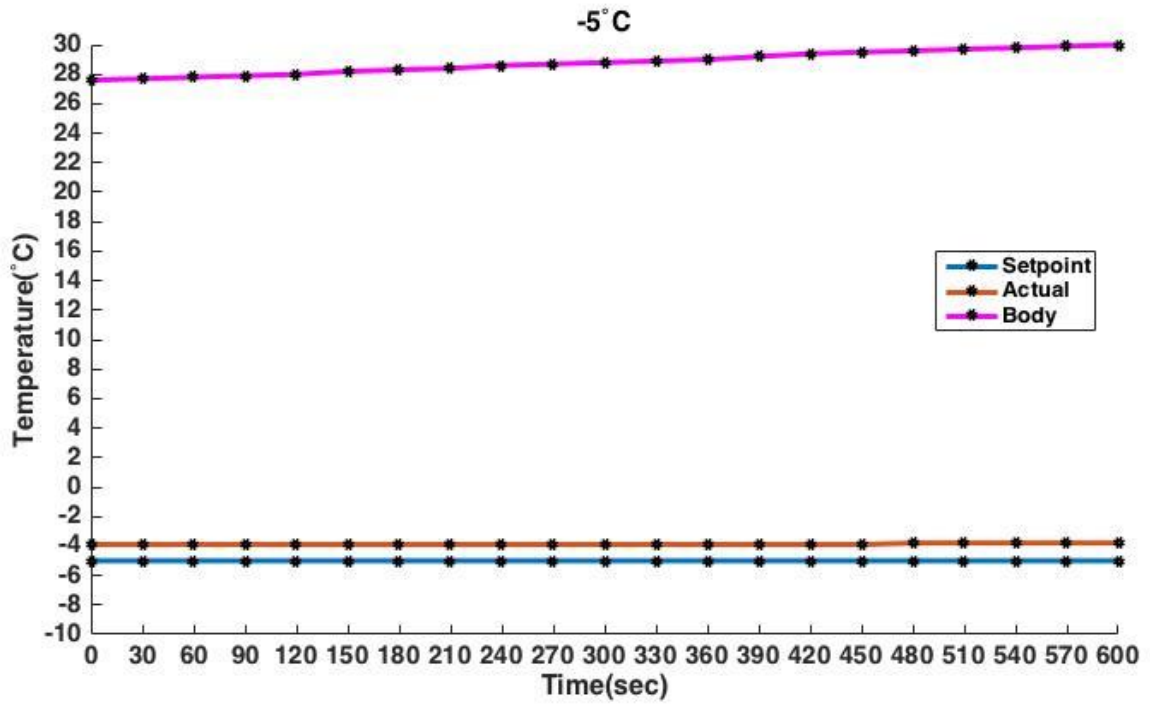


Figure 4.8: Peltier behavior under running laser at -5 °C

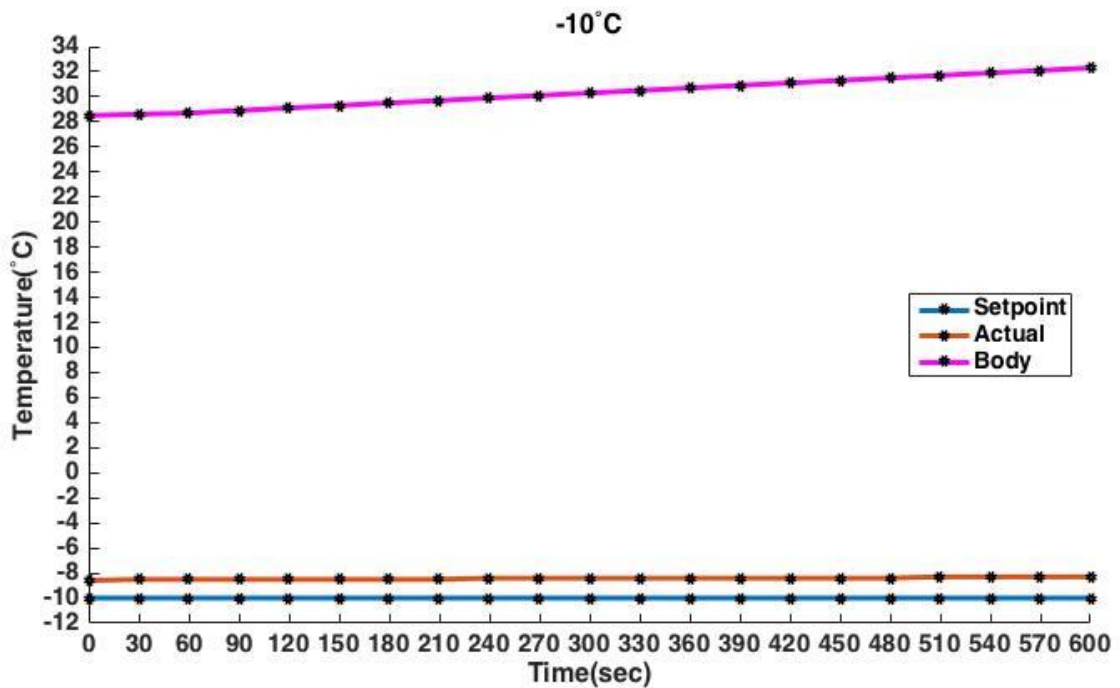


Figure 4.9: Peltier behavior under running laser at -10 °C

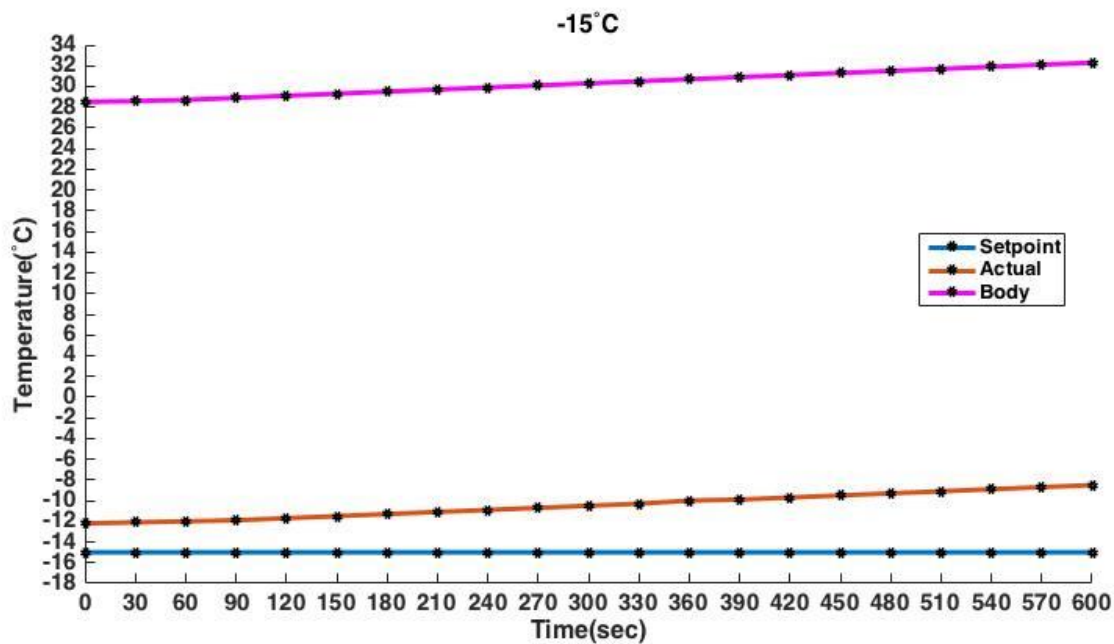


Figure 4.10: Peltier behavior under running laser at -15 °C

On the other hand, for imaging experiments at frozen state, the ablation may last between 30 to 80 minutes depending on sample size and spot size diameter which is proposed to be between 5 to 50  $\mu\text{m}$  for biological samples for obtaining better spatial resolution. To achieve this, only few temperatures can be selected. By now, the best temperature to be offered to work is at -5 °C which allows for nearly 35 minutes ablation with minimum heat dissipation to the heatsink, however, it needs further investigations to observe behavior and safety of temperatures below -5 °C for longer experiments. It will be discussed later in section 4.3.

To conclude, it is clear that the efficiency of the cooled stage performance is affected by hot temperature of the heatsink. When the heatsink cannot absorb any further heat, the surface holder of the Peltier starts becoming warmer quickly. Moreover, there is no solution to cool down the temperature of the heatsink during experiment to gain thermodynamic equilibrium, for instance, by circulating various types of coolant inside the bulky aluminum. Thus, to secure long-term stability during the ablation at frozen state without any noticeable loss, for duration of approximately 30 minutes -5 °C can be the best choice and for shorter measurements till maximum 20 minutes -10 °C can be selected. Temperatures between -10 °C and -20 °C are not possible to be applied.

## 4.2 Investigation of ablation behavior at various temperatures

### 4.2.1 Characterization of glass using cooled stage

#### A) Line scan ablation

The initial experiments were carried out on NIST 612 to inspect the effect of different temperatures on absolute signal intensity. Before ablation, the thickness of NIST was reduced to 1 mm to fit into the laser chamber and for better thermal conductivity. Since the temperature of sample surface (where the ablation process occurs) did not necessarily match the target holder temperature, measuring the sample surface was employed using a thermometer and thermal grease. Nine different temperatures were measured each for three times, the summary of the results is shown in Figure 4.11.

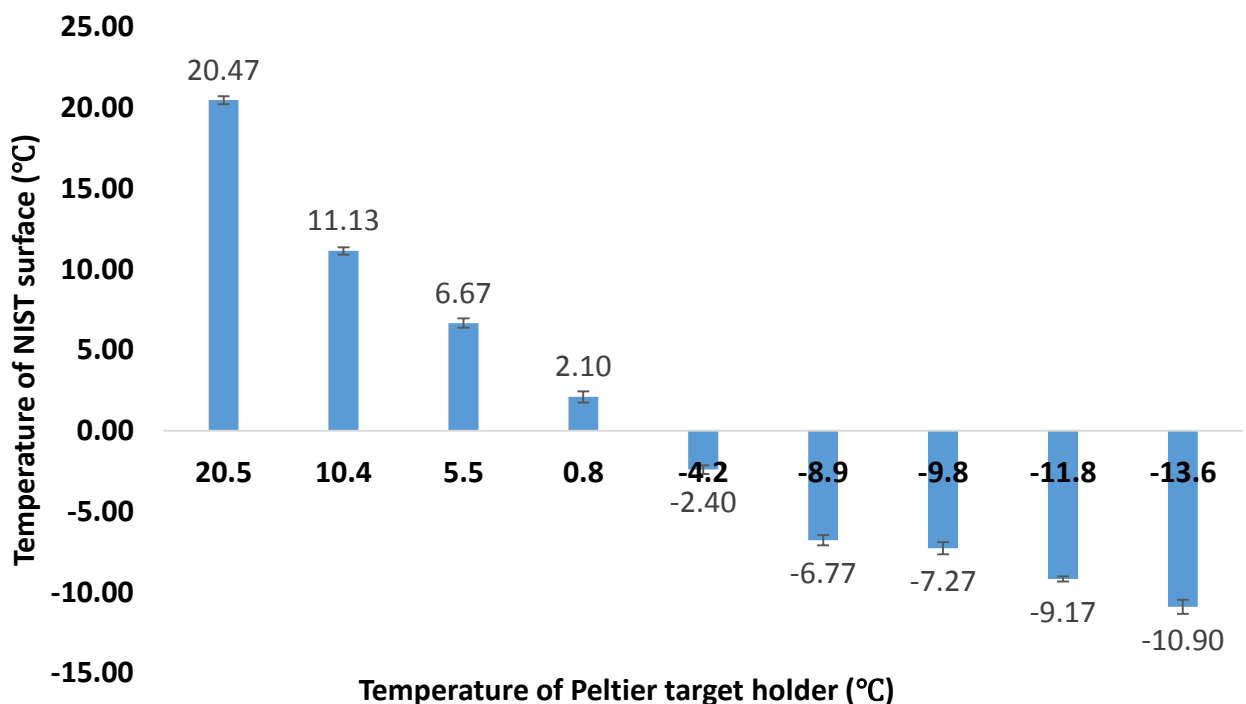


Figure 4.11: Measuring the glass surface

The results showed that temperatures of the glass surface were close to the corresponding temperatures of the target holder for temperatures above zero, but there

was a difference of one to maximum three degrees between temperature of the Peltier target holder and temperature of the glass surface for temperatures below zero. A 75 seconds single line with spot diameter of 40  $\mu\text{m}$ , scan speed of 5  $\mu\text{m/s}$  and 20 Hz repetition rate for mentioned elements in Table 3.1 was employed. Row data signal intensity was divided into four regions with equal size, calculation of average of these four regions (Figure 4.12) represented the signal intensity of the entire analysis.

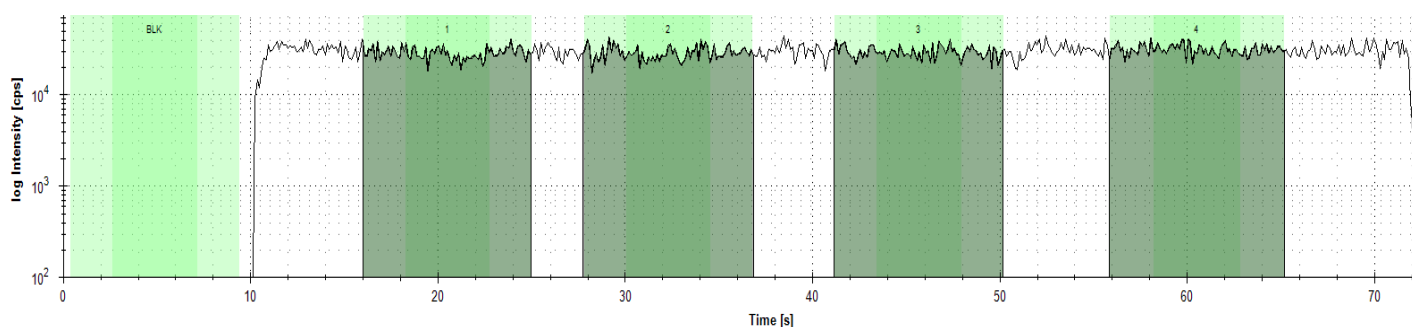


Figure 4.12: Signal intensity obtained for U

Calculation of relative standard deviations (RSD) yielded the RSD (n=4) of signal intensities below 3% at room temperature and below 2% at -5 °C and -10 °C. Figures 4. (13-15) show the intensities at four different temperatures for Al, Th and U:

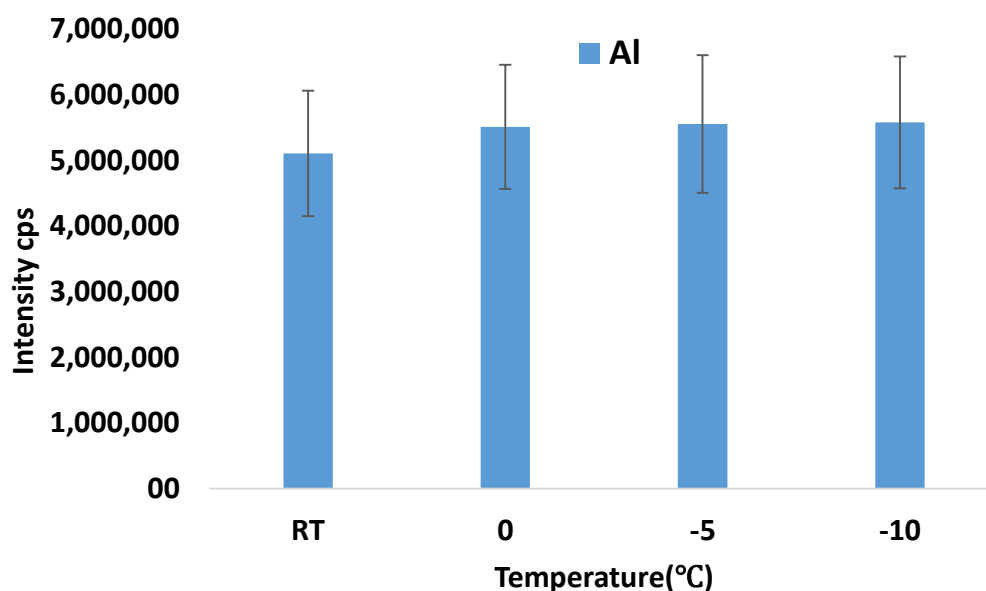


Figure 4.13: Aluminum intensity at different temperatures

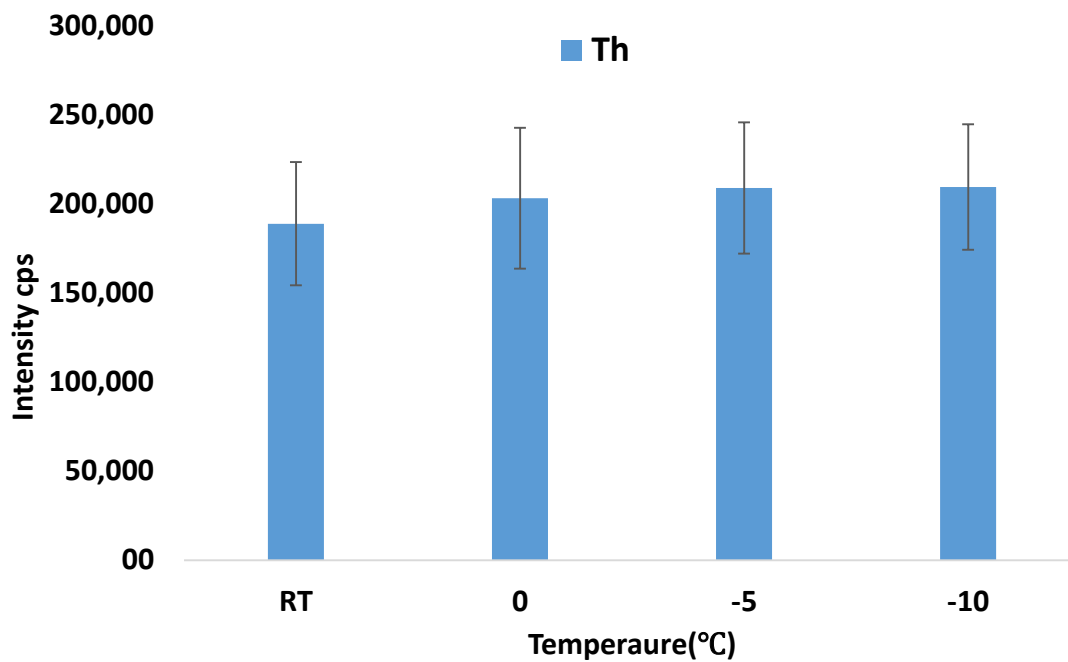


Figure 4.14: Thorium intensity at different temperatures

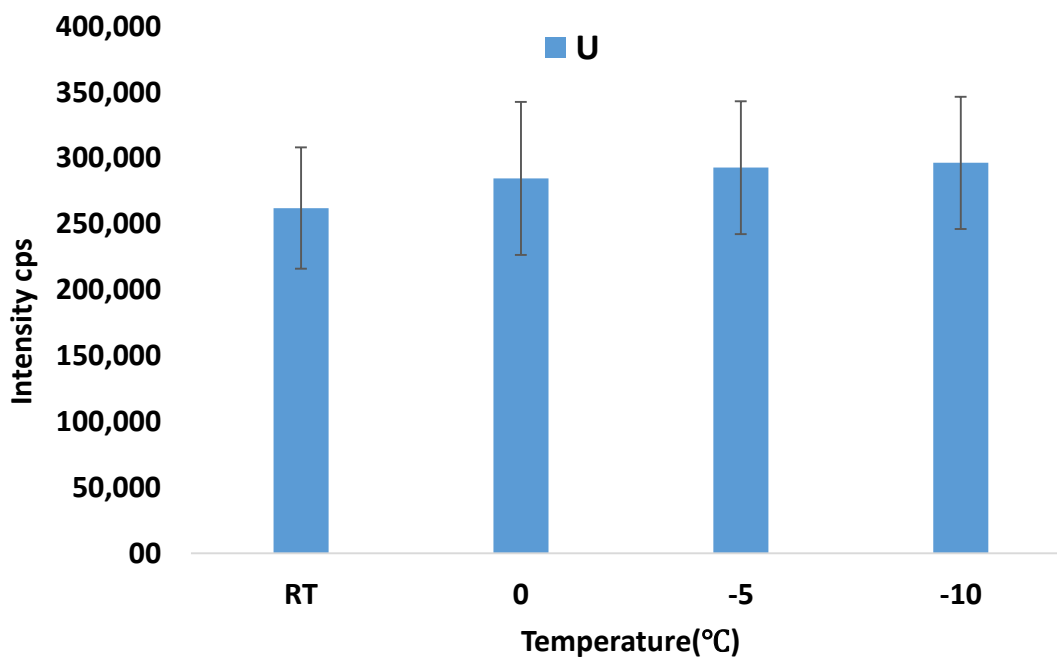


Figure 4.15: Uranium intensity at different temperatures

The Figures show that the intensities of the measured elements were slightly lower at room temperature compared with other three temperatures. For instance, the Al intensity at  $-10\text{ }^{\circ}\text{C}$  was around 9% higher than room temperature and around 10% for Th. This amount is at its maximum value around 13% for U. It was much less ( $<8\%$ )

for the other measured elements. However, the intensities differences were not significant since standard deviations of the measurements overlap each other. By looking carefully at the figures above, it is obvious that there was no considerable change between temperatures 0 °C to -10 °C. The results indicate that there is no significant influence on analytical performance of the glass reference material.

In order to tackle possible ablation differences and instrumental drifts, the signal intensities from Th and U were normalized to Al. Figure 4.16 demonstrates the normalized ratios and confirms the findings regarding the effect of various temperatures on NIST.

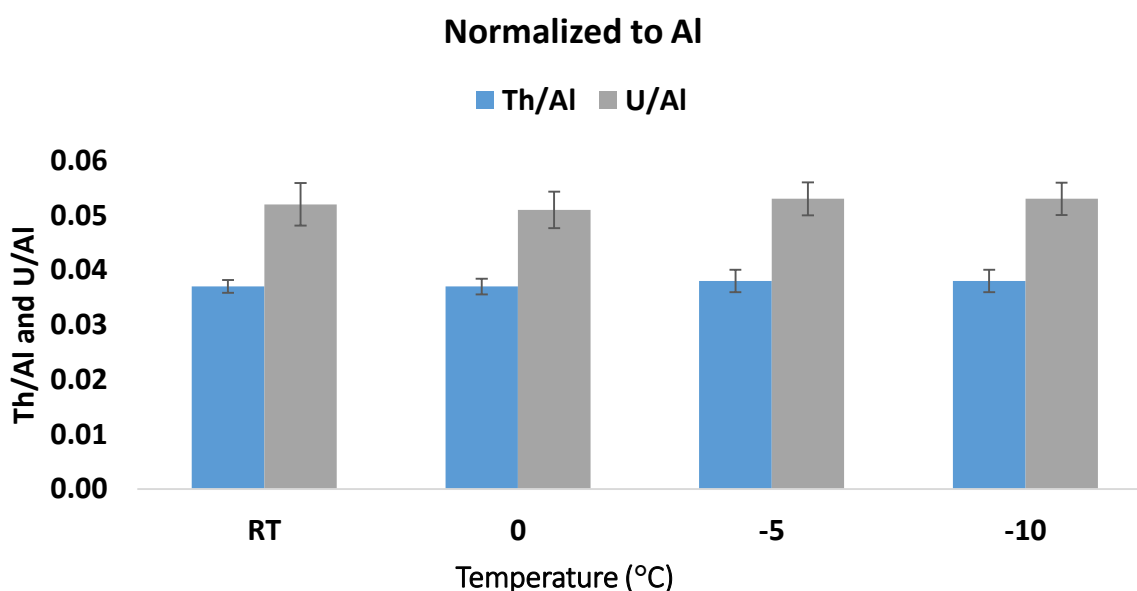


Figure 4.16: Th and U signal intensities normalized to Al

## B) Spot scan ablation

The experiment was repeated with spot scan mode. In this mode, laser holds on a defined position producing sample material from which the signal is acquired by the MS for a fix period of time before it moves to another position. Nine spots with raster spacing of 150  $\mu\text{m}$  were employed (Figure 4.17). The diameter of each spot was 80  $\mu\text{m}$  at repetition rate equal to 20 Hz and dwell time per spot of 10 seconds were selected to ablate enough materials. Three temperatures (room temperature, -5 °C and -10 °C), each with three replicates and five minutes pause between measuring of each

temperature were measured. Calculation of relative standard deviations (RSD) showed that the RSD (n=3) of signal intensities below 7 for all three temperatures. The intensities of signals did not vary so much, only slightly higher intensity at temperatures below zero (intensity at -10 °C is around 8% higher than room temperature), thus it can be concluded that there is no significant difference between non-cooled and cooled analysis and ablation is not temperature dependent for the glass reference material. Figure 4.18 shows the intensities at three different temperatures for aluminum. The similar results were obtained for other measured elements.

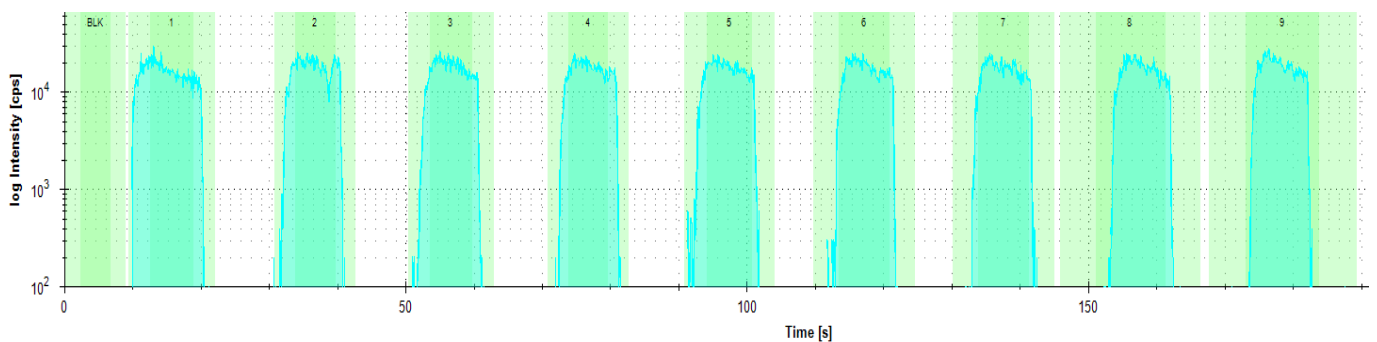


Figure 4.17: Signal intensity obtained for Co

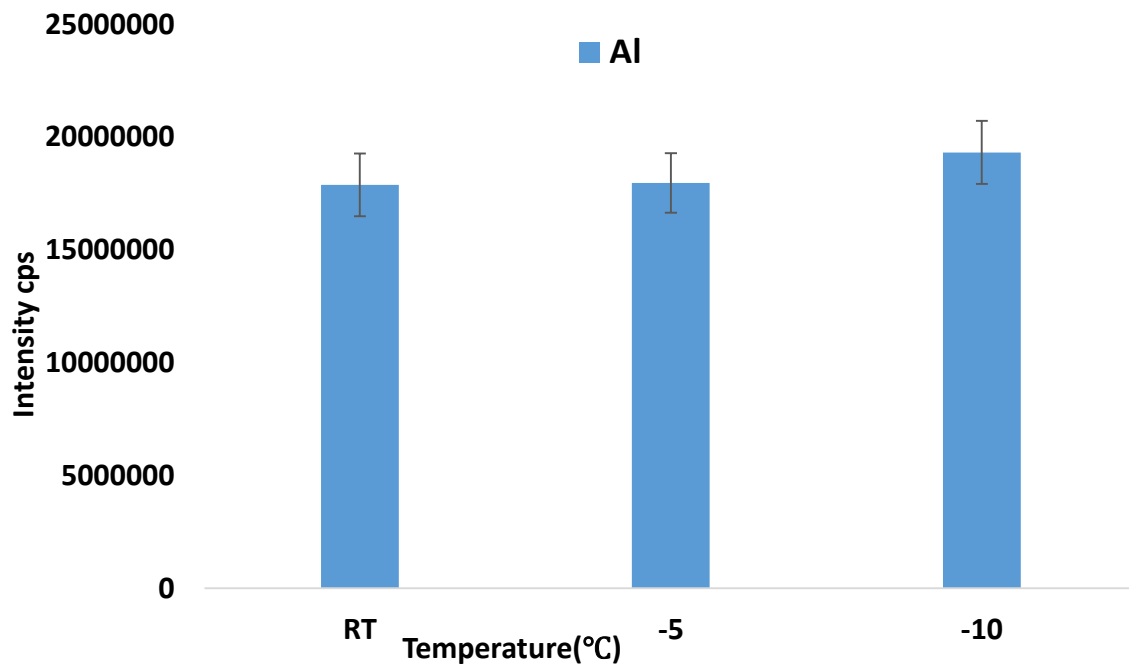
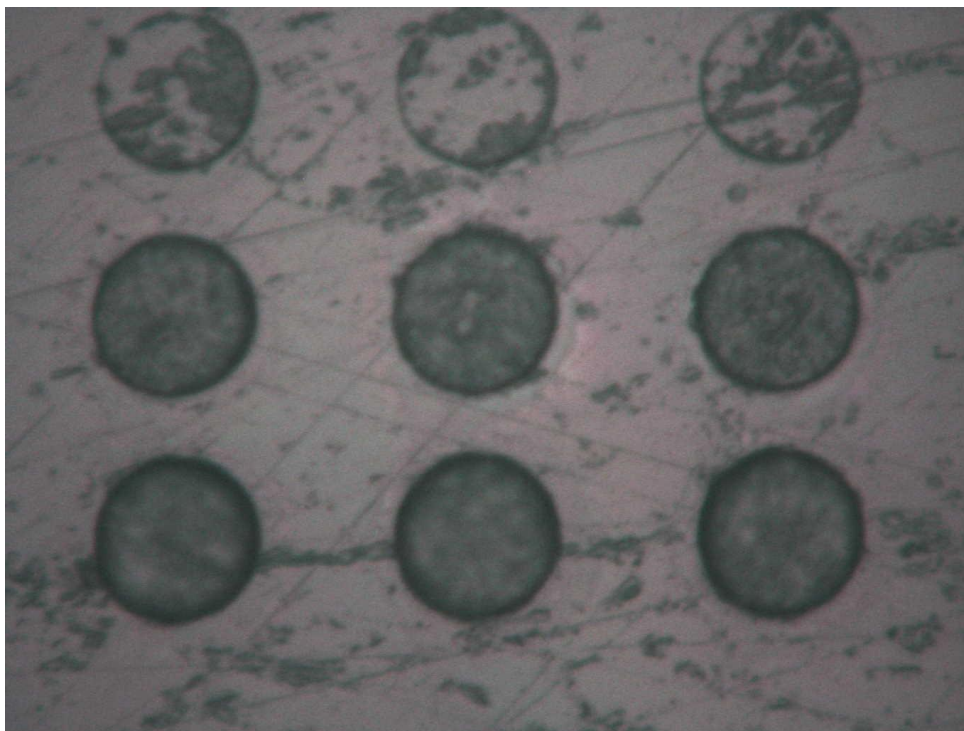


Figure 4.18: Aluminum intensity at different temperatures

Comparing the intensities of line scan and spot scan, it is obvious that the intensity was higher in case spot scans than in case of line scans. It can be explained by the size of the spot. The bigger spot size, the more materials are ablated and therefore higher intensity is expected [20, 32].

An intense interaction of laser beam with sample brings about the transfer of laser energy to the matter. Accordingly, evaporation, ejection of particles, melting can occur when the laser ablation exceeds the threshold directly in the irradiated surface and in adjacent area. The crater shapes of the glass for both cooled and non-cooled analysis are demonstrated in Figure 4. (19-20). To do this, nine spots of 80  $\mu\text{m}$  each with three replicates at three different repetition rates were applied. Dwell time of the laser firing per each spot was four seconds. First row with 5 Hz, second with 10 Hz and third with 20 Hz were ablated. It is obvious that cooled analysis does prevent re-deposition of the ablated particles in the vicinity of ablated area and spots are more distinctive compared with non-cooled analysis.



**Figure 4.19: Crater shape at frozen state**

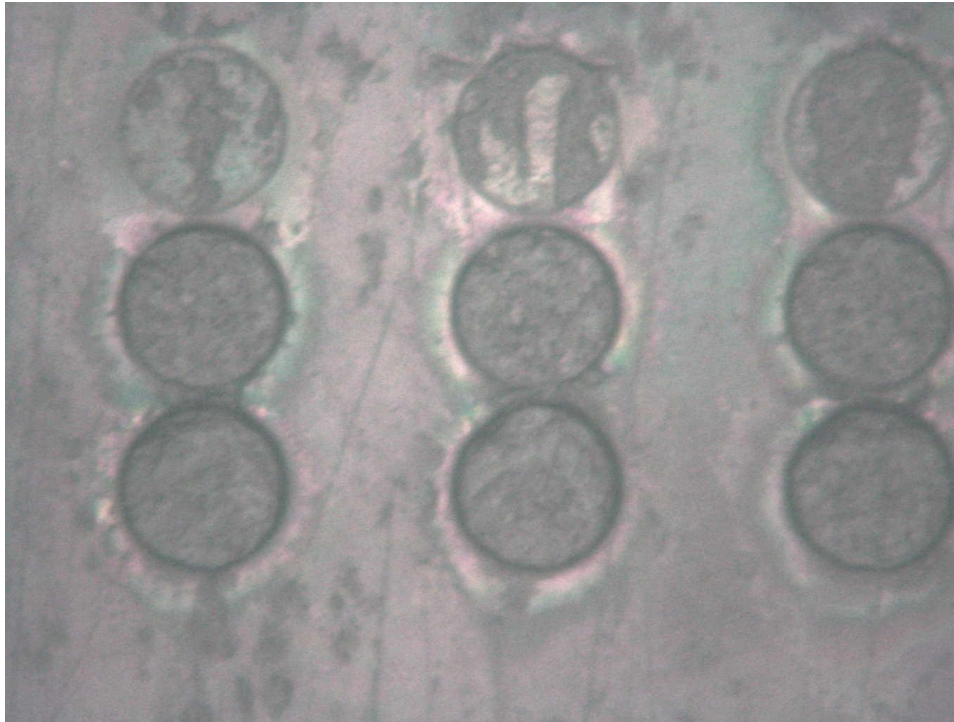


**Figure 4.20: Crater shape at room temperature**

#### 4.2.2 Characterization of metal using cooled stage

Similar experiments were conducted with the use of a metallic sample (reference material No 075 C, copper with added impurities, BCR) by means of 213 nm laser ablation ICP-MS at room temperature, -5 °C and -10 °C. A 60 seconds single line with spot diameter of 80 μm, scan speed of 10 μm/s and 20 Hz repetition rate for few elements including  $^{63}\text{Cu}$ ,  $^{56}\text{Fe}$ ,  $^{68}\text{Zn}$ ,  $^{75}\text{As}$  and  $^{208}\text{Pb}$  was employed. The obtained values for RSD (n=3) were 8% at -5 °C, 11% at room temperature and 3% at -10 °C. A possible explanation for the rather higher RSD is the fact that the surface of the copper was rough over the whole surface, resulting in different ablation behavior. The signal intensities at -5 °C and -10 °C were 32% and 46% higher than room temperature, respectively, Figure 4.21.

The same observation for the crater shapes was carried out on the copper reference material. For this, nine spots of 80 μm each with three replicates at three repetition rates started from 2 Hz, 5 Hz and 10 Hz were applied. Dwell time of the laser firing per each spot was four seconds. For better understanding of the heat effect caused by interaction of laser and matter, Figure 4. (22-23) show two spots ablated at 10 Hz repetition rate (10 shots per second). The pictures were provided using a profilometers

(DektakXT, BRUKER, USA). It is obvious that re-deposition of the ablated particles is less intense during frozen condition measurement.

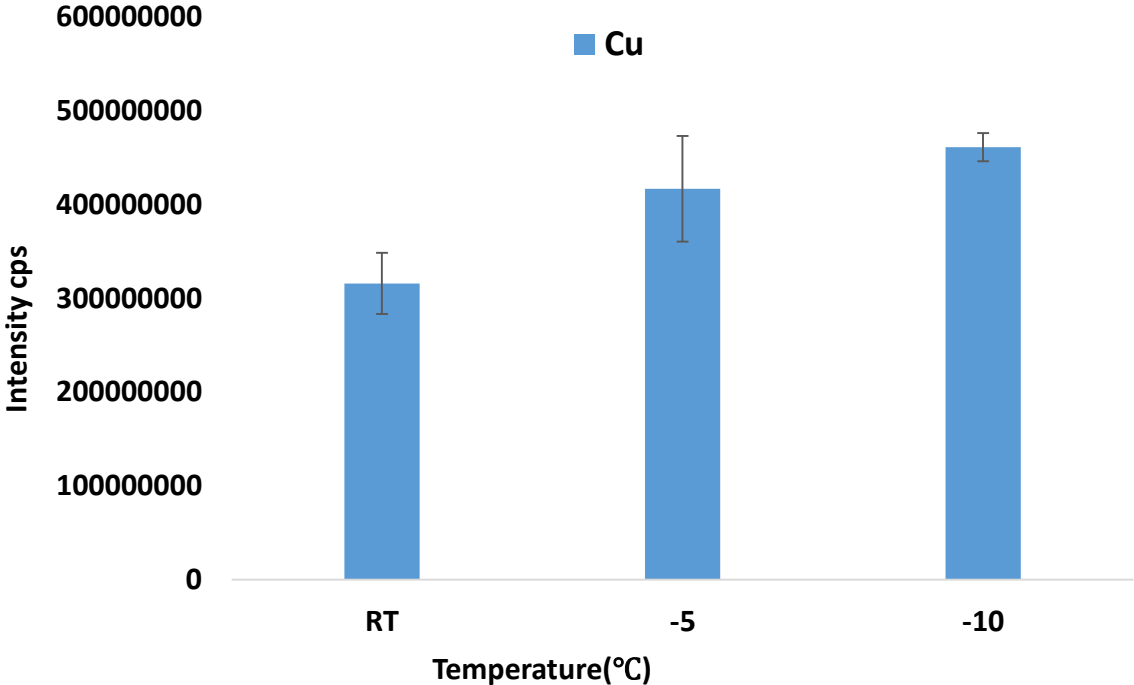


Figure 4.21: Copper intensity at different temperatures

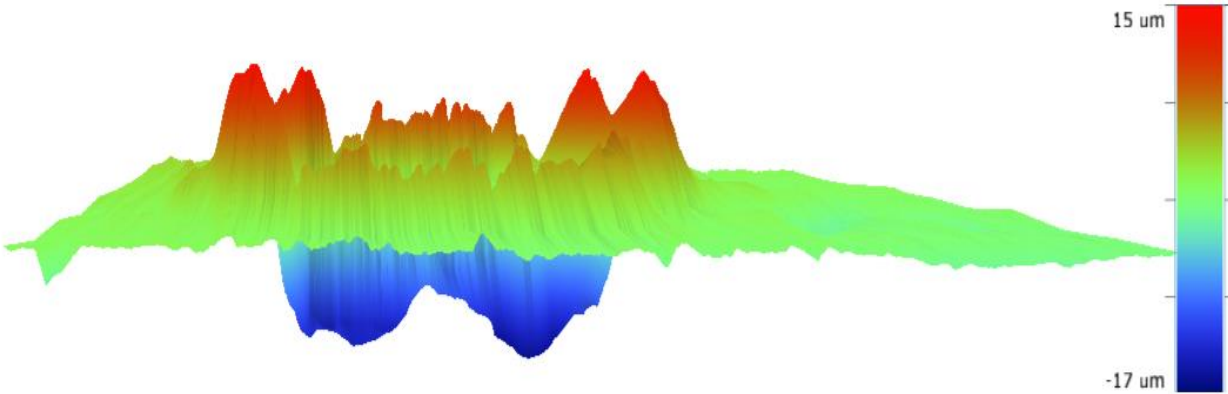
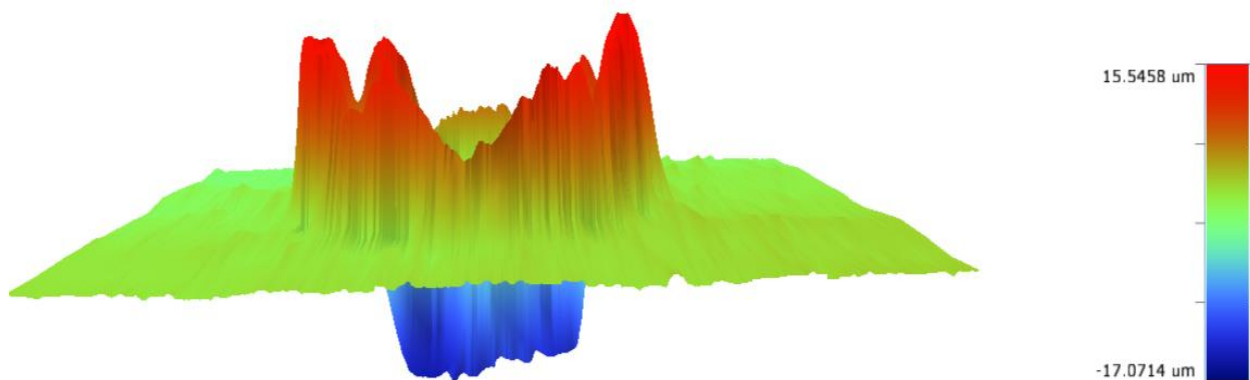


Figure 4.22: Copper crater shape at frozen state



**Figure 4.23: Copper crate shape at room temperature**

Comparing the findings from NIST and copper, in both cases the generated intensities at cooled analysis are higher than at ambient temperature, however, it is more pronounced for copper (metal). It can be explained by the excellent thermal conductivity of metals and consequently heat is instantly and effectively transferred from the ablation spot. Higher intensity also refers to better sensitivity, which can be explained by more efficient transport of the ablated particles to the plasma and in consequence better ionization. Furthermore, it can be concluded that the ablation process is only sample and not temperature dependent. A related point to consider is that all temperatures below zero produce approximately similar signal intensity. This claim is true between  $[-1\text{ }^{\circ}\text{C}$  to  $10\text{ }^{\circ}\text{C}]$ , working on the lower temperatures needs a design of more sophisticated cooled stage. Besides increasing signal intensity and stability, lowering the temperature during ablation has one more additional benefit. According to the studies, another aspect of laser ablation experiments is elemental fractionation, which occurs during the ablation process and during transport of aerosol or ionization in plasma. It is influenced by properties of the laser (pulse duration, laser wavelength and fluence) and also elemental composition and properties (ionization potential, vapor pressure, melting and boiling points and etc). This effect can be minimized by using femtosecond lasers instead of nanosecond and He as a carrier gas instead of Ar [53]. M.Jarošová, et.al [22], showed that lowering temperature to prevent sample warming was beneficial for decreasing the fractionation effects.

### 4.2.3 Gelatin matrix-matched standards for LA-ICP-MS as a proxy for biological samples

In contrast to unique features of LA-ICP-MS technique such as high spatial resolution and direct solid analysis, this analytical method suffers from sensitivity drifts, matrix effects and elemental fractionation which can produce unreliable results. To get reliable results, matrix-matched calibration standards are required. In this work, using homogenized tissue material containing the elements of interest is essential. But inadequate certified reference materials for biological tissue introduces alternative approaches such as preparation of gel standards, the use of polymeric layers or picoliter droplet dried residues as standards to obtain calibration standards. Also choosing a proper internal standard to correct instrumental drifts and differences in material ablation is imperative [54, 55].

For obtaining the multi-element calibration standards, a gelatin matrix was chosen as standard material because of its close similarity to animal tissue properties. Six concentration levels of mentioned ions were prepared. Prior to LA-ICP-MS measurements the exact concentration of prepared gelatins was determined using ICP-MS. The concentration determination was performed in four replicates of sample for each concentration level to decrease the variations occurred during sample preparation and furthermore to obtain a satisfactory reproducibility. Relative standard deviations of the replicates up to 20% were observed. These large deviations can be explained by the inhomogeneity of the prepared gelatins either during digestion by means of acid or homogenization in earlier step.

ICP-MS was washed out for 45 minutes prior to experiments to ensure stable operation condition. To make sure that distribution of the questioned analytes was homogenous, and the results are representative for laser ablation measurements spot measurements were performed. A pattern comprising of six spots adjacent to each other with 80  $\mu\text{m}$  laser beam diameter was measured on four different positions across the whole tissue slice. The patterns were placed nearby the left, right, upper, lower edges of gelatin slice to yield information about the distribution of analytes. To make sure of complete ablation of the sample material, 5 seconds dwell time per spot was selected. Repetition rate of 10 Hz and laser fluence of 3.64  $\text{J}/\text{cm}^2$  were chosen for the measurements. The Peltier-cooled stage was set at  $-10\text{ }^\circ\text{C}$  and gelatin sample stuck to its silicon wafer holder was placed at the center of target holder of cooled stage to get cooled efficiently.

After ending the first four measurements at frozen state, the Peltier was set to +20 °C, sample started thawing and water from the tissue diffused inside the tissue and evaporated after few minutes and sample became dried. The average of signal intensities of 24 spots for both frozen and room temperature states was calculated, standard deviations and relative standard deviations RSD (n=4), as well.

Figure 4.24 shows that the obtained regression line for Mn was steeper in case of frozen state for around 43%. This fact was true for other measured elements, although the coefficient of determination varied from 0.90 to 0.98. The weaker coefficient can signal some errors which can originate from various sources. It can range from contamination during preparation of gelation matrix-matched, inhomogeneity of matrix- matched standards, instrumental drifts and uncertainty in thickness of cryotome cuts. To solve the problems, normalizations of the analyte signals to europium were applied. It can be seen in Figure 4.25 that obtained fitting lines were improved and no large deviations were observed ( $R^2=0.996$ ) and RSD of the analysis was below 5% which confirmed the reproducibility of the measurements. On the other hand, regression lines were almost close to each other and there was no significant difference between frozen and room temperature conditions. The reason can be arisen from the same behavior of the internal standard to other elements, its intensity became higher during cooled ablation and became lower during non-cooled ablation. Thus, in order to show the differences, the results are presented without normalization. The reason to certify the results without normalization can be addressed to the minor and ignorable instrumental drifts during short time measurement. With the regard to this finding the experiment can be extended to biological samples because gelatin gel mimics the composition of the biological samples [54].

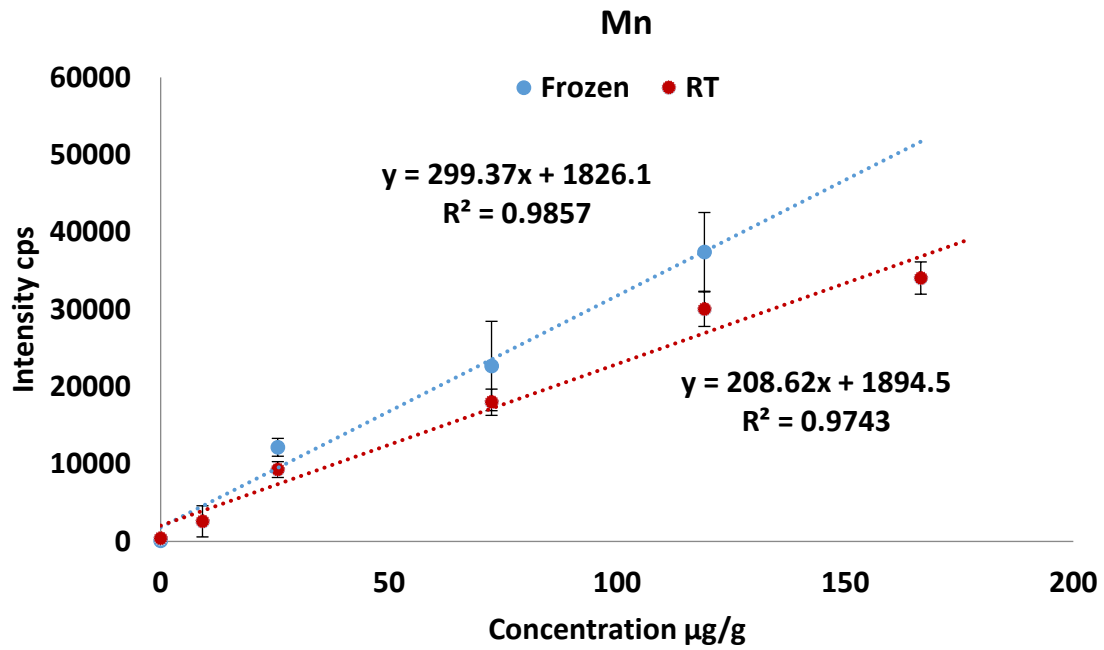


Figure 4.24: Correlation of obtained raw signal intensity from laser ablation and ions concentrations for gelatin

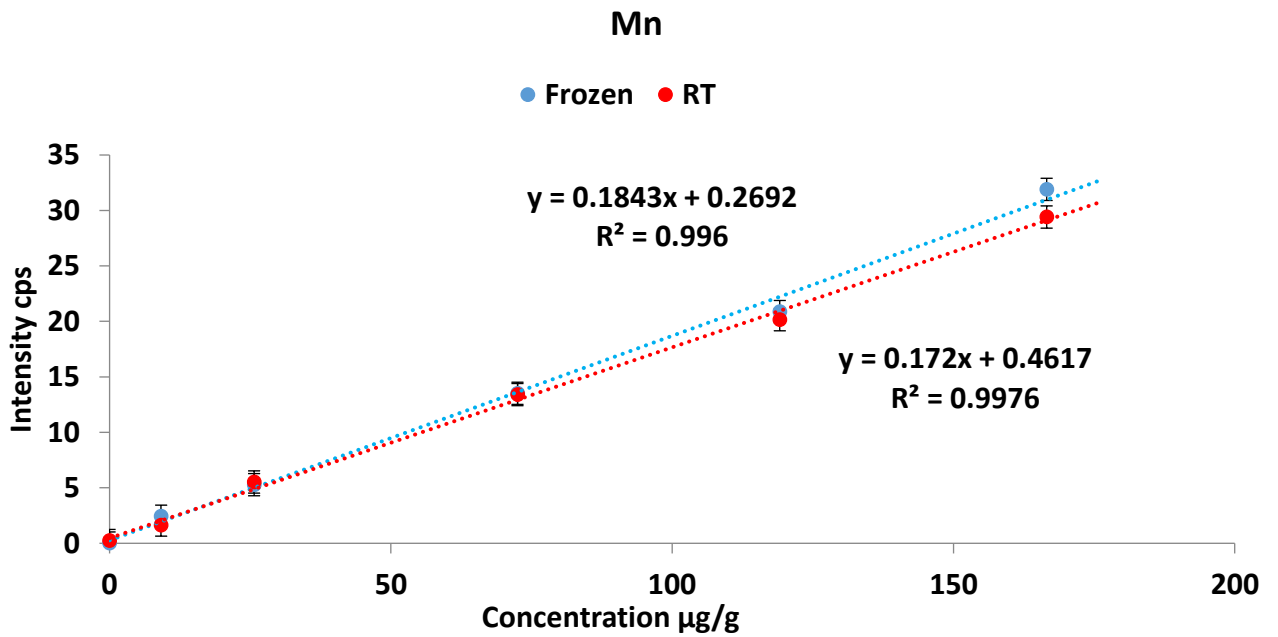


Figure 4.25: Correlation of obtained europium normalized signal intensity from laser ablation and ions concentrations for gelatin

#### 4.2.4 Characterization of matrix-matched tissue standards

The optimization of gelatin as multi-elements calibration standards confirmed the signal intensity at frozen state is higher than at room temperature and it produced a steeper regression line at frozen state for five spiked levels plus once portion for non-spiked. With the regard to this finding, the same experiment was extended to biological tissues including porcine liver and kidney showing distinct differences in their tissue properties in two different sets. In the first set, data was normalized to carbon. In the second set, indium was applied as internal standard. The effect of lowering the temperature (room temperature and -10 °C) on biological tissues during laser ablation was investigated. Prior to LA-ICP-MS measurements the accurate concentration of prepared tissues was determined using ICP-MS. The concentration determination was performed in 4 replicates of sample for each concentration level to minimize the errors occurred during sample preparation and furthermore to obtain a satisfactory reproducibility. The Relative standard deviations of the replicates were up to 15%. These large deviations can be explained by the inhomogeneity of the prepared tissues either during digestion by means of acid or homogenization in earlier step.

To ensure that distributions of the measured analytes were homogenous, spot measurements were performed. A pattern comprising of nine spots adjacent to each other with 80 µm laser beam diameter was measured on five different positions across the whole tissue slice. The patterns were placed nearby the left, right, upper, lower edges and in the middle of tissue slice to yield information about the distribution of analytes. To make sure of complete ablation of the sample material, 5 seconds dwell time per spot was selected. Repetition rate of 10 Hz and laser fluence of 3.64 J/cm<sup>2</sup> were chosen for the measurements. The Peltier-cooled stage was set at -10 °C and tissue sample stuck to its silicon wafer holder was placed at the center of target holder of the cooled stage to stay frozen efficiently.

After ending the first five measurements at frozen state, the Peltier was set to +20 °C, sample started thawing and the water from the tissue diffused inside the tissue and evaporated after few minutes and sample became dried. ICP-MS was washed out for 45 minutes prior to experiments to ensure stable operation condition. The average of signal intensities of 45 spots for both frozen and room temperature states was calculated, standard deviations and relative standard deviations RSD (n=5), as well. The obtained regression lines were steeper at frozen state than at room temperature

for all measured elements (first set of experiments used for carbon normalization). The RSD varied from 8.7% to 19.5% for non-spiked liver tissue and from 3.5% to 21.6% for non-spiked kidney tissue at both frozen and ambient states for all measured elements. Moreover, the same variations were observed in another spiked levels RSD. The reason can be explained by matrix-induced interferences or instrumental drifts which can cause troubles in transporting of particles to plasma and changing the ionization efficiency [25]. Inhomogeneity and contamination of the sample during preparing matrix– matched standards and uncertainty of the thickness of thin sections which probably was not exactly 10  $\mu\text{m}$  could be other reasons of the deviations. Rather higher deviations led to weaker coefficient of determination, as well. Correlation coefficients of all regressions also varied from 0.88 to 0.98. To overcome the obstacles, choosing proper internal standards which are matched the ionization properties of the analyte elements can compensate the interferences. It is reported that using deposited gold layer homogeneously distributed over the sample surface is a reliable method to add an internal standard. It not only can compensate changed ionization behavior because of alternation in material intake into the plasma, but also makes data obtained in independent measurement comparable [56]. Nonetheless, this method is not practically applicable to this work since preservation of tissue at frozen state is highly prominent. Carbon is also considered to be used as internal standard in biological and medical matrices. If carbon was an appropriate internal standard, it should correct instrumental drifts and eliminate any variations. The outcome showed that normalization to the  $^{13}\text{C}$  signal improved the RSD for only non-spiked kidney tissue to below 10% for all target elements, whereas this positive effect was not seen for all target elements in liver tissue. Figures 4. (26-29) illustrate the comparison of correlations between ions concentrations, raw signal intensity and normalized intensities for laser ablation. To state better, applicability of carbon as internal standard has already been in debate over years and its behavior during laser ablation is not fully understood. A good internal standard is assumed to correct any bias during the measurement, hence it should be ablated, transported, vaporized and ionized inside the ICP. But carbon shows to behave differently, its high ionization potential can lead to extreme changes in the signal intensity when the plasma conditions change even marginally. Another reason can be associated with the presence of carbon ubiquitously either inside tissue itself or as a very high background of carbon due to  $\text{CO}_2$  inside the ICP-MS. Furthermore, analyses of carbon containing matrices generates

matrix-dependent amount of gaseous carbon which causes diffusion of gaseous carbon out of axis shortly after discharging from the injector nozzle. It means the difference in diffusion loss from carbon containing species and the analytes indicates that carbon is not suitable to be considered as internal standard [57].

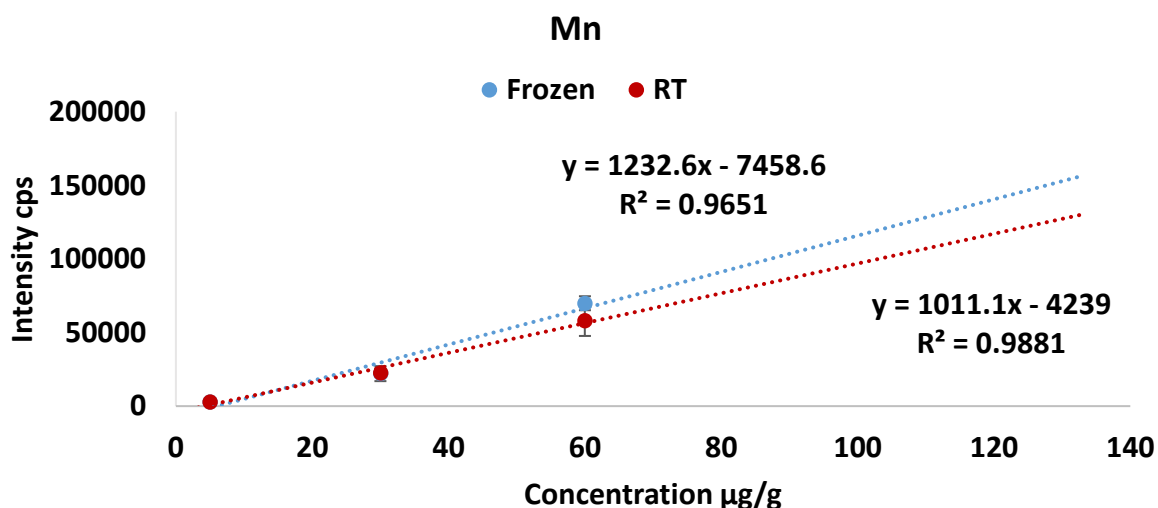


Figure 4.26: Correlation of obtained raw signal intensity from laser ablation and ions concentrations for liver

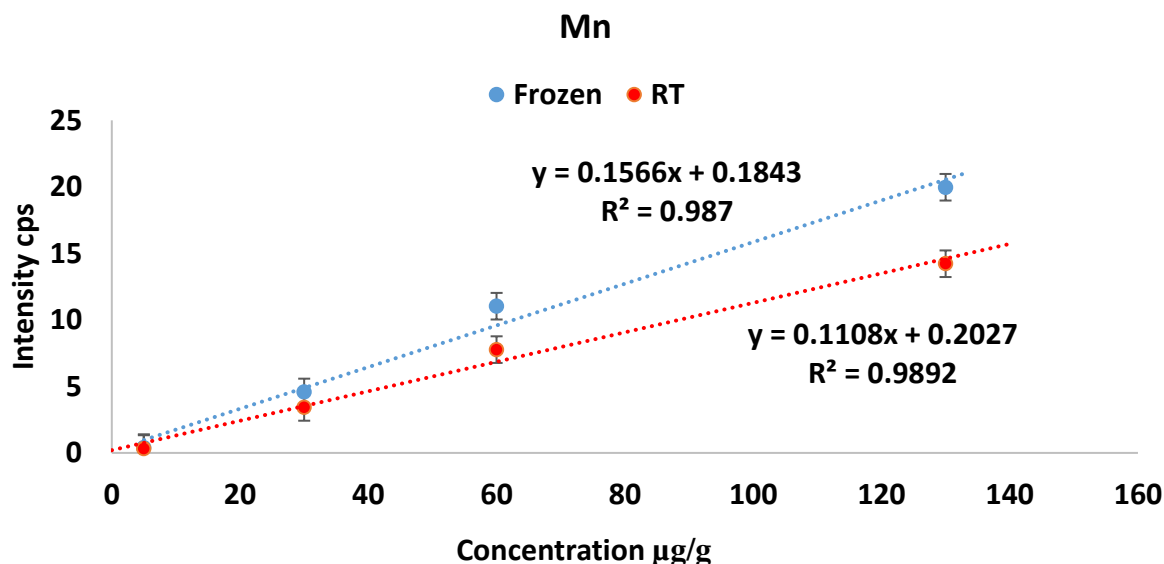


Figure 4.27: Correlation of obtained carbon normalized signal intensity from laser ablation and ions concentrations for liver

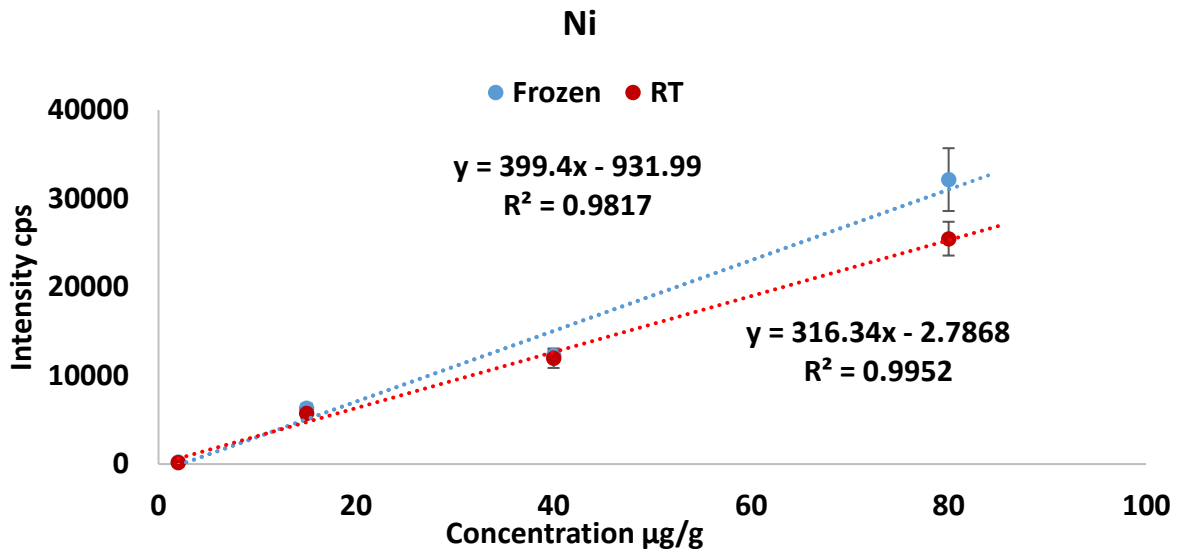


Figure 4.28: Correlation of obtained raw signal intensity from laser ablation and ions concentrations for kidney

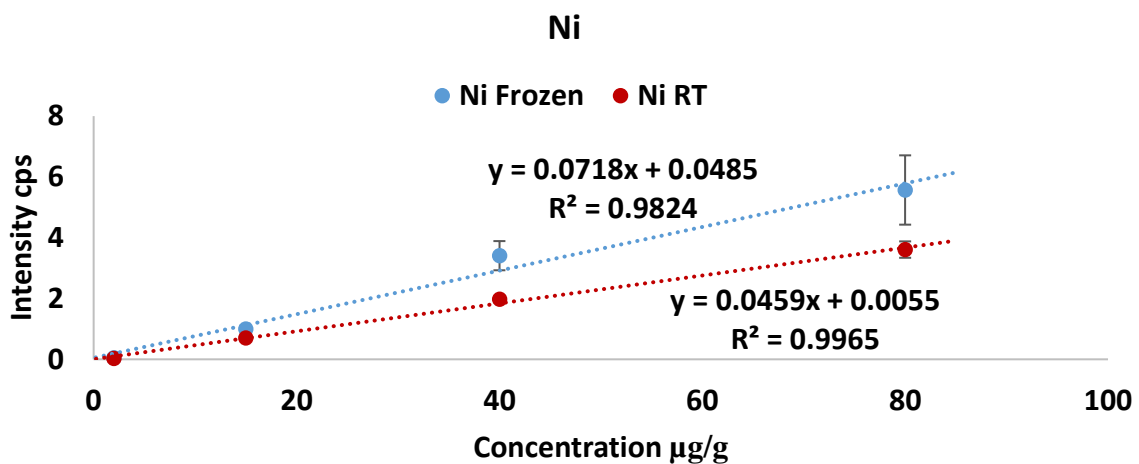
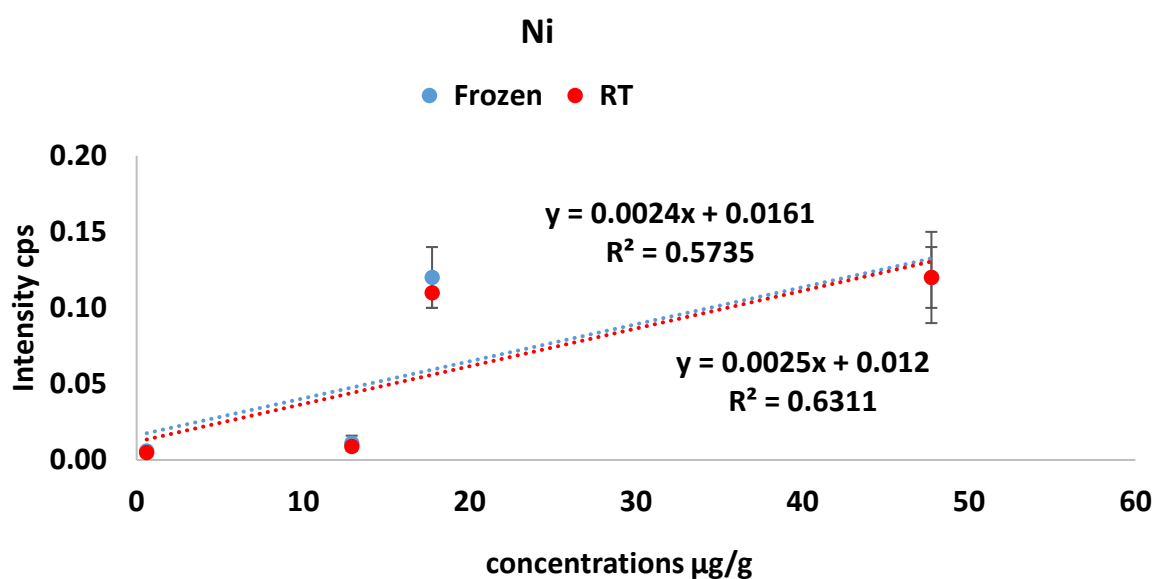


Figure 4.29: Correlation of obtained carbon normalized signal intensity from laser ablation and ions concentrations for kidney

The results corroborated that carbon did not improve the RSD for all level of concentrations. Therefore, Indium was chosen as internal standard in the second set of experiments. Indium with final concentration of 75 mg/L was added to all samples and the same settings and strategies as the first set were employed to measure the samples. Indium was supposed to overcome instrumental drifts and matrix related ablation differences due to its unique features. But in contrast to the first assumption regarding the effectiveness of normalization to indium, the results indicated that

normalization to indium not only did not help, but also it worsened the results. The indium counteracted the differences of slopes between frozen and room temperature states. The reason can be explained by the similar behavior of indium to other elements during ablation. Its intensity increased during ablation at frozen state and decreased during room temperature measurements, especially increased signals for standards measured at the frozen state. There were also quite unreasonable and large deviations. The reason can be addressed to inhomogeneity and not well distribution of indium with the tissue. Figure 4.30 illustrates the correlation of obtained indium normalized signal intensity and ions concentrations of nickel for liver tissue.



**Figure 4.30: Correlation of obtained indium normalized signal intensity from laser ablation and ions concentrations of nickel for liver**

Hence, the raw signal intensity was the best choice to show the differences in slopes for both frozen and room temperature states. Relative standard deviations up to 15% for non-spiked kidney tissue and up to 16% for non-spiked liver tissue was obtained. The signal from the LA-ICP-MS should correlate linearly with the concentrations of ions determined using ICP-MS. This was achieved for all measured elements but there were some deviations which led to a weaker coefficient of determination particularly in liver tissue. The reason can be attributed to multiple sources of errors. Since the samples were measured in separate days, instrumental drifts and matrix interferences could be the reasons of the deviations, however, these effects are not significant due

to short measurement time ( $\approx 20$  minutes) for each wafer. Inhomogeneity and contamination of sample during preparing matrix-matched standard could be another reason of the deviations. It is also likely that the thickness of the microtome cut was not precisely 10  $\mu\text{m}$  entire the tissue cut. Also, shrinkage of the rim of the tissue cuts immediately after cutting and appearing very tiny holes on the tissue section, which was probably due to existence of air bubbles in the matrix-matched standards before freezing into liquid nitrogen, confirmed the roughness of the thickness.

Figures 4. (31-32) show the correlations of obtained raw signal intensity from laser ablation and ions concentrations of copper and nickel for kidney and liver tissues, respectively. The obtained regression lines were steeper at frozen state than room temperature for all measured elements. It was around 85% higher for copper in kidney tissue and 44% for nickel in liver tissue. It can be explained by smaller size of the ablated aerosol particles at frozen state than at room temperature which would result in better and more efficient of transport process of the ablated particles to the plasma, higher sensitivity and no delay in ionization. The possible water vapors produced during the ablation of biological sample at ambient temperature may change the plasma and ionization efficiency which may be improved during the ablation at frozen state [20]. Additionally, the adsorption properties of the laser energy in ice are significantly greater than in water and dried matrix [58].

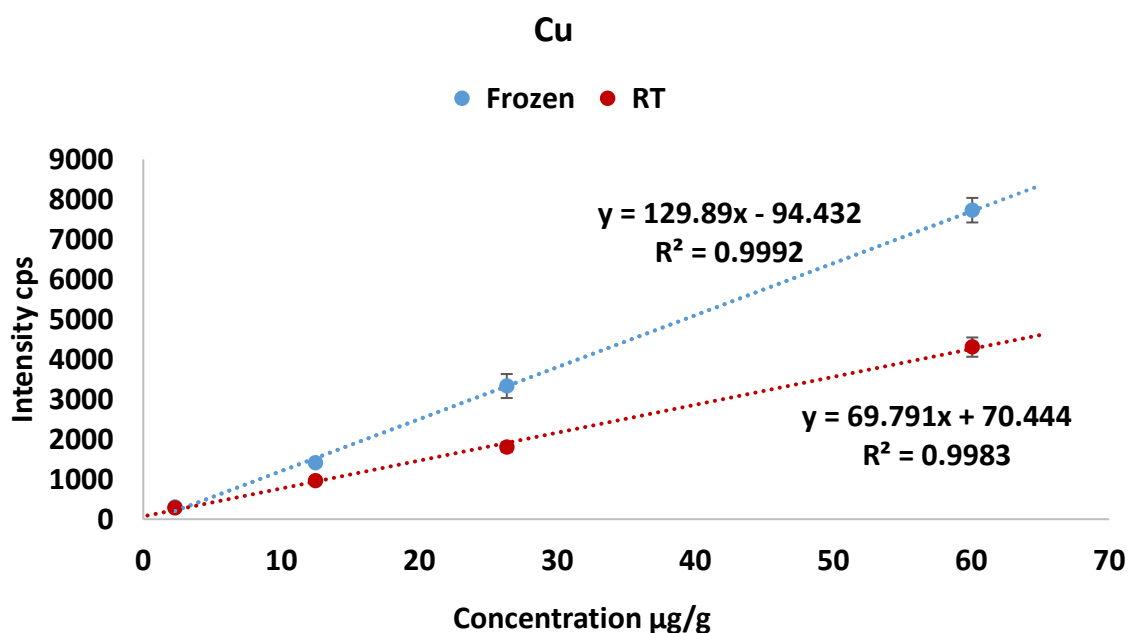


Figure 4.31: Correlation of obtained raw signal intensity from laser ablation and ions concentrations of copper for kidney

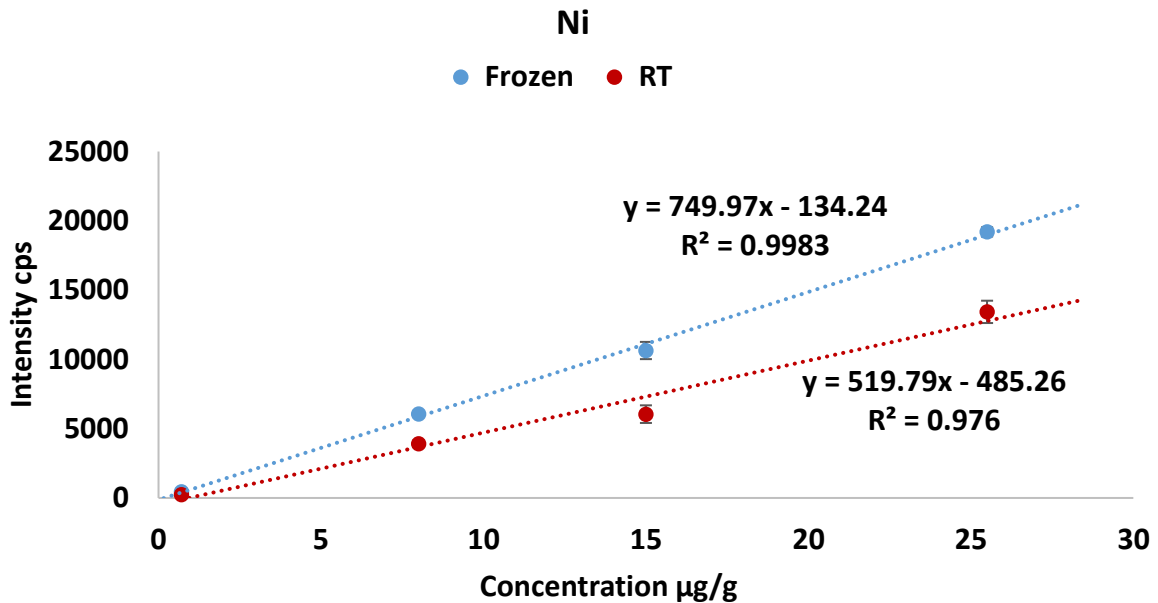


Figure 4.32: Correlation of obtained raw signal intensity from laser ablation and ions concentrations of nickel for liver

A strong interaction of a high energetic laser beam with sample leads to transfer of laser energy to the matter. This interaction can result in thermal effects which probably affect the sample, both directly in the irradiated surface and in adjacent areas. It causes re-deposition of ablated particles and contamination areas in the vicinity. Thus, an accurate control of sample temperature throughout LA-ICP-MS analysis is necessary, particularly when working with biological samples [5, 22].

Figures 4. (33-34) demonstrate the crater shapes of a biological tissue after laser ablation. Four different repetition rates each with five replicates were applied. First five upper spots from left to right ablated with 1 Hz (1 shot per second), second line of spots ablated with 2 Hz (2 shots per second), third line of spots ablated with 5 Hz (5 shots per second) and finally last line with 10 Hz (10 shots per second). It is obvious that by increasing repetition rate, more particles were ablated.

By looking carefully at figures, it can be concluded that using cooled ablation cell does prevent ablated particles aerosol from re-depositing in adjacent area. This fact can be proven by smooth and distinct rim of each spot at frozen state. It has been also shown by M.Jarošová, et.al [22] that fractionation effects can be refined using cooled ablation cell.

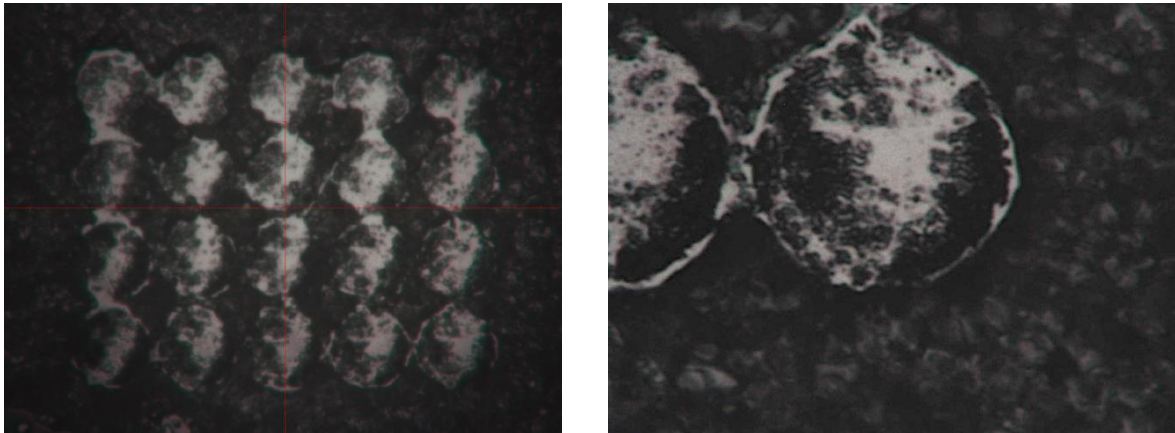


Figure 4.33: Crater shape at frozen state

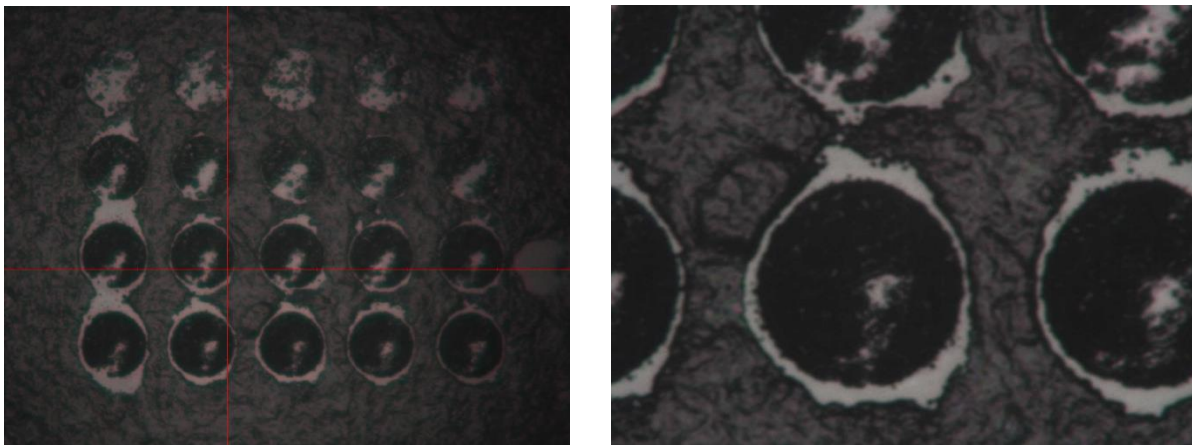
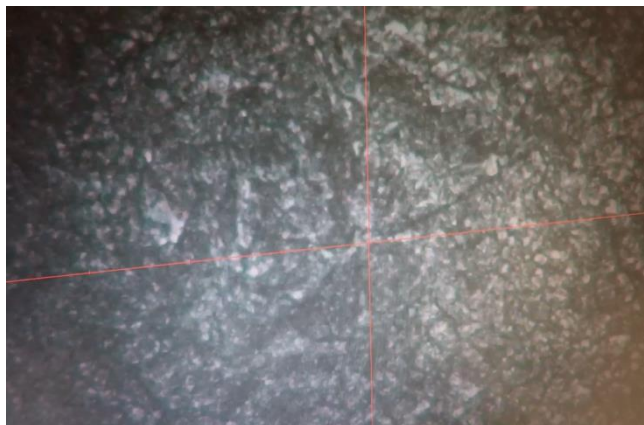


Figure 4.34: Crater shape at room temperature

### 4.3 Imaging experiments on frozen biological tissue

As mentioned in chapter one, one of the most interesting applications of LA-ICP-MS over the last years is related to imaging techniques to map the distribution of elements both metals and non-metals in biological tissues. Bioimaging of metals can be both performed in animal tissue samples and in plants for inspection of nutrient uptake [59]. One of the most essential step in biological or biomedical analysis is sample preparation and pretreatment. The reason which makes this step so important attributes to the fact that the morphology and composition of the tissue must be preserved during experiments. There are various sample preparation techniques, each suitable for specific purposes. Up to present, there have been two standard procedures in laboratories used for preparation of soft biological tissues for imaging studies:

1- formalin fixation and paraffin embedding (FFPE), 2- snap frozen of the sample in its native state. In the first case, sample preparation suffers several steps which can cause some metal losses or change the elemental distributions. In the latter case, tissue specimen becomes frozen quickly in liquid nitrogen and stored at  $-70\text{ }^{\circ}\text{C}$ . For LA- ICP- MS thin cuts of 10 or 20  $\mu\text{m}$  are prepared using cryotome. Nevertheless, ablation cell of conventional LA- ICP-MS instrumentation is operated at room temperature, thus thawing of the frozen samples is required prior to measurement. This step could introduce an additional error since trace elemental distributions might be changed. Figures 4. (35-37) illustrate thawing of the tissue sample from frozen state to a complete dried state. This process occurs in less than a minute. It initiates by diffusing water inside the tissue following by displacement of ions and ends by evaporating the water and finally dryness of tissue. Consequently, an investigation to compare the behaviour of animal tissue sections image at different sample temperatures during LA- ICP- MS was undertaken.



**Figure 4.35: Sample is still frozen, beginning of thawing**

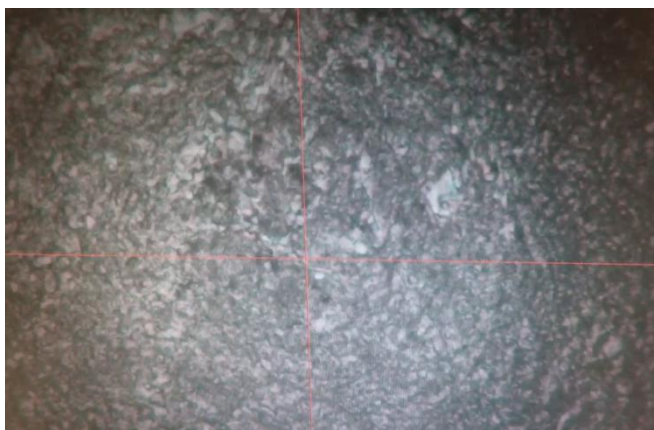


**Figure 4.36: Sample is being thawed, water diffusing**

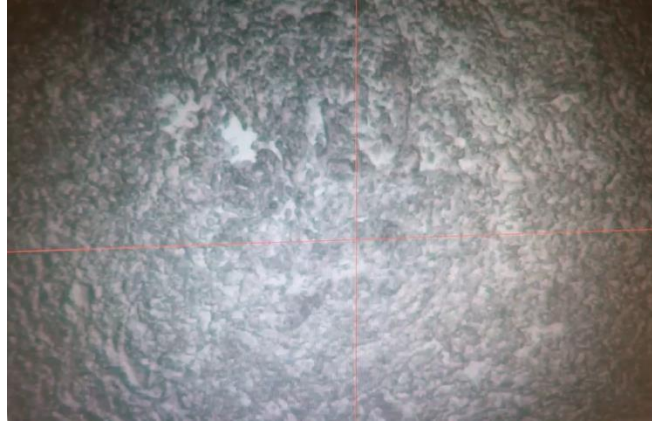


**Figure 4.37: Sample is completely dried**

M.V.Zoriy et.al [20], were the pioneer in using cooled ablation cell to demonstrate the advancements in precision and accuracy of isotopic ratios for flower leaves in 2005. A rat and a mouse brain as two biological tissues were selected and thin cuts of 10  $\mu\text{m}$  were prepared. The experimental operating parameters for the analysis histological sections should be assigned in a way to represent the structure and morphology of the tissue comprehensively. To achieve this, scan spot of 40  $\mu\text{m}$ , scan speed of 120  $\mu\text{m}/\text{s}$ , 10 Hz repetition rate, laser influence of 9.75  $\text{J}/\text{cm}^2$  and helium rate of 1 L/min were chosen. The ideal way to demonstrate the feasible differences in image quality is to ablate half of the tissue and obtain the image at frozen condition and other half at ambient temperature. But due to long measurement time required for preferred setting and inability of the Peltier cooled stage (chapter 4.1) to hold the temperature unchanged at freezing condition for longer than 30 minutes, the experiments at frozen state carried out only for some informative areas of tissues and compared with the equal areas at ambient temperature. The set temperature for measurements at frozen conditions was at  $-5\text{ }^\circ\text{C}$ . As can be seen in Figure 4. (38-39) elemental images of a rat brain is demonstrated for  $^{64}\text{Zn}$  and  $^{63}\text{Cu}$  as two prominent transition metals which play very crucial roles such as signaling, metabolism, as gene expression and as co-factors for enzymes that protect the brain from reactive oxide species (ROS) [59] (ImageLab, Epina GmbH, Pressbaum, Austria was used for image processing). The experiment was performed in two parts. The upper part ablated at frozen condition and the lower part at room temperature. The resulting elemental images have lateral resolution of 40  $\mu\text{m}$  in the horizontal and vertical direction. As proved in previous sections, measurements at frozen condition yielded higher signal intensity slopes for all

measured elements. This finding was observed for LA-ICP-MS images obtained for the brain for trace elements. Higher signal intensity is rooted in better ionization of transported particles in ICP. It is highly likely that laser energy spreads homogeneously in the cooled ablated sample and thermal fractionation effects occurring during measurement elemental analysis noticeably decreased and, in consequence particles ablated in smaller size which postulates better transportation of the particles without depositing in the tubing. It is followed by better atomization and ionization of the particles in the plasma and as a result higher sensitivity is achieved. It is obvious that at the same signal intensity scale the quality of the image at frozen state is much better than room temperature and it yields more precise elemental distributions information about the metals and their positions in tissue samples. Since there was a long time between rat brain imaging and measuring the calibration curved by LA-ICP-MS and meanwhile both laser and ICP- MS were upgrade, quantification of copper and zinc needs a new calibration curve with new LA-ICP-MS condition. Thus, the image scales are shown according to their intensity.

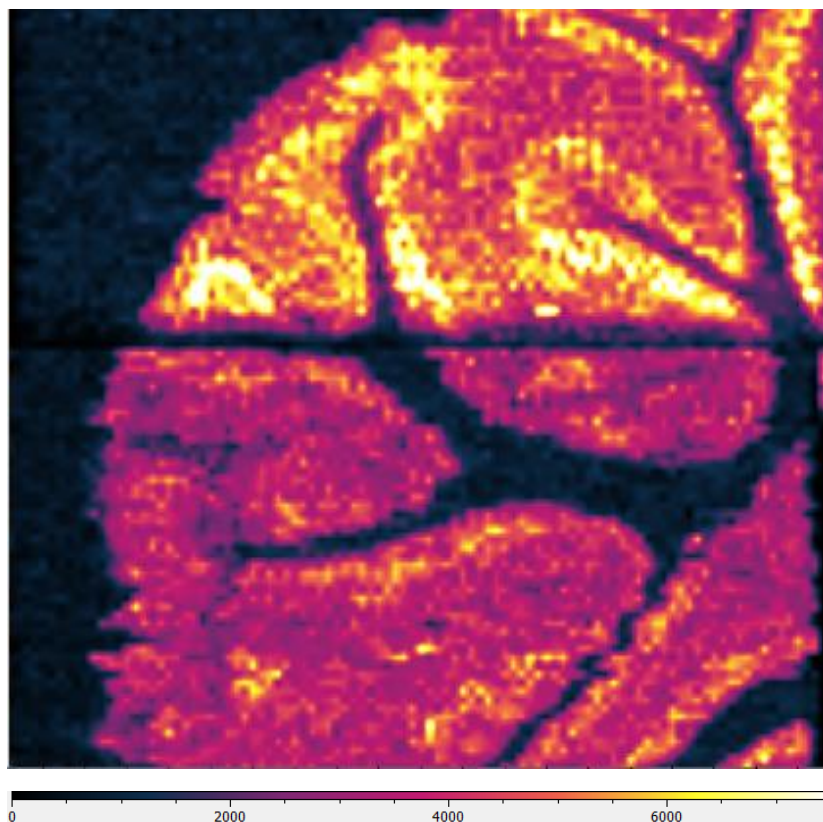


**Figure 4.38: Rat brain images obtained by LA-ICP-MS for  $^{64}\text{Zn}$  (cps) frozen (upper) and ambient (lower) state**

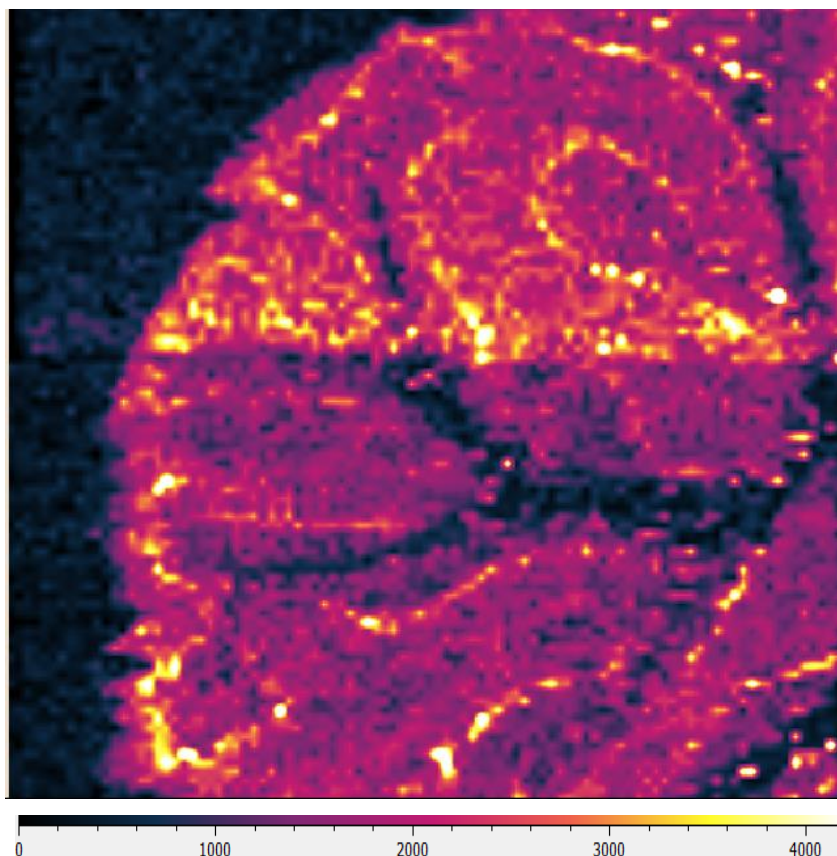


**Figure 4.39: Rat brain images obtained by LA-ICP-MS for <sup>63</sup>Cu (cps) at frozen (upper) and ambient (lower) states**

The same observation was carried out on a mouse brain with the same parameters mentioned in Table 3.1. Figure 4.40 demonstrates two images obtained at frozen state and ambient temperature. The image on the left side belongs to the measurement at frozen condition and on the right side is the image obtained at ambient temperature. By comparison, the cooled ablation image indicates higher signal intensity and the quality of the image is superior to non-cooled ablation image.

Figure 4.41 exhibits the maximum copper concentration in analyzed brain section with 60  $\mu\text{g/g}$  around two lateral ventricle regions. The calibration curve measured by LA- ICP-MS using prepared in-house-standards with defined concentrations of analyte was applied for quantification.

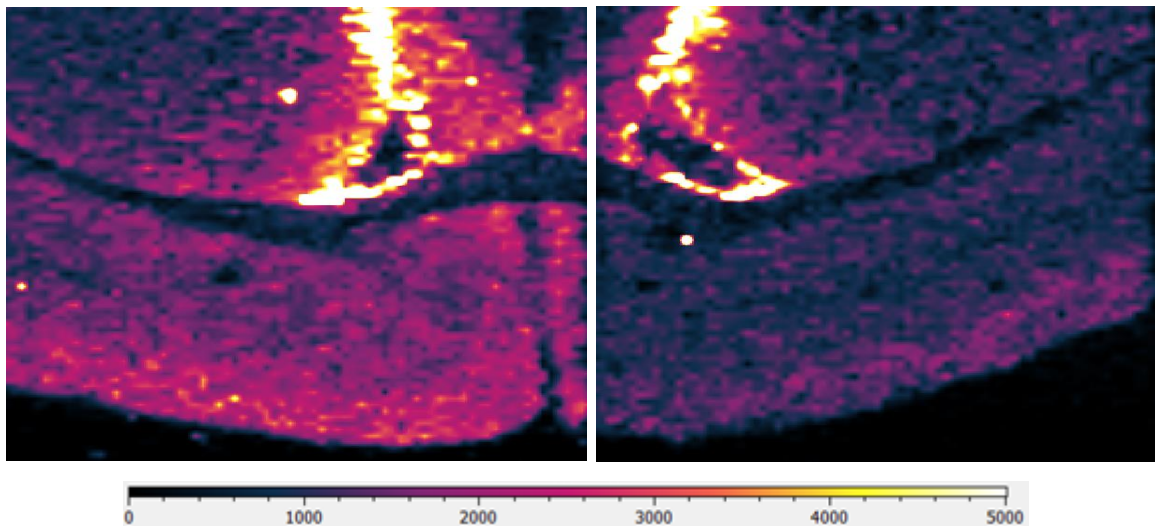


Figure 4.40: Comparison of mouse brain images obtained by LA-ICP-MS for  $^{63}\text{Cu}$  (cps) at both frozen condition (left) and ambient temperature (right)

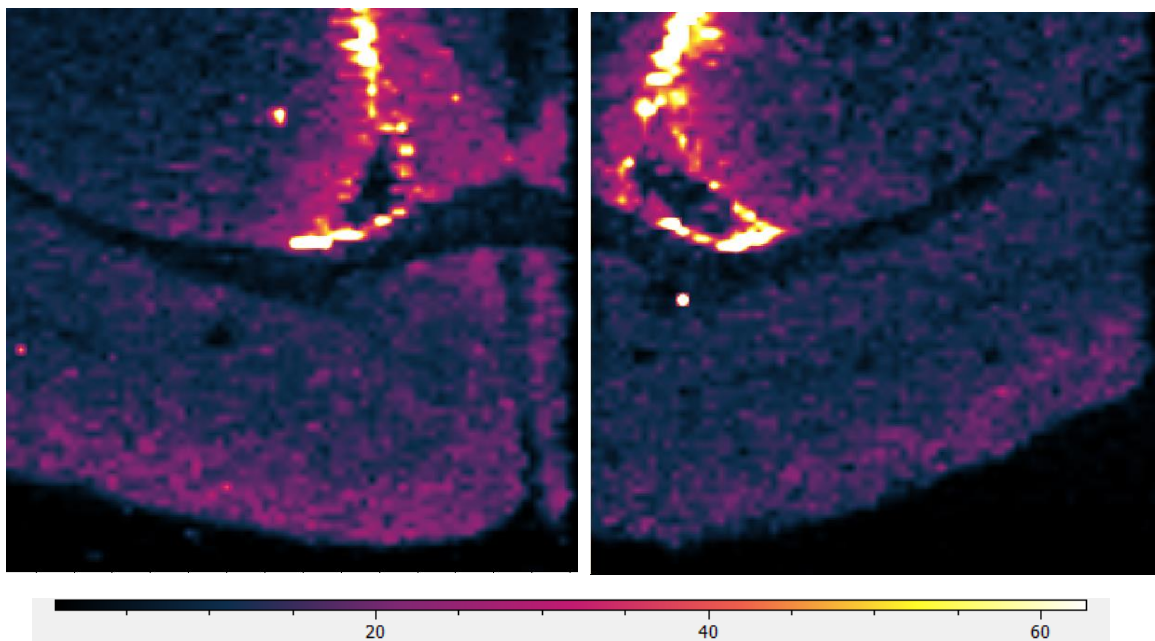


Figure 4.41: Images of copper concentration ( $\mu\text{g/g}$ ) obtained by LA-ICP-MS at frozen (left) and ambient (right) state

To summarize, imaging experiments of the soft tissues under frozen condition provide higher signal intensity. It can be explained by better transportation of ablated aerosol particles to the ICP and more efficient ionization as well. A much highlighted benefit of cooled ablation is to preserve the structure and integrity of tissue from possible damage due to less heat dissipation into adjacent area during the measurement. As a result, less re-deposition of the ablated aerosol particles leads to better image quality.

## 5. Conclusion

This work was undertaken to evaluate a Peltier-cooled ablation cell to investigate the ablation behavior of different temperatures on various materials such as glass, metal and biological samples. For this, a Peltier-cooled cell consisting of target holder (25×45 mm), two semiconductors N type and P type (cooling component, Peltier-element), two thermistors, two thermal conductors and body which is called heatsink made of bulky aluminum was designed. The Peltier was accurately characterized to guarantee the constancy of the set temperature during experiments. It was determined that for short time measurements up to 20 minutes the Peltier was allowed to be cooled down till -10 °C and for longer experiments up to 35 minutes -5 °C was the ideal temperature to be worked with. Temperatures below -10 °C were not applicable due to rapid saturation of the heatsink and inability to absorb more heat. Therefore, the target holder could not keep the set temperatures at freezing points constant for longer time.

Experimental results on glass (NIST 612) and metal (copper BCR No 075C) showed that decreasing temperature yielded higher signal intensity for measured elements. This effect, however, was more pronounced for metal object due to better thermal conductivity and signal intensity at -10 °C was 46% higher than at room temperature. This amount was maximum up to 10% for glass measurements. The obtained RSD was quite reasonable for glass and it confirmed reproducibility and accuracy of the measurements, both at room temperature and freezing point. No significant difference between temperatures below -1 °C till -10 °C (the minimum temperature could be examined) was observed.

For signal quantification in imaging experiments with biological tissue samples gelatin was chosen as matrix for the calibration standards due to its resemblance to biological tissue. Gelatin was spiked for six concentration levels and cryotome cuts were prepared with the thickness of 10 μm. The results indicated that gelatin matrix-matched calibration yielded steeper linear regression in case of frozen state with regression coefficient range varied from 0.90 to 0.98 for all measured elements. To improve the regression coefficient and tackle the instrumental drifts and ablation differences, analyte signals were normalized to europium which had been added as internal standard to all calibration standards. The regression coefficient above 0.99 and RSD below 3% were obtained, whereas normalization counteracted the slope differences

which can be interpreted as similar behavior of europium during ablation as other measured elements, in particular increased signals for standards measured in the frozen state.

Having confirmed that there are some benefits regarding cooled ablation, the experiment carried out on two distinct biological tissues. Porcine liver and kidney were homogenized and spiked for four concentration levels and tissue sections prepared using cryotome. Matrix-matched tissue standards yielded steeper regression line for cooled ablation analysis compared to non-cooled ablation. In these calibration experiments, there were some deviations observed which were related to the instrumental drifts, matrix related ablation differences and day-to-day signal variation. Choosing a proper internal standard to overcome these unwanted effects is mandatory. Thin layer of gold is reported to behave well, however, due to a restriction applied to this work associating with temperature control, it was not applicable. At first, the raw data from laser ablation was normalized to  $^{13}\text{C}$ . It could slightly improve the RSD in case of kidney tissue, although it was not observed for all measured elements for liver tissue. Since using carbon as internal standard is always disputable, indium was selected as second internal standard. However, normalization to indium disappeared the differences between cooled and non-cooled ablation and led to rather large deviations. The reason for disappearing the differences can be associated with the behavior of indium during ablation process. Its intensity altered during measuring at frozen and room temperature state, it increased during frozen state ablation and decreased during room temperature ablation process, similar behavior as other elements. Additionally, the reason for large deviations after normalization can be interpreted as not well homogenization of indium with tissue matrix-matched. Therefore, the best way to demonstrate the effects of lowering temperature and differences of measurement between both frozen and room temperature state was by using raw signal intensity data. The results showed that the correlations of obtained raw signal intensity from laser ablation and ions concentrations for all target elements yielded steeper slope in case of frozen state. It was around 85% higher for Cu in kidney and 44% for Ni in liver tissue. The most probable reason for this improvement is that in case of cooled analysis the size of ablated aerosol particles is smaller, and it results in better transport process of ablated particles to plasma and higher sensitivity. Furthermore, the adsorption properties of the laser energy in ice are significantly greater than in water matrix. Crater shape was seen to be sharper and well distinct at

frozen state with no contamination around which is usually caused by re-deposition of the ablated particles as a result of heat dissipation into neighboring areas. The results from calibration lines are acceptable without normalization since the measurements for each tissue section was performed in less than 20 minutes, therefore undesirable effects regarding the instrumental drifts cannot influence the results severely.

In recent years, LA-ICP-MS has been shown to be a strong analytical tool for imaging and distributions of metals and nonmetals in thin sections of biological tissues. However, preparation and pretreatment before analysis are the most important part to be noticed. Up to now, formalin fixation and paraffin embedding (FFPE) or snap frozen of the sample in its native state are the most common approaches. Both nevertheless have been reported to suffer several pitfalls. In FFPE method, a large number of sample preparation steps cause contamination and metal loss. In the latter case, thawing of the frozen samples is required prior to measurement. This step could introduce an additional error since trace element distributions might be altered. To overcome these barriers, frozen biological tissues were measured by means of an in-house-built Peltier cooled stage throughout the experiments to preserve their morphology and structures. Tissue cuts from a rat and mouse brain were prepared. Because of some restrictions regarding the Peltier inability to hold the temperatures constant at frozen points for longer required time, the experiments were performed only on small area of the tissues at frozen condition. The final images were provided with the lateral resolution of 40  $\mu\text{m}$ . The obtained results indicated that higher signal intensity during cooled analysis. The reason can be attributed to smaller size of the ablated particles and better ionization in the plasma. Moreover, cooled ablation showed to preserve the structure and integrity of the tissues since fractionation effect can be diminished using cooled stage. Thus, the image quality obtained during cooled analysis outshines the non-cooled analysis. Also, quantitative results for copper concentration on the mouse brain was obtained using calibration standards.

## 6. Outlook

This work offers the applicability of a Peltier-cooled ablation stage during laser ablation of different materials such as glass, metal and mainly focused on biological samples. During the work, it has been observed that ablation properties of biological samples are highly temperature dependent. Therefore, rigorously sample temperature control entire the analysis time and being able to respond instantly to any fluctuation especially during imaging experiments which acquire longer time is essential. The Peltier cooled stage used in this work could sustain the temperature below zero (-1 °C to -10 °C) rather unchanged for around thirty minutes optimally which allows only limited sample area for imaging experiments. There is no doubt that designing a new Peltier-cooled stage with the ability to work for longer measurement time to produce more reliable data analytical is beneficial.

On the other hand, for long imaging experiments of biological tissue instrumental drifts, day-to-day signal variation and matrix-matched related ablation properties differences are not ignorable, and they have their adverse influences on signal stability and quality of the image. To compensate this, using of suitable internal standards is mandatory. Gold sputtering of the samples is one the certified option, however, due to preservation of frozen tissue sections practically it is not possible after attaching the samples on the silicon wafer. Improvement can be directed toward the coating the silicon surface before attaching the frozen sections on it. Nevertheless, difficulty in collecting the samples on gold coated silicon wafer is another issue to be tackled. Using transparent conductive indium tin oxide (ITO) as a substrate to collect the samples is also of great interest. Furthermore, problems regarding inhomogeneity of biological tissue preparation can be minimized using standard homogenizer specifically designed for this purpose.

Various approaches have been performed to determine the size of particles at frozen condition by means of SEM (scanning electron microscope). It is very likely that the ablated aerosol particles were at the range of nanometer and using silicon wafer or adhesive tape was not a practical approach to collect the particles. Thus, determination of ablated particles size is a point to be considered.

Having proved the qualitative advantage of using cooled ablation stage, a new research can provide insight information into the better spatial distribution by

minimizing the beam diameter and more accurate image quantification of metals in animal and human soft tissues. It may broaden horizons of understanding the role of trace elements in diagnosis of different diseases including cancer.

# Figures

Figure 2.1: Detailed view of the ICP-MS [25].....	16
Figure 2.2: Detailed view of plasma torch and RF coil relative to ICP-MS interface [25] .....	17
Figure 2.3: Typical vacuum interface used in ICP-MS instruments [26].....	18
Figure 2.4: Schematic diagram of a quadrupole mass analyzer [28] .....	20
Figure 2.5: Schematic of a channel electron multiplier [27] .....	21
Figure 2.6: Schematic diagram of a laser ablation [1].....	23
Figure 2.7: Abundance of some elements in nonliving world compared with the abundance in organisms [33].....	26
Figure 2.8: Scan types available for LA-ICP-MS .....	31
Figure 3.1: ThermoFisher Scientific iCAP Q ICP-MS instrumentation used for the performed experiments.....	34
Figure 3.2: New Wave 213 laser ablation device employed for the performed experiments.....	35
Figure 3.3: Picture of Peltier and its components .....	37
Figure 3.4: Fluke thermometer .....	38
Figure 3.5: ThermoFisher Cryostat.....	40
Figure 4.1: Peltier behavior at 20 °C.....	43
Figure 4.2: Peltier behavior at 0 °C.....	44
Figure 4.3: Peltier behavior at -5 °C .....	44
Figure 4.4: Peltier behavior at -10 °C.....	45
Figure 4.5: Peltier behavior at -15 °C.....	45
Figure 4.6: Peltier behavior at -20 °C.....	46
Figure 4.7: Time stabilization on the sample surface.....	47
Figure 4.8: Peltier behavior under running laser at -5 °C.....	48
Figure 4.9: Peltier behavior under running laser at -10 °C.....	48
Figure 4.10: Peltier behavior under running laser at -15 °C.....	49
Figure 4.11: Measuring the glass surface.....	50
Figure 4.12: Signal intensity obtained for U .....	51
Figure 4.13: Aluminum intensity at different temperatures.....	51
Figure 4.14: Thorium intensity at different temperatures .....	52
Figure 4.15: Uranium intensity at different temperatures .....	52

<b>No table of figures entries found.</b>	
Figure 4.17: Signal intensity obtained for Co	54
Figure 4.18: Aluminum intensity at different temperatures	54
Figure 4.19: Crater shape at frozen state	55
Figure 4.20: Crater shape at room temperature	56
Figure 4.21: Copper intensity at different temperatures	57
Figure 4.22: Copper crater shape at frozen state	57
Figure 4.23: Copper crate shape at room temperature	58
Figure 4.24: Correlation of obtained raw signal intensity from laser ablation and ions concentrations for gelatin	61
Figure 4.25: Correlation of obtained europium normalized signal intensity from laser ablation and ions concentrations for gelatin	61
Figure 4.26: Correlation of obtained raw signal intensity from laser ablation and ions concentrations for liver	64
Figure 4.27: Correlation of obtained carbon normalized signal intensity from laser ablation and ions concentrations for liver	64
Figure 4.28: Correlation of obtained raw signal intensity from laser ablation and ions concentrations for kidney	65
Figure 4.29: Correlation of obtained carbon normalized signal intensity from laser ablation and ions concentrations for kidney	65
Figure 4.30: Correlation of obtained indium normalized signal intensity from laser ablation and ions concentrations of nickel for liver	66
Figure 4.31: Correlation of obtained raw signal intensity from laser ablation and ions concentrations of copper for kidney	67
Figure 4.32: Correlation of obtained raw signal intensity from laser ablation and ions concentrations of nickel for liver	68
Figure 4.33: Crater shape at frozen state	69
Figure 4.34: Crater shape at room temperature	69
Figure 4.35: Sample is still frozen, beginning of thawing	70
Figure 4.36: Sample is being thawed, water diffusing	70
Figure 4.37: Sample is completely dried	71
Figure 4.38: Rat brain images obtained by LA-ICP-MS for <sup>64</sup> Zn (cps) at frozen (upper) and ambient (lower) states	72
Figure 4.39: Rat brain images obtained by LA-ICP-MS for <sup>63</sup> Cu (cps) at frozen (upper) and ambient (lower) states	73

Figure 4.40: Comparison of mouse brain images obtained by LA-ICP-MS for  $^{63}\text{Cu}$  (cps) at both frozen condition (left) and ambient temperature (right) .....74

Figure 4.41: Images of copper concentration ( $\mu\text{g/g}$ ) obtained by LA-ICP-MS at frozen (left) and ambient (right) states .....74

## Tables

Table 2.1: Summary of the different lasers properties using for ICP-MS.....	25
Table 3.1: Parameters applied for ICP-MS instrumentation.....	35
Table 3.2: Parameters applied for laser New Wave 213.....	36

## Literature

1. Montaser, A., *Inductively Coupled Plasma Mass Spectrometry*. 1998: Wiley.
2. Konz, I., et al., Laser ablation ICP-MS for quantitative biomedical applications. *Anal Bioanal Chem*, 2012. **403**(8): p. 2113-25.
3. Mokgalaka, N.S. and J.L. Gardea-Torresdey, *Laser Ablation Inductively Coupled Plasma Mass Spectrometry: Principles and Applications*. *Applied Spectroscopy Reviews*, 2006. **41**(2): p. 131-150.
4. Giesen, C., et al., History of inductively coupled plasma mass spectrometry-based immunoassays. *Spectrochimica Acta Part B: Atomic Spectroscopy*, 2012. **76**: p. 27-39.
5. Konz, I., et al., Design and evaluation of a new Peltier-cooled laser ablation cell with on-sample temperature control. *Anal Chim Acta*, 2014. **809**: p. 88-96.
6. Galievsky, V.A., A.S. Stasheuski, and S.N. Krylov, *Capillary Electrophoresis for Quantitative Studies of Biomolecular Interactions*. *Analytical Chemistry*, 2015. **87**(1): p. 157-171.
7. J.L. Neilsen , A.A.a., J. Christensen a, P. Watson 3b, A. Cox b, C.W. McLeod b, <Laser ablation inductively coupled plasma-mass spectrometry in combination with gel electrophoresis: a new strategy for speciation of metal binding serum proteins >. 1998.
8. Sanz-Medel, A., et al., ICP-MS for absolute quantification of proteins for heteroatom-tagged, targeted proteomics. *TrAC Trends in Analytical Chemistry*, 2012. **40**: p. 52-63.
9. Rodushkin, I. and M.D. Axelsson, Application of double focusing sector field ICP-MS for multielemental characterization of human hair and nails. Part III. Direct analysis by laser ablation. *The Science of the total environment*, 2003. **305**(1-3): p. 23-39.
10. Prohaska, T., et al., Investigation of Sr isotope ratios in prehistoric human bones and teeth using laser ablation ICP-MS and ICP-MS after Rb/Sr separation. *Journal of Analytical Atomic Spectrometry*, 2002. **17**(8): p. 887-891.
11. Punshon, T., et al., Mass loading of nickel and uranium on plant surfaces: application of laser ablation-ICP-MS. *J Environ Monit*, 2004. **6**(2): p. 153-9.
12. J. S. Becker, M. V. Zoriy, C. Pickhardt, N. Palomero-Gallagher, and K. Zilles, *Imaging of Copper, Zinc, and Other Elements* 2005.

13. Giesen, C., et al., Iodine as an elemental marker for imaging of single cells and tissue sections by laser ablation inductively coupled plasma mass spectrometry. *Journal of Analytical Atomic Spectrometry*, 2011. **26**(11): p. 2160.
14. Sarafanov, A.G., et al., Analysis of iron, zinc, selenium and cadmium in paraffin-embedded prostate tissue specimens using inductively coupled plasma mass-spectrometry. *J Trace Elem Med Biol*, 2008. **22**(4): p. 305-14.
15. Hare, D., et al., Elemental bio-imaging of melanoma in lymph node biopsies. *Analyst*, 2009. **134**(3): p. 450-3.
16. Hare, D., et al., Elemental Bio-imaging of Thorium, Uranium, and Plutonium in Tissues from Occupationally Exposed Former Nuclear Workers. *Analytical Chemistry*, 2010. **82**(8): p. 3176-3182.
17. Berg, D., et al., Use of Formalin-Fixed and Paraffin-Embedded Tissues for Diagnosis and Therapy in Routine Clinical Settings, in *Protein Microarrays: Methods and Protocols*, U. Korf, Editor. 2011, Humana Press: Totowa, NJ. p. 109-122.
18. Qin, Z., et al., Trace metal imaging with high spatial resolution: applications in biomedicine. *Metallomics*, 2011. **3**(1): p. 28-37.
19. Bonta, M., et al., A comparison of sample preparation strategies for biological tissues and subsequent trace element analysis using LA-ICP-MS. *Anal Bioanal Chem*, 2017. **409**(7): p. 1805-1814.
20. Zoriy, M.V., et al., Determination of uranium isotopic ratios in biological samples using laser ablation inductively coupled plasma double focusing sector field mass spectrometry with cooled ablation chamber. *International Journal of Mass Spectrometry*, 2005. **242**(2-3): p. 297-302.
21. Hamilton, J.S., et al., Evaluation of a custom single Peltier-cooled ablation cell for elemental imaging of biological samples in laser ablation-inductively coupled plasma-mass spectrometry (LA-ICP-MS). *Journal of Analytical Atomic Spectrometry*, 2016. **31**(4): p. 1030-1033.
22. Jarošová, M., et al., Influence of temperature on laser ablation fractionation during ICP-MS analysis for 213 nm and 266 nm laser wavelength micro-sampling. *J. Anal. At. Spectrom.*, 2016. **31**(10): p. 2089-2093.
23. Ammann, A.A., Inductively coupled plasma mass spectrometry (ICP MS): a versatile tool. *J Mass Spectrom*, 2007. **42**(4): p. 419-27.

24. Woeste, S., Inductively Coupled Plasma Mass Spectrometry. Laboratory Medicine, 2004. **35**(2): p. 73-75.
25. Thomas, R., Practical Guide to ICP-MS: A Tutorial for Beginners, Second Edition. 2008: Taylor & Francis.
26. Montaser, A. and D.W. Golightly, Inductively coupled plasmas in analytical atomic spectrometry. 1987: VCH Publishers.
27. Hill, S.J., Inductively coupled plasma spectrometry and its applications. Vol. 8. 2008: John Wiley & Sons.
28. Linge, K. and K. Jarvis, Quadrupole ICP-MS: Introduction to Instrumentation, Measurement Techniques and Analytical Capabilities. Vol. 33. 2009.
29. Denoyer, E., et al., Determination of trace elements in uranium: practical benefits of a new ICP-MS lens system. Atomic spectroscopy, 1995. **16**(1): p. 1-6.
30. Neufeld, L.M., I. New Wave Research, and C. Fremont, USA, <Introduction to Laser Ablation ICP-MS for the analysis of forensic samples>. 2004.
31. Teresa E. Jeffries, S.E.J.a.H.P.L., Application of a frequency quintupled Nd5YAG source ( $\lambda=213$  nm) for laser ablation inductively
32. Diwakar, P.K., et al., Ultrafast laser ablation ICP-MS: role of spot size, laser fluence, and repetition rate in signal intensity and elemental fractionation. J. Anal. At. Spectrom., 2014. **29**(2): p. 339-346.
33. Chaffey, N., Alberts, B., Johnson, A., Lewis, J., Raff, M., Roberts, K. and Walter, P. Molecular biology of the cell. 4th edn. Annals of Botany, 2003. **91**(3): p. 401-401.
34. Heymsfield, S.B., et al., Chemical and elemental analysis of humans in vivo using improved body composition models. American Journal of Physiology - Endocrinology And Metabolism, 1991. **261**(2): p. E190-E198.
35. Sychrova, H., Yeast as a Model Organism to Study Transport and Homeostasis of Alkali Metal Cations. Vol. 53 Suppl 1. 2004. S91-8.
36. Long, S. and A.M.P. Romani, Role of Cellular Magnesium in Human Diseases. Austin journal of nutrition and food sciences, 2014. **2**(10): p. 1051.
37. Brini, M., et al., Calcium in Health and Disease, in Interrelations between Essential Metal Ions and Human Diseases, A. Sigel, H. Sigel, and R.K.O. Sigel, Editors. 2013, Springer Netherlands: Dordrecht. p. 81-137.

38. Abbaspour, N., R. Hurrell, and R. Kelishadi, Review on iron and its importance for human health. *Journal of Research in Medical Sciences : The Official Journal of Isfahan University of Medical Sciences*, 2014. **19**(2): p. 164-174.
39. Roohani, N., et al., Zinc and its importance for human health: An integrative review. *Journal of Research in Medical Sciences : The Official Journal of Isfahan University of Medical Sciences*, 2013. **18**(2): p. 144-157.
40. Zdrojewicz, Z., E. Popowicz, and J. Winiarski, [Nickel - role in human organism and toxic effects]. *Polski merkuriusz lekarski : organ Polskiego Towarzystwa Lekarskiego*, 2016. **41**(242): p. 115-118.
41. Anke, M., et al., Nickel--an essential element. *IARC Sci Publ*, 1984(53): p. 339-65.
42. Brazier, M.W., et al., Manganese binding to the prion protein. *J Biol Chem*, 2008. **283**(19): p. 12831-9.
43. Osredkar, J., Copper and Zinc, Biological Role and Significance of Copper/Zinc Imbalance. *Journal of Clinical Toxicology*, 2011. **s3**(01).
44. Todd, R.C. and S.J. Lippard, Inhibition of transcription by platinum antitumor compounds. *Metallomics*, 2009. **1**(4): p. 280-91.
45. Zitek, A., J. Aleon, and T. Prohaska, CHAPTER 9 Chemical Imaging, in *Sector Field Mass Spectrometry for Elemental and Isotopic Analysis*. 2015, The Royal Society of Chemistry. p. 152-182.
46. Lear, J., et al., Improving acquisition times of elemental bio-imaging for quadrupole-based LA-ICP-MS. *J. Anal. At. Spectrom.*, 2012. **27**(1): p. 159-164.
47. Moreno-Gordaliza, E., et al., Elemental bioimaging in kidney by LA-ICP-MS as a tool to study nephrotoxicity and renal protective strategies in cisplatin therapies. *Anal Chem*, 2011. **83**(20): p. 7933-40.
48. T.martorana, R., <Thermoelectric Temperature Control of instrumentation- A sample design>. 1975.
49. Najafi, H. and K.A. Woodbury, Optimization of a cooling system based on Peltier effect for photovoltaic cells. *Solar Energy*, 2013. **91**: p. 152-160.
50. Olivares-Robles, M.A., F. Vazquez, and C. Ramirez-Lopez, Optimization of Two-Stage Peltier Modules: Structure and Exergetic Efficiency. *Entropy*, 2012. **14**(12): p. 1539-1552.

51. Taylor, R.A. and G.L. Solbrekken, Comprehensive system-level optimization of thermoelectric devices for electronic cooling applications. *IEEE Transactions on Components and Packaging Technologies*, 2008. **31**(1): p. 23-31.
52. Austin, C., et al., Factors affecting internal standard selection for quantitative elemental bio-imaging of soft tissues by LA-ICP-MS. *Journal of Analytical Atomic Spectrometry*, 2011. **26**(7): p. 1494-1501.
53. Glaus, R., et al., Phenomenological studies on structure and elemental composition of nanosecond and femtosecond laser-generated aerosols with implications on laser ablation inductively coupled plasma mass spectrometry. *Spectrochimica Acta Part B: Atomic Spectroscopy*, 2010. **65**(9): p. 812-822.
54. Sala, M., V.S. Selih, and J.T. van Elteren, Gelatin gels as multi-element calibration standards in LA-ICP-MS bioimaging: fabrication of homogeneous standards and microhomogeneity testing. *Analyst*, 2017. **142**(18): p. 3356-3359.
55. Stark, H.J. and R. Wennrich, A new approach for calibration of laser ablation inductively coupled plasma mass spectrometry using thin layers of spiked agarose gels as references. *Anal Bioanal Chem*, 2011. **399**(6): p. 2211-7.
56. Bonta, M., et al., Application of gold thin-films for internal standardization in LA-ICP-MS imaging experiments. *Analyst*, 2014. **139**(6): p. 1521-31.
57. Frick, D.A. and D. Günther, Fundamental studies on the ablation behaviour of carbon in LA-ICP-MS with respect to the suitability as internal standard. *Journal of Analytical Atomic Spectrometry*, 2012. **27**(8): p. 1294.
58. Reinhardt, H., et al., Application of LA-ICP-MS in polar ice core studies. *Anal Bioanal Chem*, 2003. **375**(8): p. 1265-75.
59. Becker, J.S., et al., Bioimaging of metals in brain tissue by laser ablation inductively coupled plasma mass spectrometry (LA-ICP-MS) and metallomics. *Metallomics*, 2010. **2**(2): p. 104-11.